Department of Mechanics and Materials

Solid Mechanics

ISRN LUTFD2/TFHF--00/5087--SE(1-68)

Structural Mechanics

ISRN LUTVDG/TVSM--00/5103--SE(1-68)
ISSN 0281-6679

FINITE ELEMENT MODELLING OF A RUBBER BLOCK EXPOSED TO SHOCK LOADING

Master's Dissertation by

PAUL HÅKANSSON

Supervisors

ANDERS PETTERSSON,
Kockums AB

MATTI RISTINMAA,
Div. of Solid Mechanics

PER-ERIK AUSTRELL,
Div. of Structural Mechanics

Printed by KFS i Lund AB, Lund, Sweden, Novemeber 2000.

For information address:

Division of Solid Mechanics, LTH, Lund University, Box 118, SE-221 00 Lund, Sweden.
Homepage: http://www.solid.lth.se

Division of Structural Mechanics, LTH, Lund University, Box 118, SE-221 00 Lund, Sweden.
Homepage: http://www.byggmek.lth.se

Preface

This Master Thesis is accomplished in order to investigate the possibility to model the dynamic behaviour of rubber. The project is done at the request of Kockums AB with supervision from Solid Mechanics and Structural Mechanics - Department of Mechanics and Material at Lund University. The work has been done at Kockums AB in Malmö.

The thesis started in February 2000. I have in process of time learned a lot, practical test combined with theoretical studies and FE modelling have given many new aspects of the problem an engineer deal with. There are lots of people who have helped me to perform the task. I would like to direct my gratitude towards Anders Pettersson, Kockums AB, Matti Ristinmaa, Solid Mechanics, and Per-Erik Austrell, Structural Mechanics, who have supervised my work. I would also like to thank the whole department of Structural Analysis at Kockums and especially Jan Stenwall for many valuable discussions and suggestions. At Kockums, Lars Persson and Rune Persson at Kockums laboratory have also been of great help. Material tests have been accomplished at Trelleborg Automotive with help of Karl Jönsson. Without the generosity to let me do the tests, the thesis would loos some of its purpose when comparisons between simulations and experimental test could not have been done.

Malmö in October 2000

Paul Håkansson

Abstract

This master thesis is done in collaboration with the division of Solid Mechanics and the division of Structural mechanics at Lund University and Kockums AB. The assignment designates from the fact that there is no accurate method to model rubber dampers exposed of shock load. The rubber dampers are often used in submarines to protect sensible equipment from shock load and vibration. In this master thesis, different kinds of constitutive models for rubber will be investigated. The purpose is to find differences between models and to find out what properties that can be simulated and what cannot. The only investigated models are the ones that are available in LS-DYNA.

After a theoretical examine of the material models in LS-DYNA material tests were performed at Trelleborg Automotive. Simple shear tests were performed, where both purely elastic and dynamic tests were considered, since these tests are suited for calibration of both the Yeoh model and the Arruda & Boyce model. These two visco- hyper-elastic models were the only ones that were found useful for this application and the possible material tests. Unfortunately, was it impossible to manufacture suitable test specimens, the only alternative was to use the damper themselves. The disadvantage was that the deformation was not uniform, bending modes was included. This error was corrected when the fitting of the models was done. The magnitude of the error at different strains could be established with help of FE analysis by considering a simple shear case and one on a case where bending was included.

Shock tests were performed in order to evaluate the shock simulations in LS-DYNA. The shock tests were done with a drop table at Kockums laboratory. The dampers were exposed to a short acceleration, after that the dampers were allowed to oscillate. The deformation in these tests turned out to be purely compression and tension. The acceleration was controlled by the drop height while the frequency of the free vibrations was controlled by the weight of a mass. The achieved frequencies cover the range from about 9 Hz to 17 Hz. The shock accelerations were used as input in the FE simulations. The achieved accelerations and displacements were compared with the experimental ones.

The results from the simulations correspond quite well to the experimental tests. Especially the Yeoh model gives remarkably good results despite many approximations in the adaptation of the model. The response of the Arruda & Boyce model did, however, not fit very well for the lowest mass, for the two highest the response were similar to the on for the Yeoh model. Unfortunately, the rubber material depends more on the strain amplitude than the strain frequency at these relatively low frequencies. The frequency dependency can almost be neglected in this frequency range. This is a problem since the models depend only on the frequency and not the amplitude. This result in large deviations at the shock phase where the amplitude are considerable higher, due to too high damping, while the free vibration phase is better. If the interesting part is the shock phase it might be more suitable to use a purely hyperelastic model, the disadvantages is a large error at the free vibration phase. The free vibration phase is however better simulated with the visco-hyperelastic model

Contents

1 Introduction 1
1.1 Presentation of Kockums AB 1
1.2 Background to the assignment 1
1.3 Objective 1
1.4 Demarcation 2
1.5 Practical conditions 2
2 Presentation of rubber 3
2.1 History 3
2.2 The characteristic of rubber 3
3 Definitions and notations 7
4 Description of constitutive models for rubber 11
4.1 Hyperelastic material models 11
4.1.1 Strain energy 11
4.1.2 Strain energy functions 12
4.2 Viscoelastic material models 16
5 Test to determine material parameters 21
5.1 Experimental methods 21
5.1.1 Method to determine hyperelastic constants 21
5.1.2 Method to determine viscoelastic constants 23
5.2 Experimental Tests 24
5.2.1 Conditioning 24
5.2.2 Results of the hyperelastic test 24
5.2.3 Results of the viscoelastic tests 25
6 Adaptation of material models 29
6.1 Adaptation of hyperelastic material models 29
6.1.1 Yeoh model 30
6.1.2 Arruda & Boyce model 32
6.1.3 Comparison between FE model and uniaxial tests 34
6.2 Adaptation of viscoelastic material models 35
7 Shock test 39
7.1 Test arrangement and performance 39
7.2 Results 42
8 Simulation of shock test in LS-DYNA 47
8.1 Modelling of the damper 47
8.2 Element convergence study 49
8.3 Results from the shock test simulations 50
8.4 Evaluation of the results 55
8.4.1 Comparison between Arruda & Boyce and Yeoh 55
8.4.2 Amplitude dependency 55
8.4.3 Frequency dependency 58
9 Conclusion 59
10 References 61
Appendix A 63
Appendix B 65
Appendix C 67

1 Introduction

1.1 Presentation of Kockums AB

Kockums AB is an old Swedish company. It was establish in Malmö in 1840 it was known as *Kockums Mekaniska Werkstad.* The founder Frans Henric Kockum and his family had been active with business and industrial activities since 1820. *Kockums Mekaniska Werkstad* was mainly manufacturing agricultural implement, distillery devices, stoves and ovens. From 1850, they also produced railway carriage. In 1870, the first shipyard was build close to the engineering plant in Malmö. Investments under the forties and fifties in metal industry lead to *Kockums Jernverks AB* in 1875, it was after Frans Henric Kockum's death. The new company produced steel products, for example galvanised and enamelled products. At the same time *Kockums Mekaniska Werkstad* became more specialised to manufacture ship, railway carriage and bridges.

The company expanded heavily after the World War II it was not until the seventies the profitability decreased. This lead to the liquidation of *Kockums Jernverks AB* and a change of structure at *Kockums Mekaniska Werkstad*. They were now more concentrated on ship manufacturing. At the same time in 1977, the company took the name *Kockums AB.* Unfortunately, the profitability problem remained so in 1979 Kockums was taken over by *Svenska Varv AB* (since 1987 *Celsius Industrier*) owned by the Swedish government.

Kockums AB is to day only producing military equipment, such as submarines, small naval surface vessels and mobile bridges. The company is especially famous for its Stirling engines in the submarines and the stealth carbon fibre composite ship invisible to radar. Kockums AB was recently (October 1999) bought by the German shipyard *Howaldswerke-Deutsche Werft AG* or *HDW* located in Kiel.

1.2 Background to the assignment

In submarines elastic rubber mounts is used to protect sensible equipment from shock-load and vibration. Today, there is no accurate method to model rubber dampers for this kind of dynamic loading. A method commonly used in simulations is to replace the rubber dampers with linear springs and in some cases supplemented with a linear damper. This will, however, not fulfil all the properties of the rubber. The free oscillations achieved in the simulations will differ from the motion of the real physical material. It is for that reason desirable to find a rubber damper model with an accurate constitutive equation.

1.3 Objective

In this master thesis, different kinds of constitutive models for rubber will be investigated. The purpose is to illustrate differences between models and to find out what properties can be simulated and what cannot. The work can be described by the following tasks: material testing will be conducted in order to find the material parameters of the constitutive models. After that, the rubber damper will be modelled in the finite element program LS-DYNA and used in shock load simulations. Finally, the result of the simulation will be compared with the results of laboratory tests.

1.4 Demarcation

There are many different kinds of material models for rubber. As it is not possible to investigate them all, only suitable models in LS-DYNA will be considerd. Unfortunately, the limited time in a master thesis does not allow implementing models or any combinations thereof. Test specimen for the material test cannot be manufactured, again due to lack of time as well as due to the difficulties to vulcanise the same rubber quality as found in the existing rubber dampers. The material test will be performed on the existing rubber dampers.

1.5 Practical conditions

The FEM simulations were made in LS-DYNA version 950 [10] on a Hewlett Packard workstation. Some purely static calculations were also made in Abaqus version 5.8 [1] The available rubber dampers were manufactured by Trelleborg AB. The dampers have the design number **T06** and the material is **TR 4273**. They have the shape of a rectangular parallelepiped with the size according to figure 1.1.

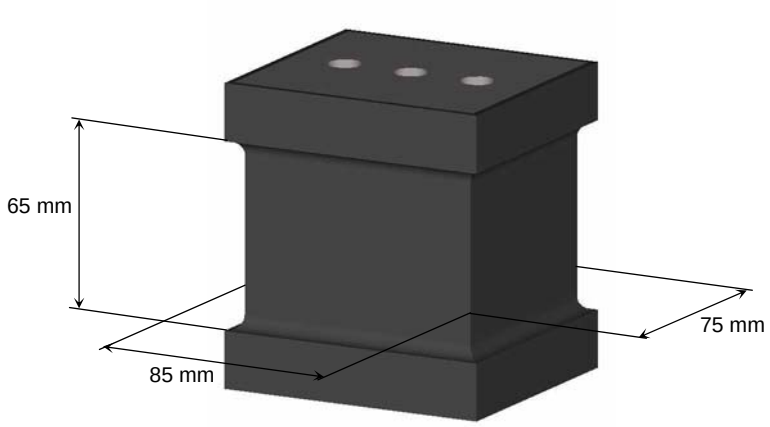

Figure 1.1. Shape and size of the rubber damper.

The rubber damper is made of natural rubber with a specified hardness of 60 IRH. The rubber is vulcanised to two steel plates. These plates are 20 mm thick and have three threaded holes each for mounting purpose.

2 Presentation of rubber

2.1 History

Rubber is a material, which today is often used in different kinds of construction elements. The important properties for this type of elements are shock absorption, vibration absorption and a dominating elastic behaviour for large deformations without any major plasticity. The Young's modulus is up to 100000 times smaller than for steel.

The history of rubber is described in the *National encyklopedin* [14] as follow: The human being has known the rubber material for many years. The Maya Indians pay homage to the rain gods by burning rubber. The industrial use arose in to Europe at the end of the 18th century. The first major applications came when Joseph Priestley in 1770 discovered that rubber removed lead from paper, hence the English name rubber.

Natural rubber is the first discovered species. It can be retrieved from more then 500 different plants. The most important source is the gumtree growing in Southeast Asia. The sap, *latex*, is collected, coagulated, washed and dried. This results in a sticky lump. In 1839, Charles Goodyear discovered that sulphur and heat transforms this sticky lump into an elastic and shape permanent material. The vulcanisation was invented. To further improve the properties of rubber different kinds of additives are added prior to the vulcanisation. For example, carbon black is used to improve the mechanical properties and organic amines or phenols are added to give the rubber a better ageing protection.

The production of synthetic rubber began under World War II, but the demand grew first under the Korean War. The reason was new inventions and a low oil price, which made the synthetic rubber economically competitive. The main raw material to manufacture synthetic rubber is namely petroleum products.

Today the total world rubber production is about 15 million tons of which 70% is used in the tyre production.

2.2 The characteristic of rubber

Rubber is built up by long molecule chains which forms a polymer. A more scientific name, which often is used, is elastomer. The raw material of natural rubber, latex, have no links between the molecule chains. It is first during the vulcanisation that these chains are connected with cross-links.

Rubber is highly elastic, of which some kinds can bear deformations of upto 500-800%. The elasticity is not linear in any way. It is usually described by a S-shaped stress-stretch curve (see figure 2.1).

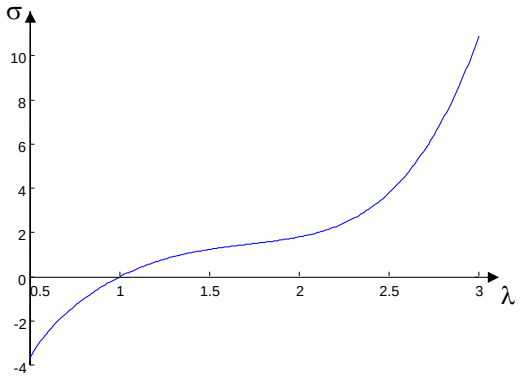

Figure 2.1. Example of a stress- stretch curve in a uniaxial stress case. $\lambda = 1$ corresponds to the undeformed state.

The behaviour of rubber material is very time dependent. The strain rate has a major effect on the stiffness, which increase dramatically in rapid processes. This behaviour can partly be described as viscoelastic. The major part of the relaxation occurs in a very short time. The relation between the shear modulus and the bulk modulus is large, the bulk modulus is usually 1000-2000 times higher than the shear modulus. This makes rubber nearly incompressible. Thus in many cases the approximation of incompressibility is quite appropriate [3].

When rubber is exposed of cyclic loading this partly viscoelastic behaviour leads, to a phenomenon called hysteresis. The consequence is that loading gives a higher stress at the same strain than unloading will give. This results in energy lost such as heat. In a case of free oscillations, the energy lost will act as damping.

The stiffness of the rubber is also affected by other factors. At a harmonic load, the frequency and the amplitude have a great influence. A higher frequency will increase the stiffness, while increased amplitude will decrease the stiffness. The temperature is an important factor as well. At temperatures over 0°C, the stiffness will be relatively constant, provided it is not close to the vulcanisation temperature. At lower temperature, the stiffness will be remarkable higher. Below -60 to -80°C the rubber will be in a glassy state [3]. Figure 2.2 shows the frequency dependency of the dynamic modulus and the phase shift of the natural rubber.

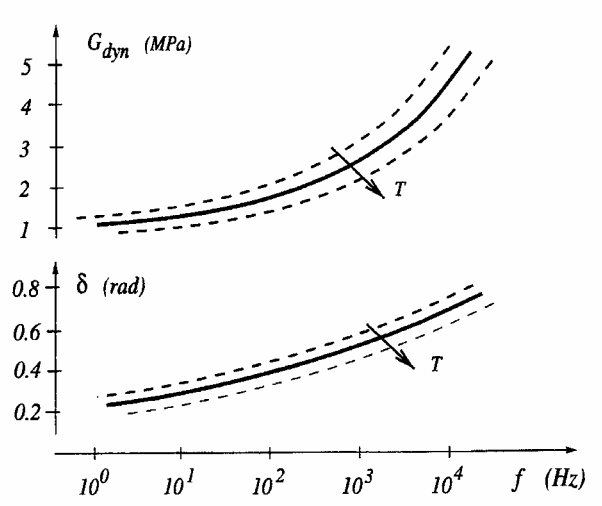

Figure 2.2. The frequency dependency of the dynamic modulus and the phase shift. (Source: Austrell [3]).

The mechanical properties of rubber are controlled by the amount carbon black mixed in the material. A higher amount of carbon black unfortunately leads to a phenomenon called Mullins´ Effect [6]. The phenomenon can be described as decreasing stiffness with strain, sometimes identified as damage. That means, the first time a material is stretched to a certain level the stress will be higher than the next time the material is stretched to the same level. The reason is that the cross-links between the molecular chain break down. If the material is allowed to rest there will, however, be some recovery.

3 Definitions and notations

The definitions and notations below are a brief summary of the designation used in the continuum mechanics to describe large deformations. The expressions are, if not stated otherwise, taken from Lundgren [11]

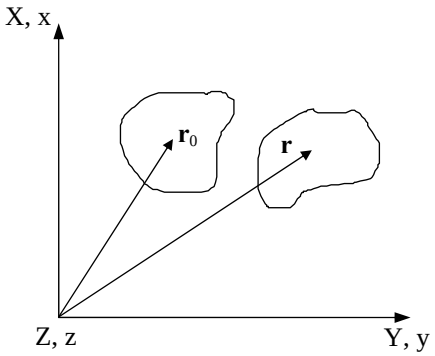

Figure 3.1. The reference and deformed configuration.

The capital letters and $\mathbf{r}_0$ denote the reference configuration while the lower-case letters and $\mathbf{r}$ denote the deformed state. $\mathbf{r}_0$ and $\mathbf{r}$ are vectors to a arbitrary point in the same body (see figure 3.1). $\mathbf{F}$ is the deformation gradient and is defined as follow

$$\mathbf{F} = \begin{bmatrix} \frac{\partial x}{\partial X} & \frac{\partial x}{\partial Y} & \frac{\partial x}{\partial Z} \\ \frac{\partial y}{\partial X} & \frac{\partial y}{\partial Y} & \frac{\partial y}{\partial Z} \\ \frac{\partial z}{\partial X} & \frac{\partial z}{\partial Y} & \frac{\partial z}{\partial Z} \end{bmatrix} = \begin{bmatrix} \frac{\partial \mathbf{r}}{\partial X} & \frac{\partial \mathbf{r}}{\partial Y} & \frac{\partial \mathbf{r}}{\partial Z} \end{bmatrix} \tag{3.1}$$

A conversion between $\mathbf{r}$ and $\mathbf{r}_0$ can now easily be made

$$d\mathbf{r} = \mathbf{F} d\mathbf{r}_0 \tag{3.2}$$

As an example a uniaxial strain deformation field can look like this

$$\begin{aligned} x &= X + kX \\ y &= Y \\ z &= Z \end{aligned} \tag{3.3}$$

This will give the following deformation gradient

$$\mathbf{F} = \begin{bmatrix} 1+k & 0 & 0 \\ 0 & 1 & 0 \\ 0 & 0 & 1 \end{bmatrix} \tag{3.4}$$

The deformation gradient **F** can then be used to form the left and right Cauchy-Greens deformation tensor

$$\mathbf{B} = \mathbf{F}\mathbf{F}^{\mathbf{T}} \quad \text{left Cauchy-Greens deformation tensor} \tag{3.5}$$

$$\mathbf{C} = \mathbf{F}^{\mathbf{T}}\mathbf{F} \quad \text{right Cauchy-Greens deformation tensor} \tag{3.6}$$

The Lagrangian strain tensor can now be defined

$$\mathbf{E} = \frac{1}{2}\left(\mathbf{C} - \mathbf{I}\right) \tag{3.7}$$

A measure of deformation is the stretch

$$\lambda = \frac{ds}{dS} \tag{3.8}$$

where ds is the length of the arbitrary vector $d\boldsymbol{r}$, while dS is the length of $d\boldsymbol{r}_0$.

The principal stretches λ_i. can be calculated as the eigenvalue to the right Cauchy-Greens deformation tensor **C**. The principal stretches can be used to calculate the strain invariants I_i

$$\begin{aligned} I_1 &= \lambda_1^2 + \lambda_2^2 + \lambda_3^2 \\ I_2 &= \lambda_1^2\lambda_2^2 + \lambda_1^2\lambda_3^2 + \lambda_2^2\lambda_3^2 \\ I_3 &= \lambda_1^2\lambda_2^2\lambda_3^2 \end{aligned} \tag{3.9}$$

An invariant that also often is used is the volume relation J

$$J = \lambda_1\lambda_2\lambda_3 = \det \mathbf{F} \tag{3.10}$$

There are several different stress tensors. The stress tensor, which represents the “true” stress, is called Cauchy stress tensor $\boldsymbol{\sigma}$. The stress definitions are taken from Ristinmaa [17].

$$\mathbf{t} = \frac{d\mathbf{P}}{da} \Rightarrow \mathbf{t}_i = \begin{bmatrix} \sigma_{i1} \\ \sigma_{i2} \\ \sigma_{i3} \end{bmatrix} \quad \text{where } \mathbf{P} \text{ is the force acting on the area } a \tag{3.11}$$

$$\boldsymbol{\sigma} = \begin{bmatrix} \mathbf{t}_1^T \\ \mathbf{t}_2^T \\ \mathbf{t}_3^T \end{bmatrix} \tag{3.12}$$

The first Piola-Kirchhoff stress tensor is defined as follow

$$\mathbf{P} = J\sigma\left(\mathbf{F}^{-1}\right)^T \tag{3.13}$$

The second Piola-Kirchhoff stress tensor

$$\mathbf{S} = J\mathbf{F}^{-1}\sigma\left(\mathbf{F}^{-1}\right)^{T} \tag{3.14}$$

Finally, the Kirchhoff stress tensor is defined as

$$\boldsymbol{\tau} = J\sigma \tag{3.15}$$

For more detailed derivations it is referred to Lundgren [11], Ristinmaa [17] or Ogden [15].

4 Description of constitutive models for rubber

The characteristic of a material is described by a constitutive model. It is a mathematical relation between the stress and the strain. The stress is in some material dependent on more than just the strain, it can for example be factors like strain rate, magnitude of strain, temperature, plasticity and strain amplitude and frequency in a case of cyclic loading. Rubber is a material which is dependent on most of the mentioned factors. There are a few different kinds of constitutive models which can be used to model rubber. The ones that will be treated here are viscoelastic, hyperelastic and a combination of them visco- hyperelastic models. These models describe different kinds of material properties, the load type decides which is most appropriate.

4.1 Hyperelastic material models

4.1.1 Strain energy

Hyperelastic constitutive models describe the elastic property of a material from the strain energy. The strain energy is a potential energy function, which means that normal potential theory is valid [15]. A potential energy function is independent of the integration path, the strain energy is thereby just dependent on the current strain. The strain energy is defined according to the following expression [17].

$$W\left(E_{ij}\right)=\int_0^{E_{ij}} S_{ij}\left(\tilde{E}_{kl}\right)d\tilde{E}_{ij} \tag{4.1}$$

where

W is the strain energy
E_{ij} is the Lagrangian strain tensor
S_{ij} is the second Piola-Kirchoffs stress tensor

In the one-dimensional case the strain energy can be described as the area below the stress- strain curve. Figure 4.1 gives an example.

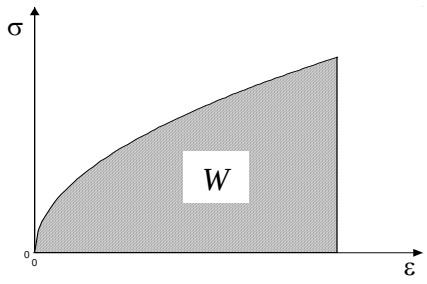

Figure 4.1. Strain energy in a one-dimensional case

If W is differentiated with respect to **E** and the derivative is worked out using (4.1), the following expression will be obtained

$$dW = \frac{\partial W}{\partial E_{ij}} dE_{ij} \quad \text{and} \quad dW = S_{ij} dE_{ij} \tag{4.2),(4.3}$$

The expression above will give the second Piola-Kirchoff stress tensor as a function of the strain energy

$$S_{ij} = \frac{\partial W}{\partial E_{ij}} \tag{4.4}$$

The second Piola-Kirchoff stress tensor, S_{ij}, can only be seen as a fictitious stress. To convert the strain energy to yield σ_{ij} and to be dependent on the strain invariants instead, the theory of conjugated tensors can be used [14]. S_{ij} is conjugated to $\frac{\partial E_{ij}}{\partial t}$ and correspond to the reference configuration, while the nominal stress tensor equal to $J\mathbf{F}^{-1}\boldsymbol{\sigma}$ corresponding to the deformed configuration is conjugated to $\dot{\mathbf{F}}$. The strain energy can thereby also be expressed as a function dependent of the left Cauchy-Green deformation tensor **B**, which for an isotropic material means that the dependency is reduced to the principal stretch λ_i. The strain energy can now be written as

$$W(\mathbf{B}) \Rightarrow W(I_1, I_2, I_3) \quad \text{where } I_i \text{ are the strain invariants}$$

If incompressibility is assumed then $I_3 = 1$. The following expression can be derived [3]

$$\boldsymbol{\sigma} = 2\left(\frac{\partial W}{\partial I_1} + I_1 \frac{\partial W}{\partial I_2}\right)\mathbf{B} - 2\frac{\partial W}{\partial I_2}\mathbf{B}^2 + p\mathbf{I} \tag{4.5}$$

Where $\boldsymbol{\sigma}$ is the Cauchy stress tensor and p is an independent field quantity.

4.1.2 Strain energy functions

The specific form of the strain energy controls the elastic material properties of the model. There are many different kinds of functions. They all try to follow the stress-stretch curve for different loading cases. At the same time they shall be as uncomplicated as possible. The simplest ones are built as a polynomial. They are usually written in the following form [15]

$$W = \sum_{i,j,k=0}^{\infty} C_{ijk}(I_1 - 3)^i (I_2 - 3)^j (I_3 - 1)^k \tag{4.6}$$

In the case of incompressibility (4.6) is reduced to

$$W = \sum_{i,j=0}^{\infty} C_{ij}(I_1 - 3)^i (I_2 - 3)^j \tag{4.7}$$

The threes appearing in the equations the makes strain energy equal to zero in an undeformed state where $\lambda_i = 1$.

Neo-Hook

A couple of famous strain energy function is based on the polynomial approach (4.7). A Neo-Hook function uses only the first term. It will be a polynomial of the first order with one constant to determine [15]

$$W = C_{10}(I_1 - 3) \tag{4.8}$$

The figures below show that the stiffness of the Neo-Hook model increases when it is exposed to compression, while the stiffness decreases in a case of extension. The relation between shear stress and deformation is purely linear. Figure 4.2 and 4.3 illustrate the relations. The model has of course the disadvantage that it does not completely describes the response of the rubber at large deformation. Moreover, it is hard to adjust the model by a laboratory experiment with just one constant.

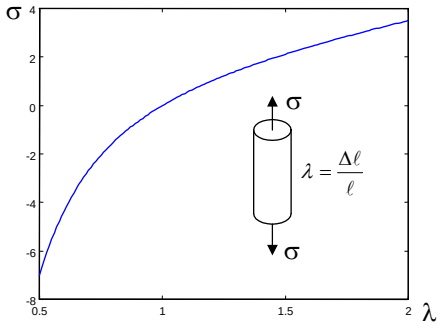

Figure 4.2. Fundamental tension/compression curve for the Neo-Hook model

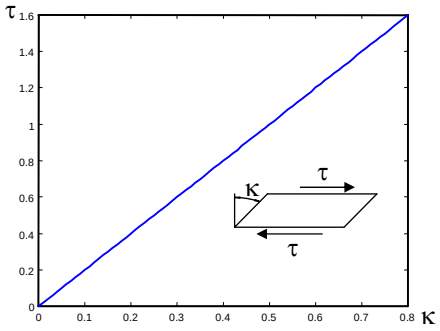

Figure 4.3. Fundamental shear curve for the Neo-Hook model

Mooney-Rivlin

Another model derived from (4.7) is the well-known Mooney-Rivlin function. It is gained if two terms is included [15]

$$W = C_{10}(I_1 - 3) + C_{01}(I_2 - 3) \tag{4.9}$$

This strain energy function shows similar characteristics as the Neo-Hooke model. The main difference is that there are two parameters to determine. The possibility to adjust the model to experimental data will be better.

Multiparameter polynomial functions

The ability to adjust the strain energy function to a stress-stretch curve will increase with more parameters and a higher order of the polynomial. An example of a third degree polynomial with only three constants is the Yeoh model [18]. It contains only three terms dependent on the first strain invariant I_1, i.e.

$$W = C_{10}(I_1 - 3) + C_{20}(I_1 - 3)^2 + C_{30}(I_1 - 3)^3 \tag{4.10}$$

The constants can in an approximate way be obtained from the initial shear modulus. The approximate relations are as follow

$$C_{10} = \frac{G}{2}$$
$$C_{20} = -\frac{G}{20} \tag{4.11}$$
$$C_{30} = \frac{G}{200}$$

These multiparameter functions are much better to reflect a stress-stretch curve from a laboratory test. However, the work needed to determine the constants grows with the number of terms. The rest of the multiparameter functions look like the Yeoh model, the only difference is different sets of constants and therefore they will not be treated any further. An example of an uniaxail and a shear curve is shown in the figures below.

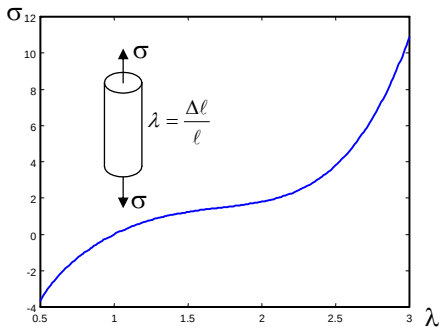

Figure 4.4. Fundamental tension/compression curve for Yeoh model

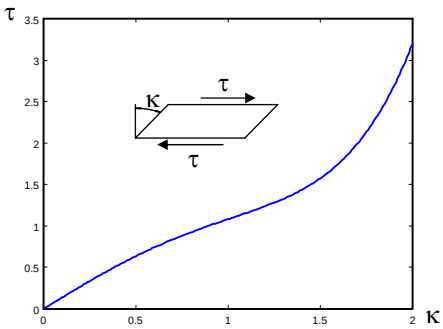

Figure 4.5. Fundamental shear curve for Yeoh model

Ogden model

Ogden [15] has developed a model, which also has its roots in the polynomial (4.7). The differences are that Ogden uses principal stretches λ_i instead of strain invariants I_i. In addition to the integer exponent in the ordinary polynomial Ogden uses real numbers. The benefit of this method is better adjustment possibilities to experimental curves.

$$W(\lambda_1, \lambda_2, \lambda_3) = \sum_{p=1}^{N} \frac{\mu_p}{\alpha_p} \left(\lambda_1^{\alpha_p} + \lambda_2^{\alpha_p} + \lambda_3^{\alpha_p} - 3 \right) \tag{4.12}$$

When the stress is to be calculated the derivative of W with respect to I_i must be converted to derivative with respect to λ_i this can be done using the chain rule. The disadvantages of this function is that it is complicated to obtain the material constants μ_p and α_p. An iterative method must be used instead of a simple least squares method.

Arruda & Boyce model
Arruda & Boyce [2] have in this model assumed that an element consist of eight chains. These link the corner of the cube to the centre. The chains decides the characteristic of the model. Factors, which affect the behaviour are the length of the chain and the number of cross-links between them. In [2] it was conducted that the strain energy can be written as

$$W = nk\Theta\left[\frac{1}{2}(I_1 - 3) + \frac{1}{20N}\left(I_1^2 - 9\right) + \frac{11}{1050N^2}\left(I_1^3 - 27\right)\right] + \\ + nk\Theta\left[\frac{19}{7000N^3}\left(I_1^4 - 81\right) + \frac{519}{673750N^4}\left(I_1^5 - 243\right)\right] \tag{4.13}$$

The advantage of the model is that there are only two parameters to determine, despite that, the model is easy to adjust to a stress-stretch curve, according to Arruda & Boyce. The constant N is the amount of cross-links between the chains. The factor $nk\Theta$ can be seen as one constant but n and Θ can be seen as a measure of the chain density and a temperature factor respectively. $nk\Theta$ is dependent on the initial shear modulus while N controls when the shear modulus shall rise after the decrease.

Strain energy function of compressible materials
The strain energy functions above are derived with the assumption of incompressible material. The explicit code in LS-DYNA can, unfortunately, not handle complete incompressibility, the material models must of that reason be modified. The presented hyperelastic functions can also be used for compressible material if the deformation is divided into one isochoric and one dilatational part. The dilatational part is a purely hydrostatic part. In incompressibility, the relative volume change J is equal to 1 i.e.

$$\lambda_1\lambda_2\lambda_3 = 1 \tag{4.14}$$

For the compressible case the relative volume change J is equal to $\lambda_1\lambda_2\lambda_3$. To be able to use the earlier functions without any changes the principal stretches is modified [15]

$$\lambda_i^* = J^{-\frac{1}{3}}\lambda_i \tag{4.15}$$

which gives

$$\lambda_1^*\lambda_2^*\lambda_3^* = 1 \tag{4.16}$$

the invariants will in a corresponding way be defined as

$$I_1^* = I_1 J^{-\frac{2}{3}} = I_1 I_3^{-\frac{1}{3}} \\ I_2^* = I_2 J^{-\frac{4}{3}} = I_2 I_3^{-\frac{2}{3}} \\ I_3^* = 1 \tag{4.17}$$

In the same way a deformation gradient related to the isochoric deformation can be defined as $\mathbf{F}^* = \mathbf{F}J^{-1/3}$.

The remaining part is to add the hydrostatic part to the strain energy. A simple form of a hydrostatic term can be expressed by the following [8]

$$W_H(J) = \frac{K}{2}(J-1)^2 \tag{4.18}$$

Where K is the bulk modulus. The hydrostatic stress is equal to

$$p = \frac{\partial W^*}{\partial J} \qquad W^* \text{ is the modified strain energy calculated of } I_i^* \tag{4.19}$$

4.2 Viscoelastic material models

Hyperelastic material models only describe the purely elastic properties of a material. These models are thereby most suited for static calculations. In dynamic applications phenomenon such as damping and hysteresis must be included in the simulation. Viscoelastic models are based on rate dependent linear dampers and linear elastic springs, these elements in different combinations form a rheological model. The most common model describing rubber, is the Zener model [3]. It consists of one elastic spring connected in parallel with a Maxwell element. See figure 6

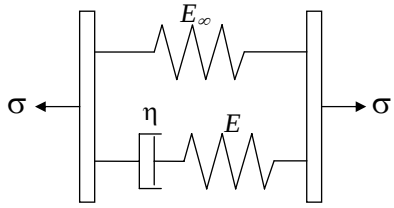

Figure 4.6. The Zener model. η denotes a rate dependent damper and E an elastic element

For a special strain history the stress in a one-dimensional loading case can be calculated as the sum of all stress changes up to a time t_2. This expresses an integral [3]

$$\sigma(t_2) = \int_{-\infty}^{t_2} E_R(t_2 - t)\frac{d\varepsilon}{dt}dt \tag{4.20}$$

where E_R is the relaxation modulus, i.e. stiffness dependent on time. See figure 4.7.

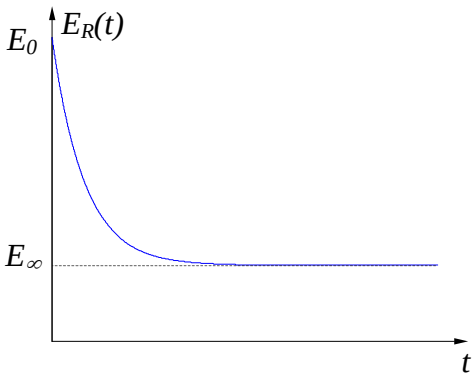

Figure 4.7. Relaxation modulus as a function of time.

The expression for the relaxation modulus can be derived as

$$E_R(t) = E_\infty + (E_0 - E_\infty)e^{-t/t_r} \tag{4.21}$$

where t_r is the relaxation time, which influence the shape of the curve.

A more general form of the viscous model can be done if several different Maxwell elements are included in the model. This results in more parameters to determine and an increased possibility to fit the model to experimental data. The relaxation modulus can be expressed by Prony series [3]

$$E_R(t) = E_\infty + \sum_{j=1}^{n} E_j e^{-t/t_{rj}} \tag{4.22}$$

In the three-dimensional case equation (4.20) can according to Christensen [4] be expressed as

$$\boldsymbol{\sigma} = -p\mathbf{I} + \mathbf{B}\left[g_0\mathbf{I} + \int_0^t g(t-\tau)\frac{\partial \mathbf{E}(\tau)}{\partial \tau} d\tau \right] \tag{4.23}$$

where g_0 corresponds to E_0, while g corresponds to $\sum_{j=1}^{n} E_j e^{-t/t_{rj}}$

Hysteresis is the energy that is lost during one cycle when a rubber element is subjected to harmonical loading. The energy lost can be described by the area enclosed by a stress-stretch curve. The hysteresis phenomena can be mapped in a shear case if a harmonic strain is assumed

$$\varepsilon(t) = \mathrm{Re}\left(\varepsilon_0 e^{i\omega t}\right) \quad \Rightarrow \quad \mathbf{F} = \begin{bmatrix} 1 & \varepsilon(t) & 0 \\ 0 & 1 & 0 \\ 0 & 0 & 1 \end{bmatrix} \tag{4.24}$$

This example follows Christensen [4]. If (4.24) is used in (4.23) and the variable change $s = t-\tau$ is made. The following expression is obtained.

$$\begin{aligned} \sigma(t) &= g_0\varepsilon_0 \sin(\omega t) + \frac{\omega\varepsilon_0}{2}\int_0^\infty g(s)\sin(\omega s)\,ds \cdot \cos(\omega t) \\ &- \frac{\omega\varepsilon_0}{2}\int_0^\infty g(s)\cos(\omega s)\,ds \cdot \sin(\omega t) \\ &+ \omega\varepsilon_0^3\int_0^\infty g(s)\sin(2\omega s)\,ds \cdot \cos(3\omega t) \\ &- +\omega\varepsilon_0^3\int_0^\infty g(s)\cos(2\omega s)\,ds \cdot \sin(3\omega t) \end{aligned} \tag{4.25}$$

The hysteresis curve is plotted in figure 4.8. The three, different, curves represent different frequencies.

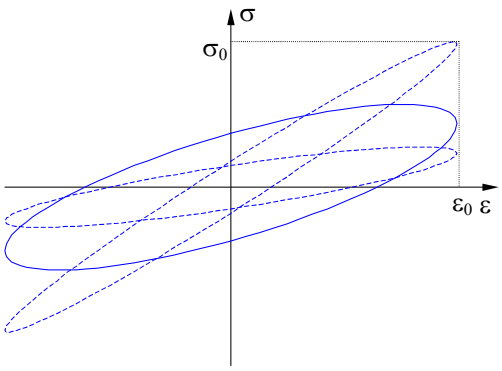

Figure 4.8. Hysteresis curve, The three curves are made for different frequencies. The most horizontal has the lowest frequency.

In figure 4.8, it is clearly seen that the hysteresis change with the frequency. The frequency for the middle curve has the largest enclosed area and consequently the largest damping in a free oscillating case. It can also be seen that the dynamic modulus is dependent on the frequency, where the dynamic modulus is defined as

$$E_{dyn} = \frac{\sigma_0}{\varepsilon_0} \tag{4.26}$$

The dynamic modulus can be derived by using a complex harmonic strain like the one in equation (4.24). The complex stress can then be expressed as [3]

$$\sigma^* = E_\infty e^* + E\frac{i\omega t_r}{1+i\omega t_r}e^* \qquad \text{where } e^* = e_0 e^{i\omega t} \tag{4.27}$$

The complex modulus can now be obtained

$$E^* = E_\infty\left(1+\frac{E}{E_\infty}\frac{i\omega t_r}{1+i\omega t_r}\right) \tag{4.28}$$

In a generalised model with an arbitrary number of Maxwell element complex modulus would become

$$E^* = E_\infty + \sum_{j=1}^{n} E_j \frac{i\omega t_{rj}}{1+i\omega t_{rj}} \tag{4.29}$$

The dynamic modulus is equal to the absolute value of E^* and the phase angle, which is the phase shift between the stress and the strain, is the argument of E^*.

$$\begin{aligned} E_{dyn} &= \left|E^*\right| \\ \delta &= \arg\left(E^*\right) \end{aligned} \tag{4.30}$$

The phase shift is strongly connected to the damping. The energy dissipation can be expressed as $U_c = \pi\sigma_0 e_0 \sin\delta$.

Visco- hyperelastic material models

The viscoelasic models are better than the hyperelastic to reflect the dynamic behaviour of rubber, one imperfection is that the elastic behaviour is linear. A solution to that problem is to consider a combination of hyper- and viscoelastic models. The Cauchy stress is given by an expression where the viscoelastic part is added to the hyperelastic stress and the hydrostatic pressure [8]

$$\sigma = \sigma^{e} + \sigma^{ve} + \sigma^{h} \tag{4.27}$$

where $\boldsymbol{\sigma}^{e}$ correspond to the viscoelatic part of equation (4.4) while $\boldsymbol{\sigma}^{h}$ is the hydrostatic pressure. The viscoelastic deviator stress $\boldsymbol{\sigma}^{ve}$ is as follow (cf. equation (4.23)).

$$\sigma^{ve}(t) = \int_0^t g(t-\tau)\frac{\partial \mathbf{E}(\tau)}{\partial \tau} d\tau \tag{4.28}$$

where

$$G(t) = G_0 \sum_{i=1}^{N} g_i e^{-t/t_{ri}} \qquad G_0 \text{ is the initial shear modulus} \tag{4.30}$$

The model can be described as the *Zener model* in figure 4.6 with the difference that the single spring E_∞ is non-linear. Similarly to the viscoelasic material models the visco-hyperelastic models show a hysteresis curve when they are cyclically loaded. In figure 4.8, it is clearly seen how the non-linearity in the Neo-Hook model has affected the curve.

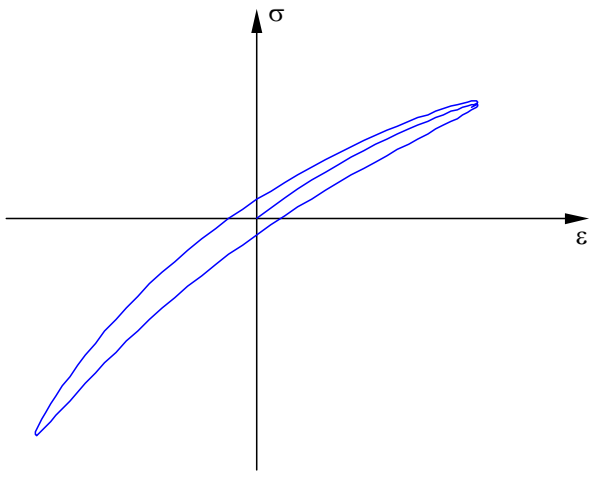

Figure 4.9. Hysteresis curve for a uniaxial loaded Neo-Hook model. The non-linearity is clearly seen compared to a linear case. See figure 4.5.

These models are, as the hyperelastic models applicable to compressible materials. The isocoric part of the principal stretch is separated from the dilatational part and a hydro-static work term is added. See equation (4.14-19).

5 Test to determine material parameters

The material models are mathematical expressions, which try to mimic the properties of the rubber as accurately as possible. To determine the parameters in the models, it is necessary to have experimental data of the rubber material. In this chapter, suitable measuring methods will be presented. The test results will, in the next chapter be used to calibrate the material model and to determine the parameters with a least squares method. Unfortunately, it was not possibility to manufacture test specimens. This mean that all tests have to be done on the damper itself, which can affect the precision of the test results.

5.1 Experimental methods

LS-DYNA has just one type of material model useful for large deformations of rubber material in dynamic applications, namely the visco- hyperelastic model. More complicated models like visco- hyperelasticity combined with viscoplasticity must be implemented by the user himself. As the time scope of this thesis does not allow this, this task must unfortunately be left as a suggestion for further studies. There are three different possibilities to model visco- hyperelasticity. Based on three different kinds of hyperelasticity namely the Ogden model, the polynomial model and the Arruda & Boyce model. The viscoelastic behaviour is implemented as outlined by Christensen [4], cf. also section 4.2. The hyperelastic part can, also, be separated from the rest and be treated alone.

5.1.1 Method to determine hyperelastic constants

The hyperelastic behaviour can be measured if the strain rate in the shear test is kept low enough during the deformation. The three hyperelastic strain energy functions describe the same behaviour of the rubber, it is therefore convenient to find a measuring method suitable for all functions. A shear test will give different stretches but the strain invariants I_1 and I_2 will be equal. This test is sufficient for the Ogden model (dependent of the stretches) and the Arruda and Boyce model (dependent of just the first strain invariant I_1). It is, however, not sufficient for an arbitrary polynomial function dependent of both I_1 and I_2. The Yeoh strain energy function is, however, just dependent of the first strain invariant and it is according to Yeoh [18] and Austrell [3] well suited for modelling the hyperelastic behaviour of carbon black filled rubber. The Ogden model will not be treated any further. It is deemed too complicated to determine the parameters and it is according to the *Abaqus User's Manual* [7] hard to calibrate the model with just one deformation mode.

Shear test can be divided into pure shear and simple shear. A pure shear test is usually performed on a thin rectangular rubber strip attached to metal strips. The height of the rubber shall be small compared to the length. The shear deformation is measured with stretch. The deformation field, which leads to deformation gradient **F** can be expressed as follow (incompressibility is assumed)

$$\begin{aligned} x &= \lambda X \\ y &= \frac{1}{\lambda} Y \\ z &= Z \end{aligned} \qquad \Rightarrow \qquad \mathbf{F} = \begin{bmatrix} \lambda & 0 & 0 \\ 0 & \frac{1}{\lambda} & 0 \\ 0 & 0 & 1 \end{bmatrix} \tag{5.1}$$

The strain invariants I_1 and I_2, equation (3.9), can now be calculated out of the eigenvalues of the right Cauchy-Greens deformation tensor **C**, equation (3.6).

$$I_{1,2} = \lambda^2 + 1 + \frac{1}{\lambda^2} \tag{5.2}$$

An easier shear test, more adapted for ordinary uniaxial testing machines is the simple shear test. There are at least two different test objects, for example the quadruple shear test and the double shear test. The quadruple shear test specimen consist of four rubber pieces placed as shown in figure 5.1.

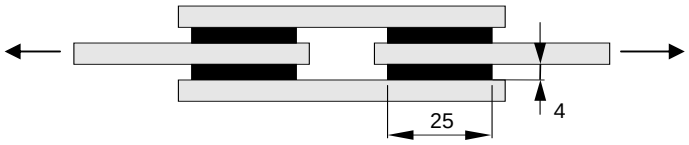

Figure 5.1. Quadruple shear specimen

Both the force and the displacement are doubled. The shear deformation is measured with the shear strain κ. The height of the rubber is not held constant in the quadruple shear test. A specimen easier to manufacture is the double shear specimen, it consists of two rubber pieces mounted in a fixture so the height of the rubber is constant. (See figure 5.2)

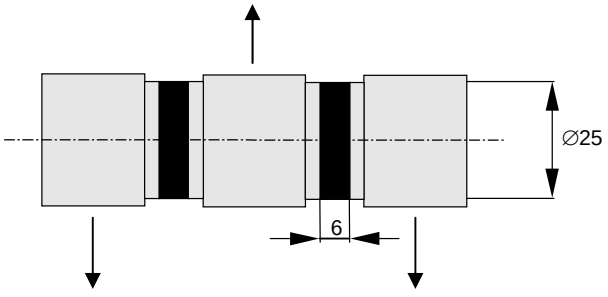

Figure 5.2. Double shear specimen

This is the method, which is most applicable to our rubber damper. The relation between shear stress and strain can, in the simple shear case, be derived from the deformation field, which yields the deformation gradient ***F***.

$$\begin{aligned} x &= X + \kappa Z \\ y &= Y \\ z &= Z \end{aligned} \qquad \Rightarrow \qquad \mathbf{F} = \begin{bmatrix} 1 & 0 & \kappa \\ 0 & 1 & 0 \\ 0 & 0 & 1 \end{bmatrix} \tag{5.3}$$

where κ is the shear strain defined as $\kappa = \frac{\delta}{h}$, δ is the displacement and *h* the height. Equation (5.3) leads to the expression of the invariants.

$$I_1 = I_2 = 3 + \kappa^2 \tag{5.4}$$

Note that $J = 1$ for this loading situation, i.e. $I_1^* = I_1$ and $I_2^* = I_2$, cf. equation (4.17). Equation (5.4) put in (4.6) yields

$$\tau = 2\left(\frac{\partial W}{\partial I_1} + \frac{\partial W}{\partial I_2}\right)\kappa \tag{5.5}$$

In the stress calculation connected with the calibration of the material models, incompressibility will be assumed.

5.1.2 Method to determine viscoelastic constants

The dynamic behaviour of the rubber is simulated by the viscoelastic models. Both damping and stiffness are dependent on the frequency and the amplitude. The viscoelastic model handle the strain rate dependent energy dissipation, but to be able to completely model the frequency and amplitude dependency is it also necessary to include an energy dissipating term, which is not dependent on the strain rate. This term is on the other hand not implemented in LS-DYNA.

The test can be performed with the same double shear test specimen as in the determination of the hyperelastic parameters. To determine the parameters several different stress-strain curves is measured. Each curve comes from a cyclic deformation with a specific amplitude and frequency. The model can then be fitted to the curves and the dynamic modulus.

5.2 Experimental Tests

The material tests are made at Trelleborg Automotive with a MTS 810 dynamic testing machine. It is a hydraulic machine with capacity of 100 kN static loading. A test rig is built where the rubber dampers are exposed to simple shear. The rig consists of a bridle, which keep the outer distance of the damper constant and a plate between the damper. See figure 5.3.

Figure 5.3. Test rig for the dampers.

The rig is attached to the test machine by a screw joint.

5.2.1 Conditioning

A rubber material become softer at repeated deformation, i.e. if a material is deformed to a certain strain the material will be softer the next time it is deformed up to that strain. This is designated as Mullin´s effect [6]. If the test shall be done on a conditioned test specimen or on an unconditioned one is controlled by the application of the rubber element. A rubber element which is just statically loaded is better evaluated with an unconditioned test specimen. In this case is it realistic just to perform conditioned tests, because it would otherwise be necessary to change rubber dampers for every test. The results would also be less accurate in that case because of dispersion of the rubber quality.

There are a lot of different methods of conditioning. The easiest way is to apply a cyclic loading to the specimen, with an amplitude which is as large as the largest in the test, until the stress-strain curve is stabilised. There are of course better methods but they are more complicated and it is hardly meaningful to use them with out any closer examination.

5.2.2 Results of the hyperelastic test

To determine the non-linear elastic behaviour the deformation rate must be so slow that the viscoelastic behaviour can be neglected. Yeoh [18] recommend a stretch rate of maximum 50 % min^{-1}, which is equal to a shear strain rate of 0.83 min^{-1}, according to a combination of equation (5.2) and (5.4). However Austrell [3] have found that a stretch rate lower than 3% min^{-1}, equal to a shear strain rate of 0.06 min^{-1}, is needed to eliminate the viscoelastic behaviour.

The test specimen in form of rubber dampers has an allowed shear strain, κ, of 1.3. To cover the whole region, the dampers were deformed to a shear strain of about 1.5. Due to lack of time at Trelleborg Automotive the strain rate was set to 0.18 min^{-1}. It appears that the stress in loading was higher than the one in unloading. This is caused by the strain rate independent energy dissipation and it can also be an effect of a not completely eliminated viscoelactisity, due to too high strain rate. The curve can be seen in figure 5.4.

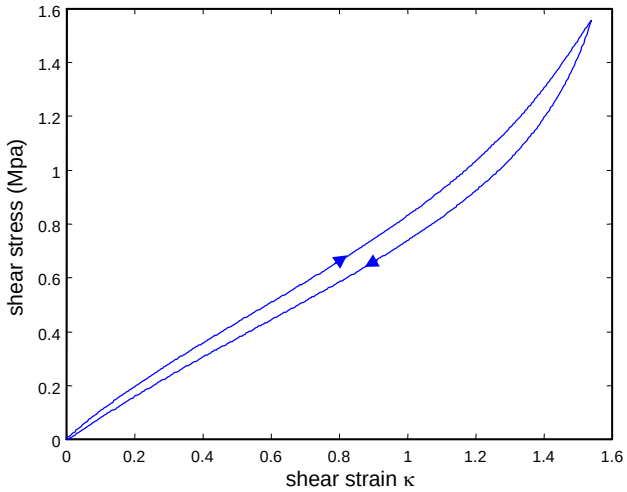

Figure 5.4. Stress- strain curve, simple shear

The shear stress is calculated as the engineer stress $\tau = F / A$, where A is the original area.

5.2.3 Results of the viscoelastic tests

The viscoelastic behaviour, which include rate dependent stress and damping, can be evaluated if several cyclic stress-strain curves is made for different amplitude and frequencies. The tested amplitude and frequency shall correspond to the ones, which can be achieved in a shock test with drop table. It is not likely to get a frequency less then 10 Hz of the oscillations after the shock. It is however possible to obtain larger amplitudes then the test machine can make. Frequencies were of that reason tested from 1 Hz to 20 Hz with shear strain amplitudes from 0.015 up to the limit of the test machine. The combinations can be seen in figure 5.5.

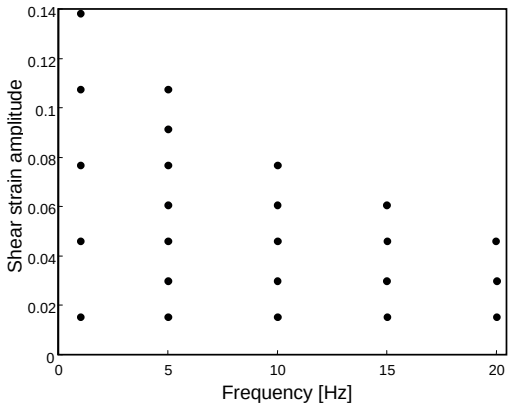

Figure 5.5. Tested combinations of frequencies and amplitudes

The higher frequencies were tested at twice as many amplitudes as planed, to avoid overloading the testing machine when the amplitude was increased. Unfortunately, we missed to go back and fill in the missing amplitudes at the lowest frequency. The lowest frequency was tested with the largest strain amplitude first in order to see the deformation softening. It was however impossible to see any major difference. The tests were made with a constant prestrain of 0.15. The prestrain was adjusted to be a little bit larger than the largest amplitude. The constant prestrain is necessary if the different frequency and amplitude combination shall be compared with each other. It is also desirable to be able to extrapolate the missing part of the frequency - amplitude plane. Unfortunately, the curves in the higher frequencies were not reliable, the registered forces were to small when the strain increased and to big when it decreased. The reason is probably that the load cell could not make a correct registration at that high rates and the inertia of the rig and other masses attached to the load cell could reduce the force in the load cell. This phenomenon is clearly seen in a graph over the dynamic modulus. See figure 5.6. The results is also presented in numbers in appendix A. The dynamic modulus is calculated as

$$G_{dyn} = \frac{2\sigma_0}{2\varepsilon_0} \tag{5.8}$$

Where the maximum resp. minimum stress and strain is manuelly read from the curves.

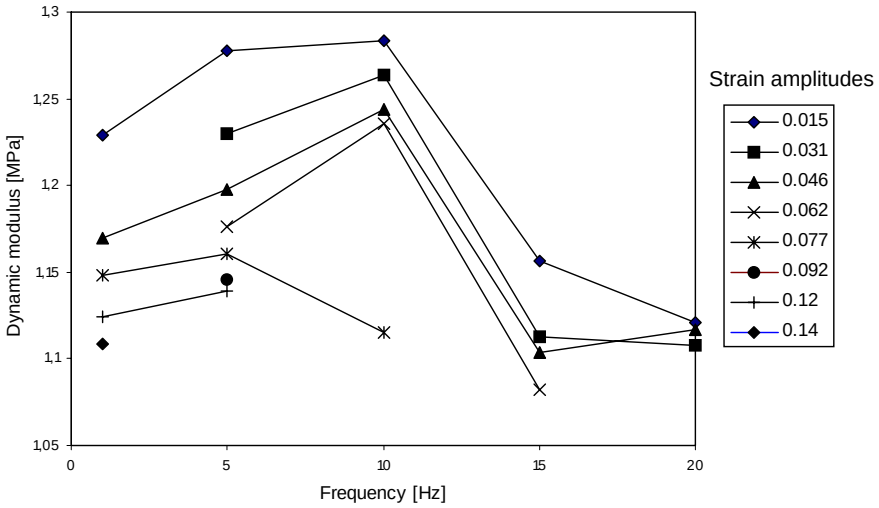

Figure 5.6. Dynamic modulus dependent of the frequency and the amplitude.

The result in figure 5.6 is impossible to use to determine the viscoelastic behaviour. One alternative is to continue the work with theoretical values, there is however a possibility that an estimation of the missing points could be done. Hopefully, such a estimation given in figure 5.7 are better than completely theoretical values. The estimation is based on the values in the lower frequency and figure 2.2 (showing the frequency dependency of natural rubber).

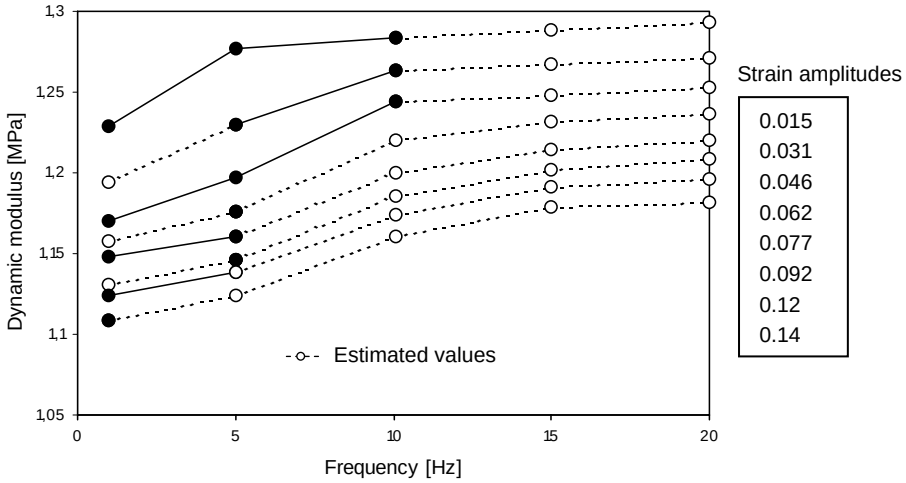

Figure 5.7. Estimated dynamic modulus dependent of the frequency and the amplitude.

The phase shift δ between the force and displacement curve is measured. The resolution on the curves and disturbance made it impossible to find out any major differences between the amplitudes. It can however be seen that the phase shift increase when the frequency gets higher. In the same way as the dynamic modulus are the values at the higher frequencies incorrect especially the ones at 15 Hz. δ is calculated as $\delta = \omega \Delta t$, where Δt is the phase shift in time. The measured values are visualised in figure 5.8.

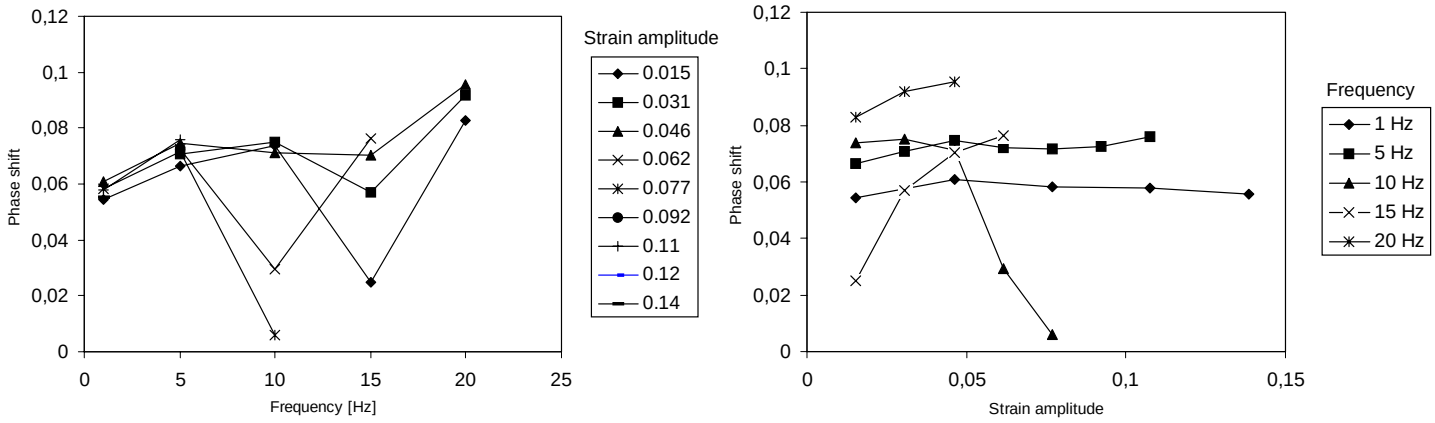

Figure 5.8. The phase shift dependent on the frequency at left and on the strain amplitude at right.

6 Adaptation of material models

6.1 Adaptation of hyperelastic material models

To calibrate the model the stress strain curve, which reflect the elastic behaviour will be considered. As previously discussed in section 5.2.2 it turned out that a too high loading rate was used, i.e. small viscous effects could be detected, therefore an average curve will be used. The average curve is shown in figure 6.1

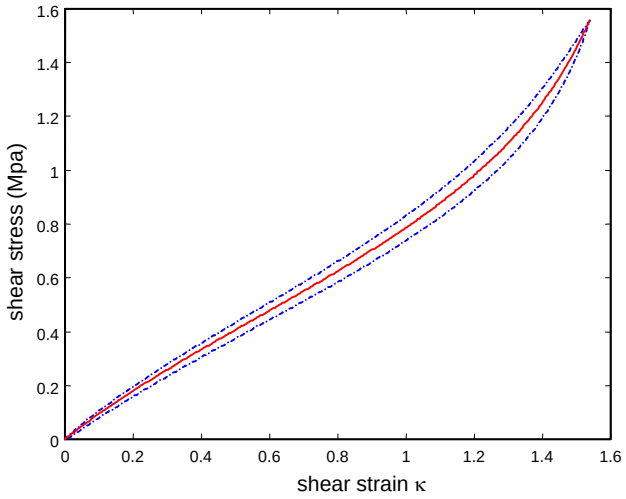

Figure 6.1. Average curve (solid line) of loading and unloading curve (dash-dot line).

The damper is unfortunately not optimum device for use as a shear test specimen, the damper is much weaker compared to values found in the literature of the same rubber quality. The reason is the influence of bending induced by the relative big height compared to the length of the damper. The material parameters will therefore not be accurate if the experimental values are accepted as they are. A solution to the problem is to fit the parameters with help of a FE analysis. Since the load case is purely static, the FE analysis is made with Abaqus ver 5.8 [1].

Finite element model in Abaqus
The geometry is very simple, the damper is modelled as a rectangular parallelepiped with 8 node brick element. The chosen elements are fully integrated hybrid elements, with a large deformation element formulation. Hybrid element is recommended by *Abaqus User's manual* [7] when the material is incompressible or nearly incompressible. To model the damper 15×15×15 elements are used. The nodes in the bottom surface are locked in all direction, while the nodes on the opposite surface are locked in two directions and the third is given a prescribed displacement. See figure 6.2.

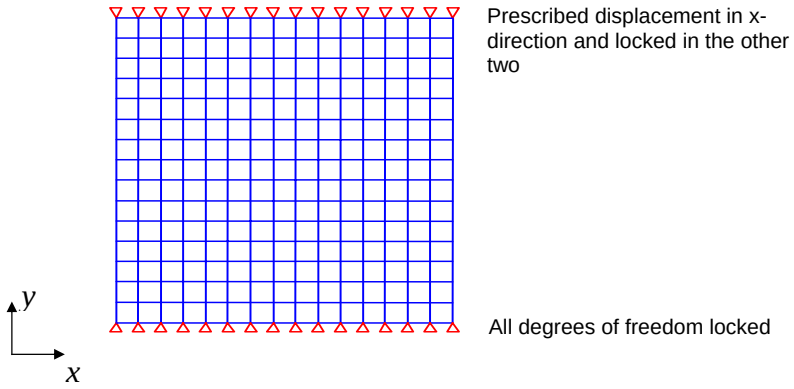

Figure 6.2. Side view of the 3 dimensional mesh. Shear with bending included

The model in figure 6.2 is compared with a model where just the shear stresses are present. The simple shear stress state can be obtained if only one element between the surfaces are used. Otherwise are the two models equal. The mesh and boundary conditions used to obtain the simple shear stress state are shown in figure 6.3

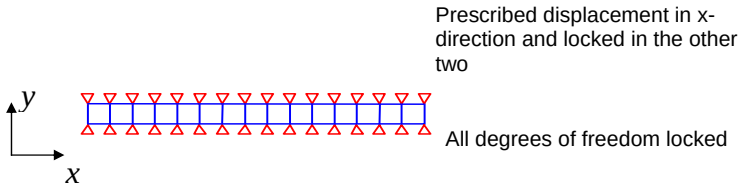

Figure 6.3. Side view of the 3 dimensional mesh. Simple shear.

The shear stress is calculated as the engineers stress, i.e. the sum of the nod force at the constraints divided with the original area. The strain comes from the displacement divided with the original height.

6.1.1 Yeoh model

In the Yeoh model the constants can in an approximately way be obtained from the initial shear modulus. The three constants can however in a more accurate way be determined by a simple least squares method from a stress strain curve.

Recall the Yeoh model

$$W = C_{10}(I_1 - 3) + C_{20}(I_1 - 3)^2 + C_{30}(I_1 - 3)^3 \tag{6.1}$$

The theoretical value of the strain energy in the different experimental data points (i) can be expressed as a linear equation system.

$$W_i^{teor} = \begin{bmatrix} I_{1,i} - 3 & (I_{1,i} - 3)^2 & (I_{1,i} - 3)^3 \end{bmatrix} \cdot \begin{bmatrix} C_{10} \\ C_{20} \\ C_{30} \end{bmatrix} \tag{6.2}$$

The relative residual **e** can be expressed as

$$\mathbf{e} = 1 - \frac{\mathbf{Ac}}{\tau^{\exp}} \tag{6.3}$$

Where $\tau^{teor}=\mathbf{Ac}$ is obtain by using (5.4) and (6.2) in (5.5). To find the minimum of **e** the L_2- norm $\mathbf{e}^T\mathbf{e}$ is used, i.e.

$$\min \|\mathbf{e}\|_2^2 = \min \mathbf{e}^T\mathbf{e} \tag{6.4}$$

Calculating the derivative with respect to C_i and the following linear equation system is obtained

$$\mathbf{A}^T\mathbf{Ac} = \mathbf{A}^T\tau^{\exp} \tag{6.5}$$

Where the solution **c** to the equation system determines the material parameters. Applying least squares method the follow C_{i0} constant were found

C_{10} = 0.4512
C_{20} = -0.0660
C_{30} = 0.0225

The fit between the Yeoh model and the FE analysis of both simple shear and shear with bending can be seen in figure 6.4.

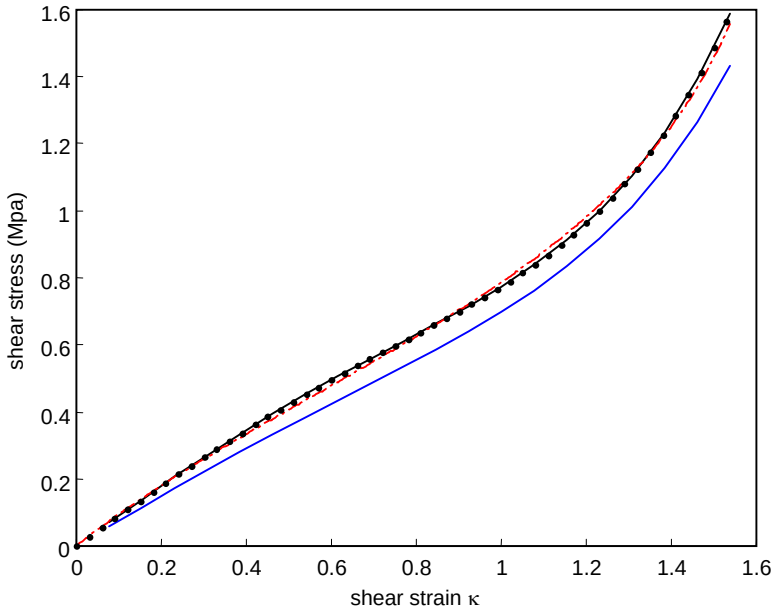

Figure 6.4. Calibration of the Yeoh model to experimental data. The dots are the analytical simple shear model, while the upper solid line is the FE model of simple shear. The lower solid line is the FE model where bending is included. Finally the dash-dotted line is the experimental curve.

A comparison between the shear with bending and without reveals that the maximum error is about 17%. To find better estimates of the material parameters an iterative process is performed. The error, dependent on κ, is added to the experimental data and a new fit is made and continued until a closer agreement between the results obtained from the FE analysis and the experimental data is obtained The following material parameters were obtained from this iterative procedure.

$C_{10} = 0.529$
$C_{20} = -0.0958$
$C_{30} = 0.0293$

The fit between the FE analysis and the experimental data can be seen in figure 6.5.

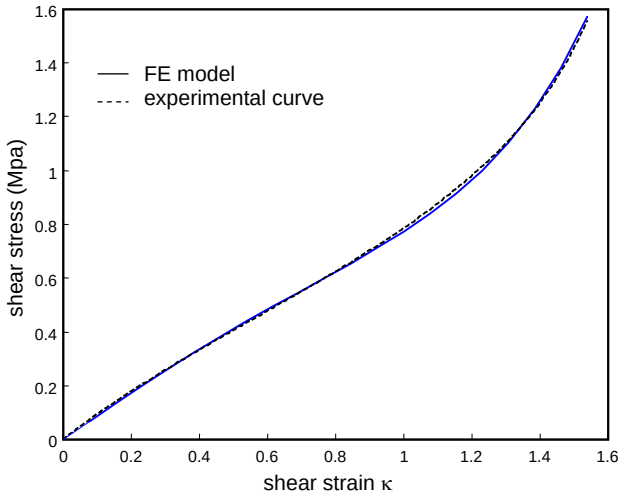

Figure 6.5. Calibration of the Yeoh FE model, to experimental data. Bending is included.

The material parameters can, unfortunately, after this approximation only be seen as an estimation of the parameters obtained from a real simple shear test.

6.1.2 Arruda & Boyce model

The Arruda & Boyce model have also constants related to physical properties. One of the constants controls the initial shear modulus whereas the other one controls the location where a stiffness change in the stress-strain curve takes place.

$$W = nk\Theta\left[\frac{1}{2}(I_1 - 3) + \frac{1}{20N}(I_1^2 - 9) + \frac{11}{1050N^2}(I_1^3 - 27)\right] + \\ + nk\Theta\left[\frac{19}{7000N^3}(I_1^4 - 81) + \frac{519}{673750N^4}(I_1^5 - 243)\right] \tag{6.6}$$

Where $nk\Theta$ controls the initial shear modulus and N controls the up bend. To determine the two constants a non-linear least squares method has to be used. In the optimisation algorithm the residual $e = 1 - \tau^{exp}/\tau^{teor}$ is minimised for all experimental data points. This is done with a Nelder-Mead algorithm, which is a built in function (*fminsearch)* in

Matlab ver. 5.3 [12]. In *fminsearch* a L_2-norm of the residual $\boldsymbol{e}$ is minimised. The used norm is

$$\|\mathbf{e}\|_2^2 = \mathbf{e}^T\mathbf{e} \tag{6.7}$$

The Nelder-Mead algorithm is a slow converging algorithm, there exists much faster algorithms. But the Nelder-Mead has however the advantage that no gradient of the function has to be determined as in the case of a Levenberg-Marquardt method. The theoretical values of shear stress are worked out with equation (5.4), (5.5) and (6.6).

From the minimasation proces the following material parameters were obtained.

N = 3.3605
nkΘ = 0.5853

The fit of the model compared to the experimental points is shown in figure 6.6 The FE analysis on shear with and without bending can also be seen.

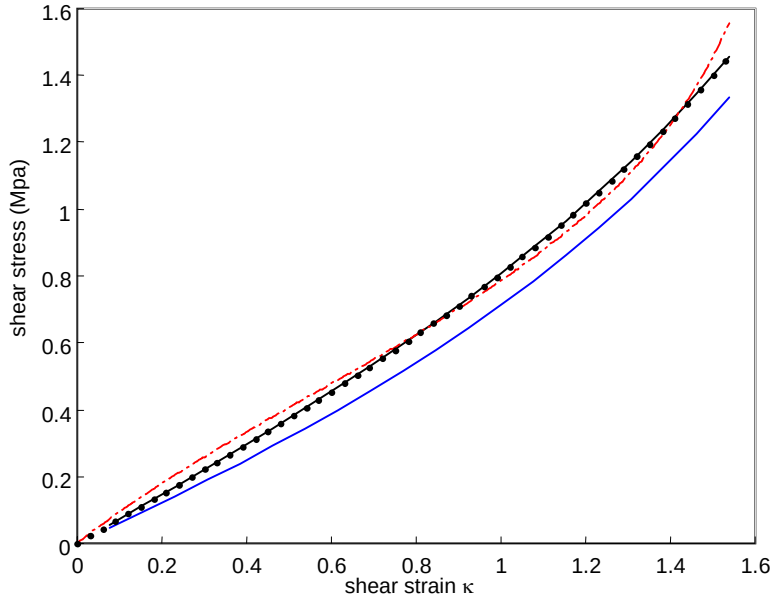

Figure 6.6. Calibration of the Arruda & Boyce model to experimental data. The dots are the analytical simple shear model, while the upper solid line is the FE model of simple shear. The lower solid line is the FE model where bending is included. Finally the dash-dotted line is the experimental curve.

The maximum error between the result obtained in the FE analysis and the experimental data has about the same magnitude as the Yeoh model i.e. about 17%. To obtain a better estimation of the material parameters an iterative process similar to the one used for the Yeoh model is adapted. From this iterative procedure the following parameters were found.

N = 4.09
nkΘ = 0.705

In figure 6.7 it is shown that the shear curve including bending differs slightly from the experimental curve, but as revealed by figure 6.6 and 6.7 the difference in the FE solution is not remarkable.

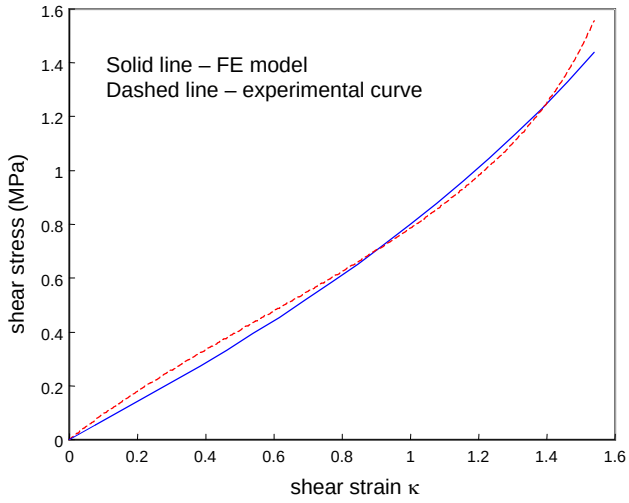

Figure 6.7. Calibration of the Arruda & Boyce FE model to experimental data. Bending is included.

6.1.3 Comparison between FE model and uniaxial tests

In the shock tests only compression and stretch will take place. The response of the material models during stretch and compression is therefore very important. The tension and compression deformation field can be described as

$$\begin{aligned} x &= \lambda X \\ y &= \lambda_{\perp} Y \\ z &= \lambda_{\perp} Z \end{aligned} \qquad \Rightarrow \qquad \mathbf{F} = \begin{bmatrix} \lambda & 0 & 0 \\ 0 & \lambda_{\perp} & 0 \\ 0 & 0 & \lambda_{\perp} \end{bmatrix} \tag{6.8}$$

which reveals that first strain invariant can be written as

$$I_1 = 2\lambda_{\perp} + \lambda \tag{6.9}$$

but due to incompressibility i.e. $\lambda_1\lambda_2\lambda_3 = 1$ it follow that

$$\lambda_{\perp}^2 = \frac{1}{\lambda} \tag{6.10}$$

i.e. the first strain invariant takes the form

$$I_1 = \frac{2}{\lambda} + \lambda^2 \tag{6.11}$$

The FE analysis is done with the same model that was used for shear with bending included. The only difference is the boundary condition. In this case there is a prescribed displacement in y-direction and the other directions are locked see figure 6.2. The results of the simulations are shown in figure 6.8. At large compression the results can be affected by some boundary effects, since those effects near the boundary conditions are not considered in this simple model. The experimental test data are obtained from a report concerning the dampers [9] as well as compressions test made at Kockums laboratory. The used test machine is a Zwick Z250, it is a thread rod machine with a capacity of 250 kN. The damper was loaded until the compression was about 35 mm. The speed was set to 0.09 mm/s that corresponds to a shear strain rate of 0.18 min^{-1}. The

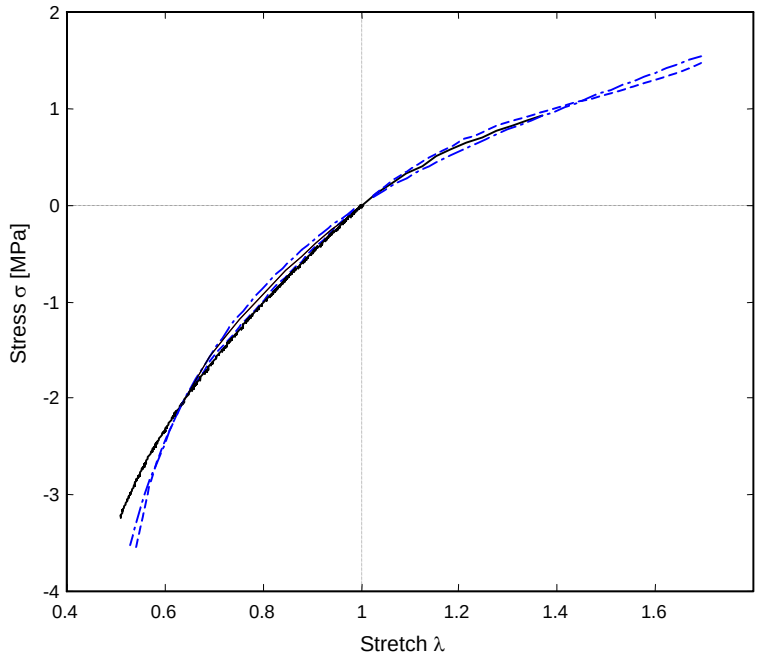

Figure 6.8. Stretch comparison between Abaqus simulation and experimental tests. Solid lines are from the experimental tests. The lower curve is the compression test made at Kockums laboratory. The dashed line is the Yeoh model, while the dashed-dotted is the Arruda & Boyce model.

comparison is made by letting the rate of the first strain invariant be equal in (6.11) and (5.4).

From figure 6.8 it follows the response of material models are in good agreement with the experimental tests at stretches between 0.6 and at least 1.4. Below 0.6 are the models far to stiff. At moderate stretches the Arruda & Boyce model displays a softer response than the Yeoh model. All results from the compression tests are presented in appendix B.

6.2 Adaptation of viscoelastic material models

The viscoelastic part of the model will now be calibrated to the harmonic curves. One way of doing this is to propose a function for the stress strain relation and optimise that to the different curves. That is however a rather complicated process and very time consuming. Fortunately, for moderate prestrain and strain amplitudes the calibration can

be done in a much easier way. The almost linear stress- strain relation makes it possible to assume linear elasticity, which means that the prestrain does not affect the dynamic modulus. The model can of that reason be fitted to the measured dynamic modulus and phase shift by using the complex modulus and its absolute value (dynamic modulus) and argument (phase shift). The complex modulus is given by

$$G^* = G_\infty + \sum_{j=1}^{n} G_j \frac{i\omega t_{rj}}{1 + i\omega t_{rj}} \tag{6.12}$$

There is however a problem with the measured dynamic modulus and phase shifts, the values at higher frequencies are not accurate, cf. the discussion in section 5.2.3. The fit must be done on the estimated values given in figure 5.7, this will of course affect the result, but the alternative would be continued calculations on theoretical values. Another problem is that the bending of the damper makes it considerably weaker than a uniform shear case. To compensate that the dynamic modulus is corrected based on the error obtained in the hyperelastic shear test. In the dynamic modulus calculations the maxima respective the minima of the stress in the cycle are increased with the calculated error from the hyperelastic parameter fit. That makes an increase of the dynamic modulus with 16.5% for a strain amplitude of 0.015 and 12.6% for the strain amplitude of 0.15.

The calibration is done with a non-linear least squares method similar to the one for the Arruda & Boyce model. A suitable number of terms are four i.e. eight parameters. It was not possible to follow both the phase shift and the dynamic modulus with fewer parameters. To obtain the long-term modulus G_∞ the equation (5.5) is used as well as the Yeoh model restricted to small deformations, i.e. $\tau = 2C_{10}\kappa = G_\infty\kappa$, accordingly G_∞ = 1.06 MPa The calibrations are made for both the smallest and the largest amplitude. The calibration for the largest amplitude is the one used for the shock test simulations. The material parameters obtained from the minimisation process are given by

Strain amplitude 0.015

G_1= 0.432 MPa	G_2= 0.230 MPa	G_3 =0.0740 MPa	G_4= 0.0181 MPa
t_{r1} = 1.24 s	t_{r2} = 0.00718 s	t_{r3} =0.0443 s	t_{r4} = 0.00327 s

Strain amplitude 0.14

G_1= 0.487 MPa	G_2= 0.241 MPa	G_3 = 0.123 MPa	G_4= 0.00190 MPa
t_{r1} = 0.00119s	t_{r2} = 0.690 s	t_{r3} = 0.0196 s	t_{r4} = 0.248 s

The fit of the dynamic modulus can be seen in figure 6.9 and of the phase shift in figure 6.10

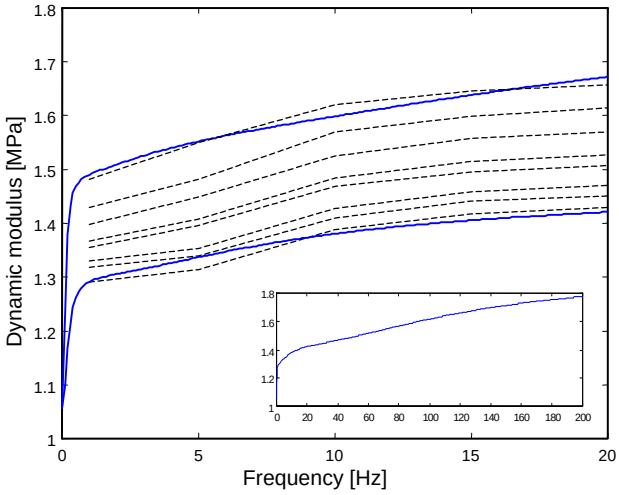

Figure 6.9. Fit of the viscoelastic parameters to the estimated dynamic modulus. The solid lines are the models and the dashed ones are the estimated curves, where the smallest amplitude is the top curve. The behaviour of largest amplitude up to 200 Hz is shown in the small graph.

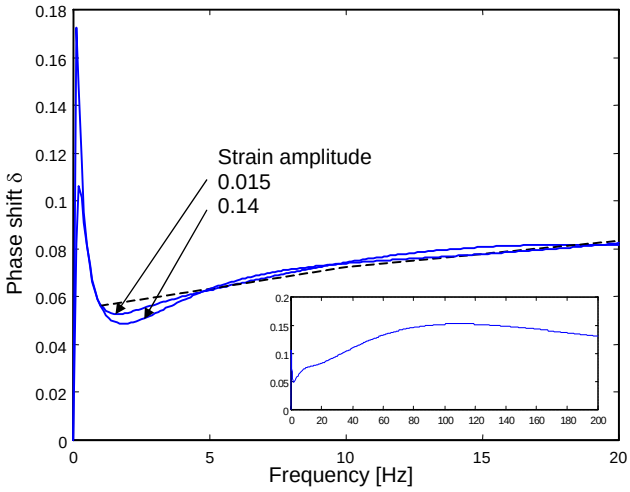

Figure 6.10. Fit of the viscoelastic parameters to the measured phase shift. The dashed line is the measured values. The small graph shows the behaviour of the largest strain amplitude up to 200 Hz.

The peek in the phase shift is a result of the calibration of the viscoelastic parameters to a long-term modulus G_∞ equal to the elastic shear modulus. This relation is not completely correct, since the amplitude dependency of the rubber gives a considerably higher long-term modulus. The largest amplitude would probably have a long-term modulus of about 1.28 MPa. It is, however, necessary to use the same modulus as LS-DYNA, i.e. the elastic modulus. There have been no experimental tests of the rubber dampers at higher frequencies. The most important is however that nothing dramatically happen in the models when the frequency rise. It can be seen in figure 6.9 and 6.10 that the dynamic stiffness increase slowly, just like the phase shift below 120 Hz after that there is a decrease. This decrease is not correct but it would probably not affect the results of simulations with oscillations of 5 to 25 Hz. In the determination of the viscoelastic parameters severals of approximations and assumptions were made so the parameters can only be seen as estimated values.

FE analysis of the experimental harmonic curves.

To control the result of the viscoelastic parameters a FE analysis in LS-DYNA is performed. That gives a possibility to verify the results and the estimations. The model consist of a mesh containing 7×7×15 elements. The 15 elements are between the plane with boundary conditions. Otherwise is the model similar to the one used to determining the hyperelastic behaviour, except that the prescribed displacement is replaced with a strain history. The strain history consist of a ramp up to the prestrain after that is the strain kept constant for about 3 seconds in order to let the material relax completely, then the sinus shaped harmonic strain is started. The used material model is the Yeoh model with viscoelasticity. In LS-DYNA completely incompressibility can not be assumed. That makes it necessary to specify a Poisson's ratio or a bulk modulus. The Poisson's ratio is assumed to be 0.499. In figures 6.11 - 6.13 the viscoelastic parameters related to the strain amplitude of 0.015 are used and in figure 6.14 the ones related to the amplitude of 0.14 are used.

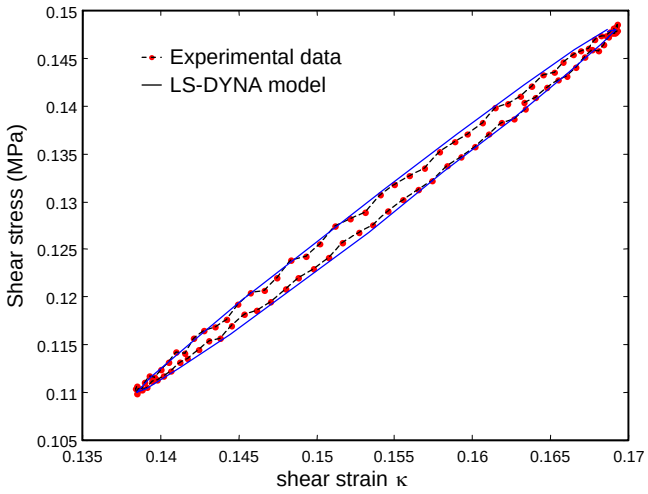

Figure 6.11. Comparison of harmonic loading between experimental data and LS-DYNA model. The frequency is 1 Hz. The strain amplitude is 0.015.

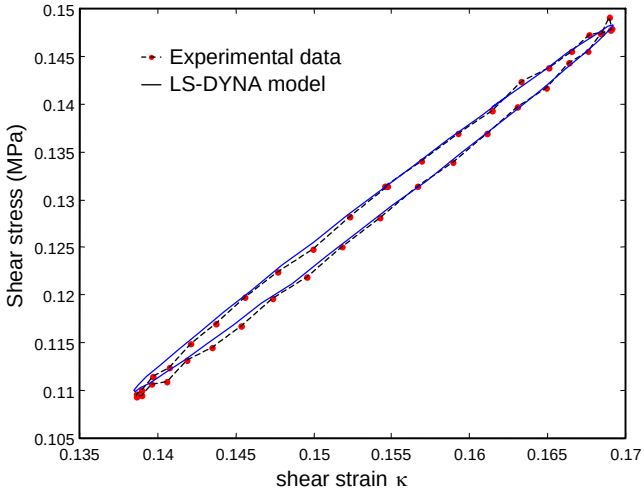

Figure 6.12. Comparison of harmonic loading between experimental data and LS-DYNA model. The frequency is 5 Hz. The strain amplitude is 0.015.

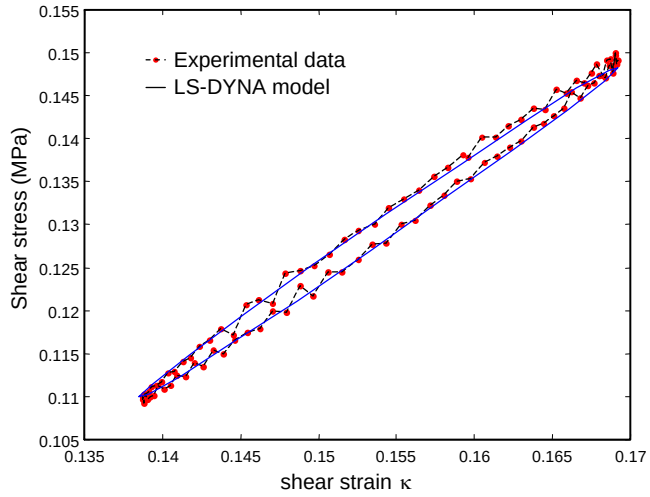

Figure 6.13. Comparison of harmonic loading between experimental data and LS-DYNA model. The frequency is 10 Hz. The strain amplitude is 0.015.

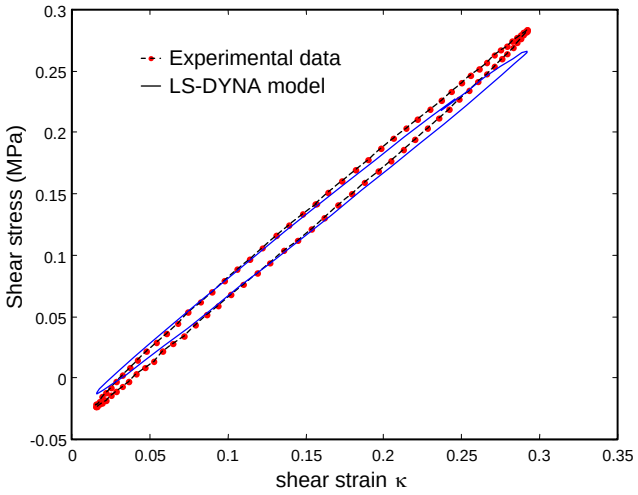

Figure 6.14. Comparison of harmonic loading between experimental data and LS-DYNA model. The frequency is 1 Hz. The strain amplitude is 0.14.

The experimental curves are lowered to the ones from the simulations. This is done because of a force offset in the data from Trelleborg. It was impossible to track the right level. The curves from the simulation fit quit well, the one with the largest amplitude is a bit too weak. It is, however, the one with almost completely estimated viscoelastic parameters.

7 Shock test

The shock test was done in order to have experimental results to verify the shock simulations in LS-DYNA. The test was made with a machine with a drop table. It is an *Impac 3636* delivered from *Montery Research Laboratory INC*, se figure 7.1. The table consists of a mass of about 700 kg, the test object is mounted on top of the mass. The mass and the test object are then released from a predestined height of fall. The table will hit a dashpot, which gives the mass an acceleration in shape of a half sinus wave. The test machine can handle test object weights of up to 2000 kg and accelerations of about 2000g, with a weight of 2000 kg the accelerations can be up to 350g. The duration of the half sinus pulse can be varied from 1.4 to 45 ms.

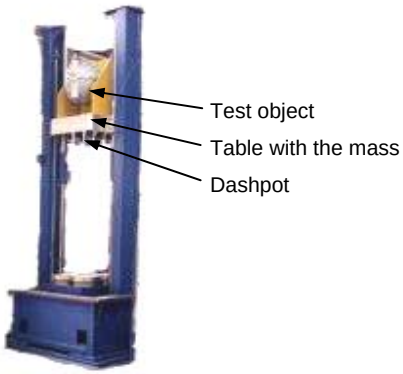

Figure 7.1. The shock test machine

The object of this test is to measure the response of the rubber dampers when they are exposed to a shock. The impulse was measured so it can be used as input in LS-DYNA. The responses of the rubber dampers were measured both for the shock and for the oscillations afterwards.

7.1 Test arrangement and performance

The shock test of the rubber dampers was performed with the arrangement of four dampers attached to the table and a weight fixed on top of them. The deformation of the dampers are exclusively compression and tension. The weight controls the frequency of the oscillations after the shock. The accelerations were measured with a few accelerometers, one was placed on the table and it registered the impulse (see figure 7.2), another one was placed in the middle of the weight and one as close to a damper as possible. The two accelerometers on the weight were placed so in order to estimate distortions in the fundamental oscillations. In the same way, two accelerometers measured the acceleration perpendicular to the direction of motion of the table. A displacement transducer gave the distance between the table and the weight, i.e. the deformation of the rubber dampers. This displacement transducer was placed as close to the damper with the accelerometer as possible. The arrangement of the accelerometers and displacement transducer is shown in figure 7.3 and 7.4.

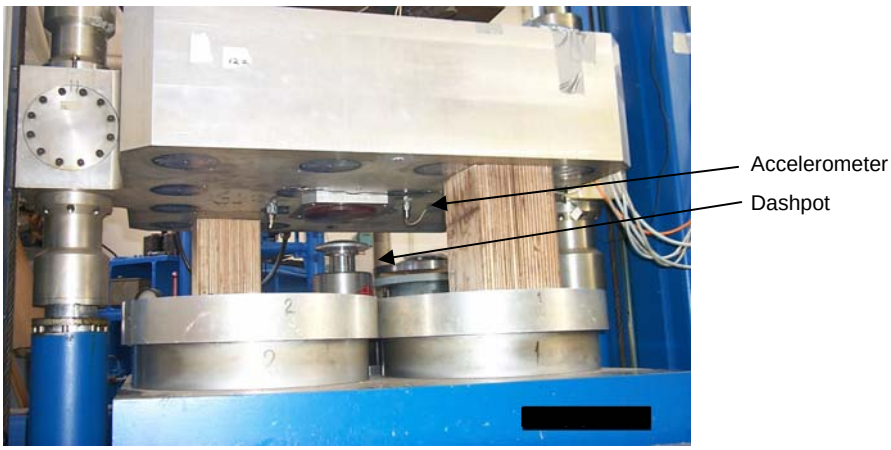

Figure 7.2. Photo of the drop table. The accelerometer measuring the impulse and the dashpot giving the impulse are in the middle of the picture.

Figure 7.3. The arrangement of four accelerometers on the mass (marked with arrows). The displacement transducer is located to the left in the picture.

Figure 7.4. The displacement transducer.

The used accelerometers have an upper limit of 200 g, it is piezoresistive meter model *2262A-200* from *Endevco*. They were supplied with a voltage of 5 V the output from the accelerometer were then after an amplification and a A/D transformation recorded by a DAT recorder. The used tape recorder was a *Heim DATaRec-A160*, the current supply and the receiving of the signal from the accelerometers were done by the module *Strain gage amplifier typ SGA4*. The displacement transducer type *ACW 2000B/7* was manufactured by *RDP electronics*. It was connected to an extern amplifier type *S7AC* also from *RDP electronics* and an alternating current source. The output signal was in this case sent to the tape recorder through a *Direct input module DIC 20.* The recorded signals were transformed into tables in ascii format with the parallel signal processor *Zonic 7000.* The signal processor contains also a digital filter, which reduce the higher superposition frequency. The whole scheme is visualised in figure 7.5.

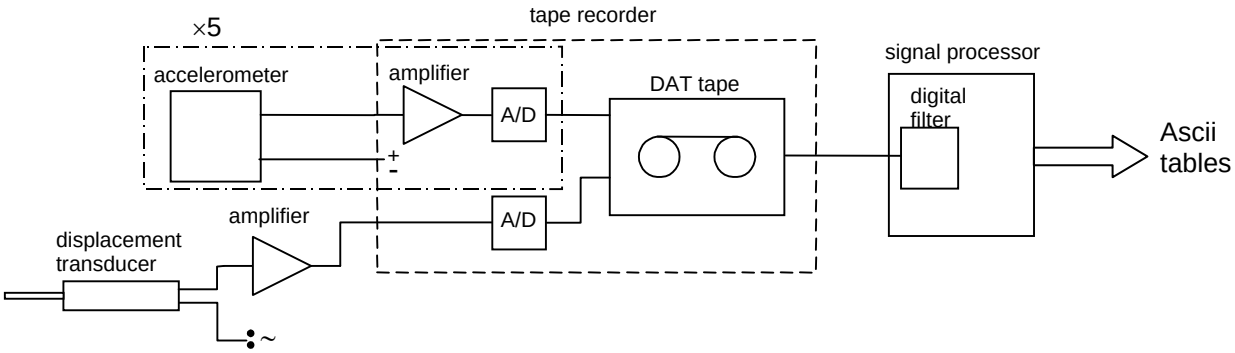

Figure7.5. Scheme over the gauging equipment.

The accelerometers measure acceleration related to the ground, which corresponds to the *fixed reference axis* in figure 7.6. While the displacement transducer measure the distance between the table and the weight corresponding to the coordinate *x*.

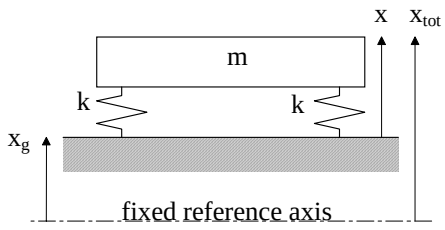

Figure 7.6. Definition of coordinate system and reference coordinate system

The acceleration related to the x-coordinate can be expressed as

$$\ddot{x} = \ddot{x}_{tot} - \ddot{x}_g \quad \text{or} \quad a = a_{tot} - a_g \tag{7.1}$$

The test was made with different masses to achieve different frequencies of the oscillations. To obtain various amplitudes the initial velocity when the table hit the dashpot was varied. That means different height of falls. The height was calibrated to

achieve a maximum compression of about 50%. The peak acceleration on the table is controlled by the initial velocity and the properties of the dashpot on the test machine. The used dashpot was a liquid spring that gives a duration of the acceleration pulse of about 20 ms dependent on the total mass of the table and the test object.

7.2 Results

The tests were made with three different masses when each mass was tested with several fall heights. The highest height is controlled by the maximum compression. The lower heights have in some cases been too small so the brake in the table did not work, which results in that the table bounced against the damper. The masses, the fall heights, maximum compression, the maximum acceleration of both the table and the mass and a approximate achieved frequency is presented in the table below.

Mass 210 kg

Fall Height [mm]	Compression [mm]	Acceleration table [m/s^2]	Acceleration mass [m/s^2]	Frequency [Hz]
75*	13	89	130	17.5
150	18	140	218	16.5
190	21	165	260	16.2
225	23	182	295	16.1
300	26	221	365	16.0

Mass 460 kg

Fall Height [mm]	Compression [mm]	Acceleration table [m/s^2]	Acceleration mass [m/s^2]	Frequency [Hz]
50*	15	65	102	12.7
75*	19	85	141	13.5
100	22	102	173	11.1
125	24	119	209	11.1
150	26	135	241	11.1
175	28	149	273	11.1
200	30	163	305	11.1

Mass 570 kg

Fall Height [mm]	Compression [mm]	Acceleration table [m/s^2]	Acceleration mass [m/s^2]	Frequency [Hz]
25*	11	38	58	9.2
50*	16	60	97	9.2
75*	21	82	137	9.5
100	24	99	172	10.2
125	26	115	205	10.2
150	29	132	243	10.2

A * marked fall height indicate that the table have bounced. The frequencies related to those heights are very approximate. Curves for the table and the mass acceleration and the displacement of the mass are shown for a few different masses and fall heights in figures 7.7-7.10. The rest of the tests can be found in appendix C. It shall be noticed that the used accelerometers have a certain sensitivity for transversal acceleration in their measuring direction. That is a great importance when the curves over the transversal acceleration of the mass are studied. About 1% of the principal acceleration is added to the real transversal acceleration.

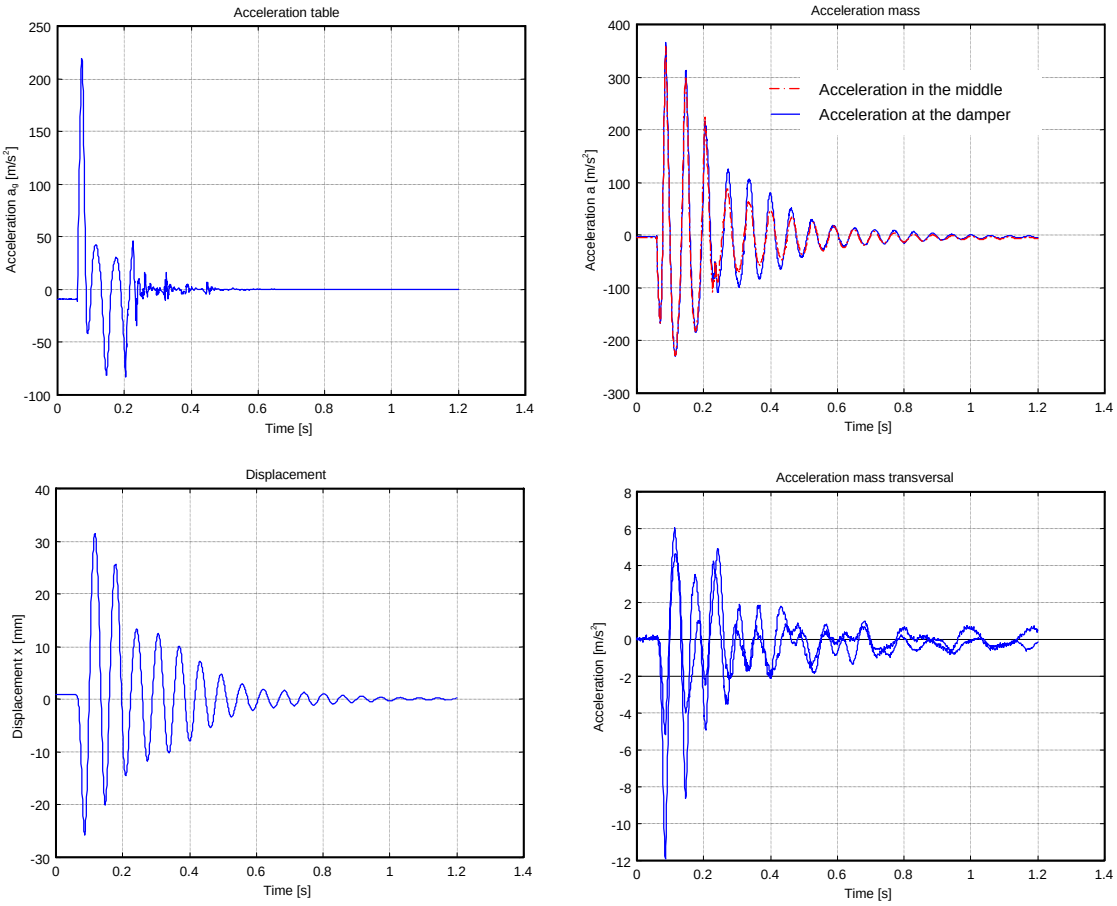

Figure 7.7. Accelerations and displacement of the mass and acceleration of the table. The displacement and the acceleration except the transversal of the mass are relative the table. The mass is 210 kg and the fall height is 300 mm.

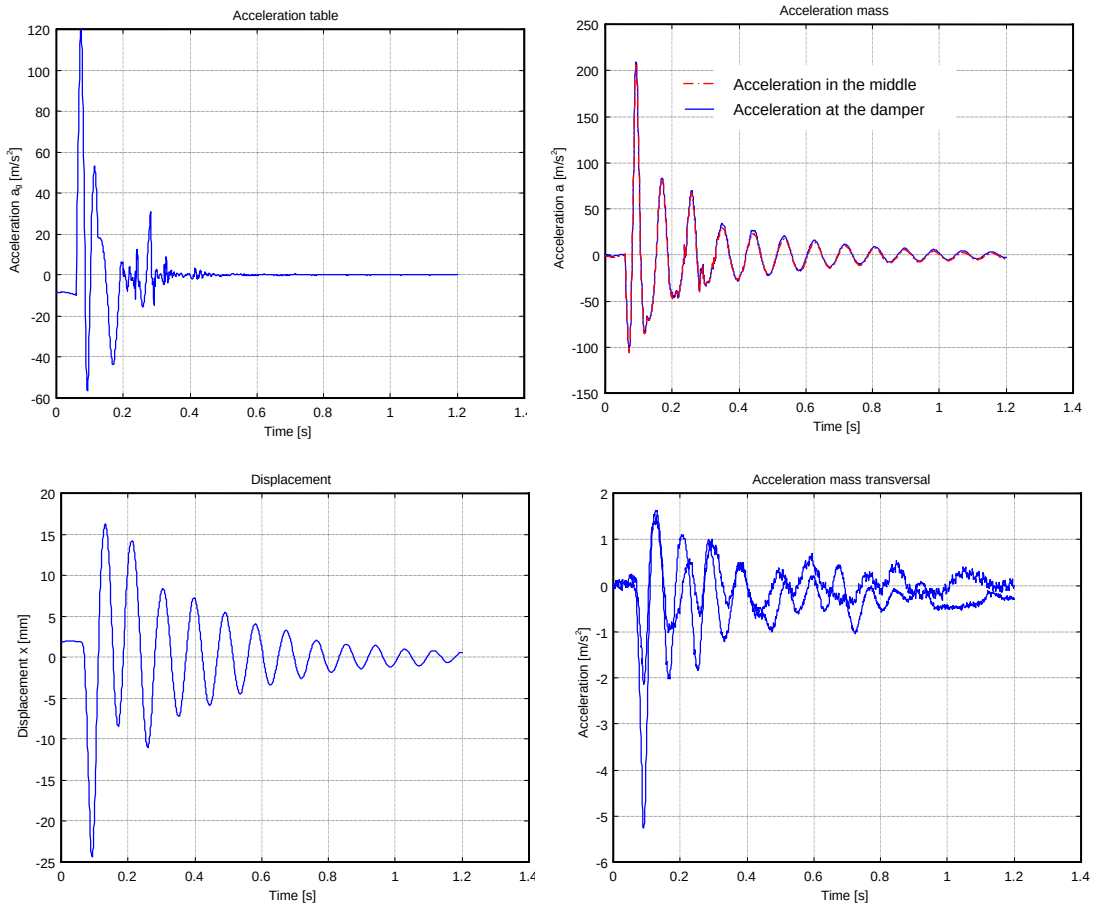

Figure 7.8. Accelerations and displacement of the mass and acceleration of the table. The displacement and the acceleration except the transversal of the mass are relative the table. The mass is 460 kg and the fall height is 125 mm.

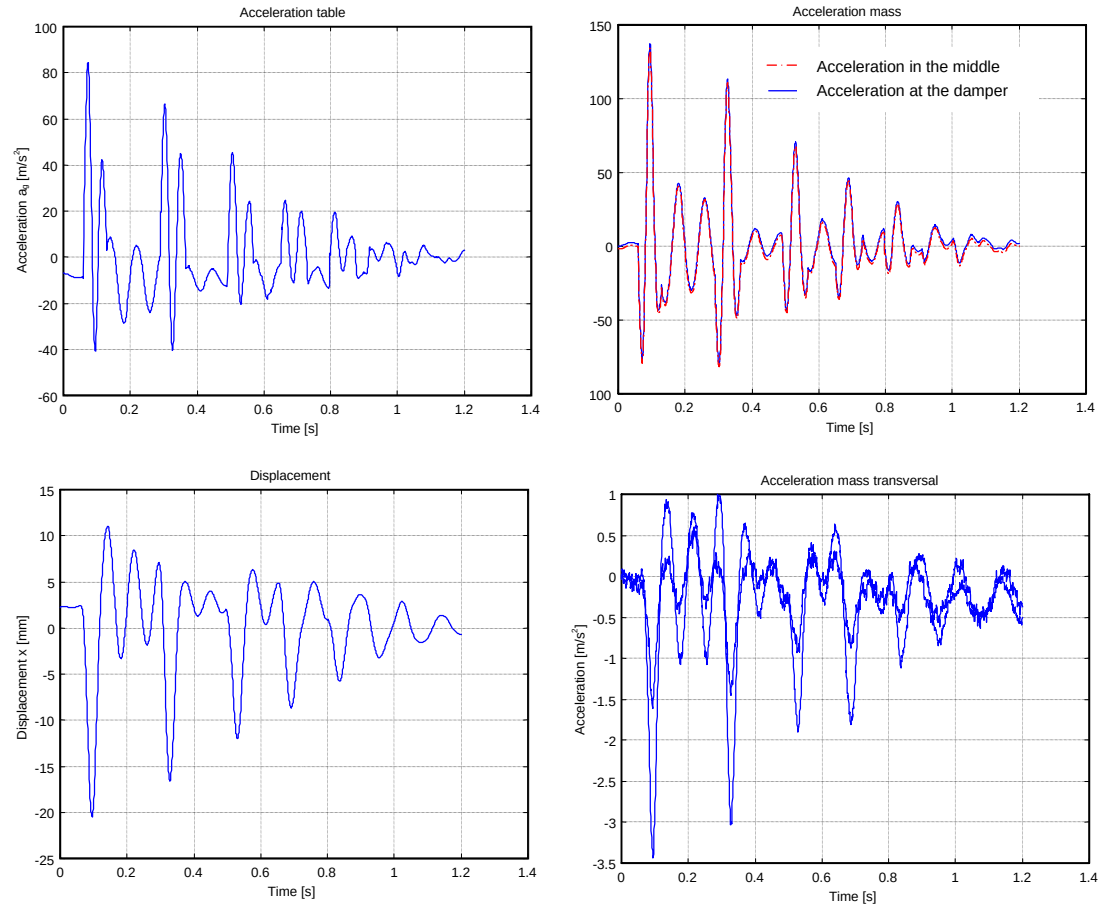

Figure 7.9. Accelerations and displacement of the mass and acceleration of the table. The displacement and the acceleration except the transversal of the mass are relative the table. In these curves can it clearly be seen that the table has bounced. The mass is 570 kg and the fall height is 75 mm.

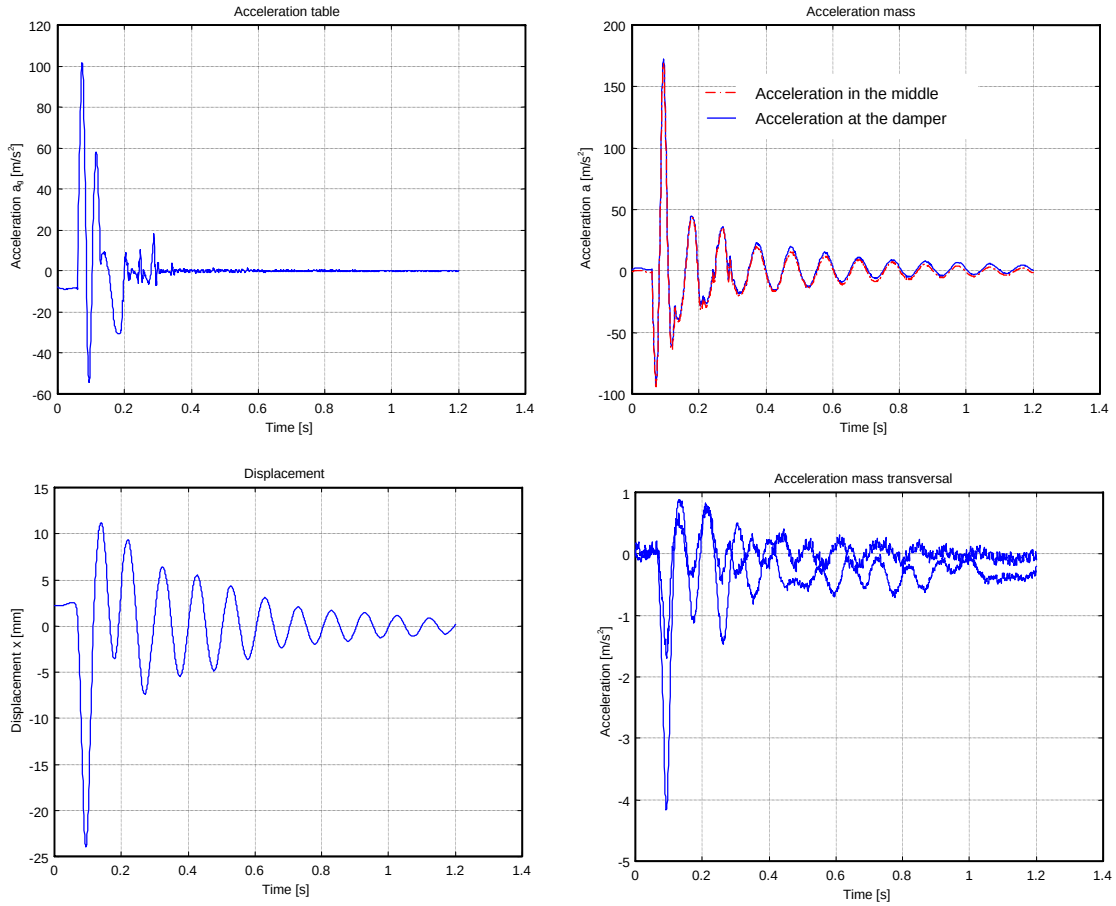

Figure 7.10. Accelerations and displacement of the mass and acceleration of the table. The displacement and the acceleration except the transversal of the mass are relative the table. The mass is 570 kg and the fall height is 100 mm.

The rather equal acceleration on the mass, i.e. at the damper and in the middle, together with the relative small acceleration in the transverse direction indicates that the oscillation have been in the planed direction without any major disturbance. The brake is supposed to lock the table when its velocity is zero. The time it takes for the brake to lock the table can be seen as a disturbance in the acceleration curve for the table.

8 Simulation of shock test in LS-DYNA

The test results of the shock test are used to evaluate the material models. The acceleration on the table on the shock test machine is used as input in LS-DYNA and the relative displacement and acceleration between the table and the mass is compared with the results from the FE simulation.

8.1 Modelling of the damper

The damper is modelled as simple as possible. The shape of the damper makes it natural to choose brick elements, the used element formulation is a constant stress formulation which is default in LS-DYNA. The element is uniformly distributed along the sides. To save processing time the damper is split at its symmetry planes and just a fourth of the damper is modelled. The mass consists of a plane of element with density corresponding to the weight of the mass. The material used in the mass is linear elastic with material constants for steel except the density. The surface between the different material is constrained in order to prevent bending and strain perpendicular to the direction of motion on the mass element. The boundaries between the steel plates and the rubber are complicated to model in an accurate way. If nothing is done with these boundaries the rubber elements at the boundaries will be very distorted and they will finally penetrate the mass elements. This is solved by extending the mass with one row of elements on each side of the rubber. The LS-DYNA option *CONTACT_NODES_TO_SURFACE* prevents the nodes in the rubber elements to penetrate the mass. The deformation of the model will in this way be similar to the deformation of the damper. A similar mass is attached to the opposite side for the same reason. The surface between is however locked in all direction so the extra mass will not affect the dynamic behaviour. The model with boundary conditions and constraints can be seen in figure 8.1.

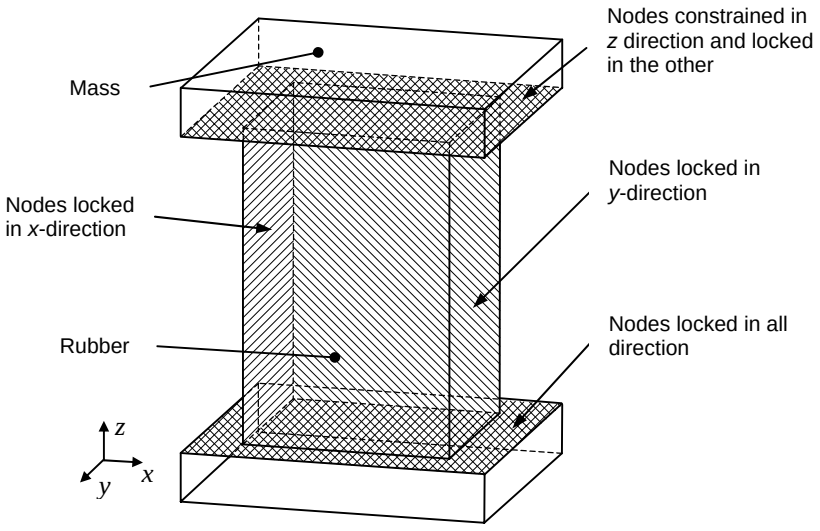

Figure 8.1. Model of the damper with boundary conditions and constraints.

The evaluated material models are the Yeoh model and the Arruda & Boyce model with viscoelasticity. The Yeoh model is implemented in LS-DYNA as *general hyper elastic rubber* material type 77 adapted for the Yeoh model i.e. the constants C_{ij} except C_{10} , C_{20} and C_{30} are zero. The model *Arruda and Boyce rubber* material type 127 provides the Arruda & Boyce model. The used hyperelastic material parameters are presented in chapter 6.1. The mass density approximated to be 1100 kg/m^3 and the Poisson's ratio is assumed to be 0.499 that corresponds to a bulk modulus of 520 MPa. The relation between Poisson's ratio ν and the bulk modulus K is derived from the following equations

$$K = \lambda + \frac{2}{3}\mu \tag{8.1}$$

cf. Ogden [15] and λ and μ are defined as [16]

$$\begin{aligned} \mu &= G \\ \lambda &= \frac{2G\nu}{1-2\nu} \end{aligned} \tag{8.2}$$

the bulk modulus can then be expressed as

$$K = \frac{2}{3}\frac{G(1+\nu)}{1-2\nu} \tag{8.3}$$

The viscoelastic material parameters are the same in both models, they are taken from chapter 6.2. The decay constant t_r is in LS-DYNA denoted as $\beta = 1/t_r$.

The acceleration from the drop table is applied to all nodes on the model as body loads. That corresponds to a prescribed base acceleration equal to $\ddot{x}_g$ in figure 7.6. As input the measured acceleration on the drop table and the gravity g are used. The brake on the table causes some acceleration, which has been neglected due to the high frequency. The distortion in the pure tension-compression deformation mode is also neglected. This would be rather complicated to apply and since this distortion is not significant, it is neglected. An example of an input curve can be seen in figure 8.2.

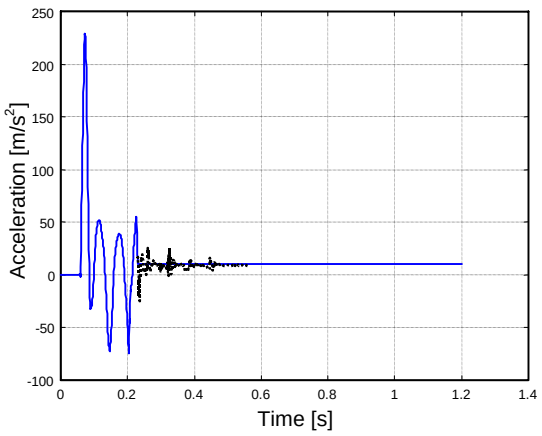

Figure 8.2. Example of acceleration used as input to LS-DYNA. The doted line is the neglected acceleration from the brake

To determine a suitable number of elements is a simple convergence study performed in next section.

8.2 Element convergence study

It is almost impossible to know, in before hand, how many elements necessary in order to obtain an accurate solution. It is therefore convenient to do some kind of simple convergence study. Normally is the accuracy of the result driving the processing time. But the solution usually seems to converge to a curtain number of elements. The quarter of the damper is modelled so the height has twice as many elements as the sides. The elements have all the same size. The convergence study is performed on the case with the highest compression. The study is only made for the Yeoh model, this test controls the element and it is not likely that the Arruda & Boyce model would give a tendency different from this one. The acceleration and displacement curves are shown in figure 8.3.

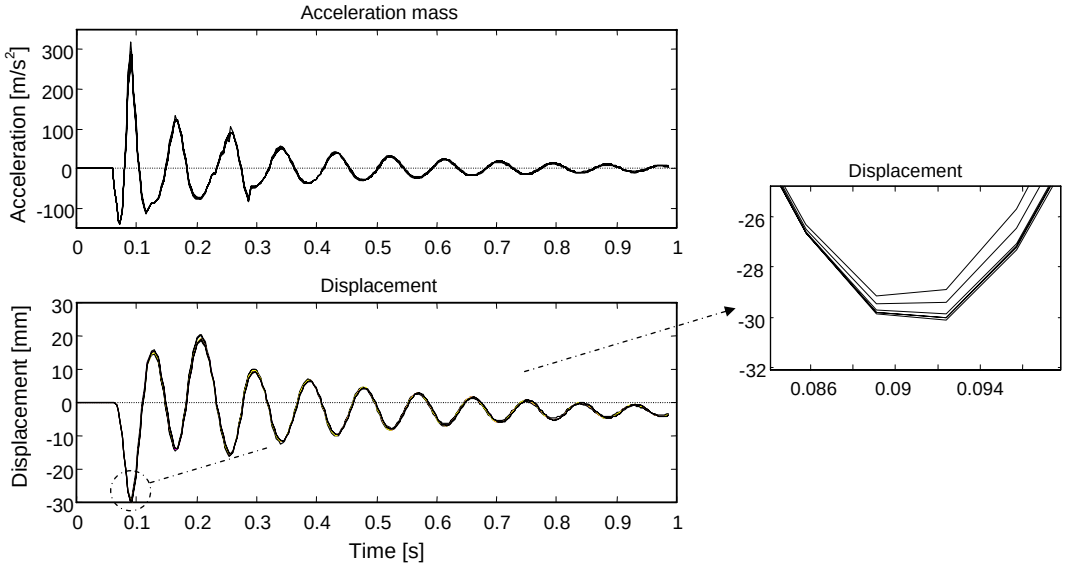

Figure 8.3. Acceleration and displacement curves from different numbers of elements. In the magnification is the curve from the smallest number of elements, 6×3×3, on top and the one from the largest number, 30×15×15, at the bottom. The input, which generates the largest compression, is used.

The used processing time is presented below. If the damper is used as a component in a larger model these values are probably not accurate, but they can perhaps serve as an estimation of time consumption in relation to the different numbers of elements. The time step and consequently the processing time are controlled by the bulk modulus. A higher bulk modulus gives a higher wave propagation velocity, which leads to a smaller time step. The length of the smallest element side is also affecting the time step.

Number of elements	Cpu processing time
6×3×3	9 min
10×5×5	30 min
15×8×8	2 h 27 min
20×10×10	8 h 5 min
24×12×12	15 h 1 min
30×15×15	91 h 27 min

It is not an obvious choice, which element configuration that is most suitable to use. The differences are, however, so small that any number of elements could do. 10×5×5 elements seems to be a good balance between processing time and accuracy. The deformed 10×5×5 element model can bee seen in figures 8.4 and 8.5. The deformed shape is taken from the highest compression in the case with a mass of 473 kg, the compression is about 30 mm. Figure 8.4 shows the corner of the model while figure 8.5 is a view over the symmetry plane. Although, the elements near the boundary are very distorted the convergence test reveals that the results are not very sensitive to the numbers of elements. No test have been made on larger compressions, so it is not advisable to use this model for those case without further evaluation.

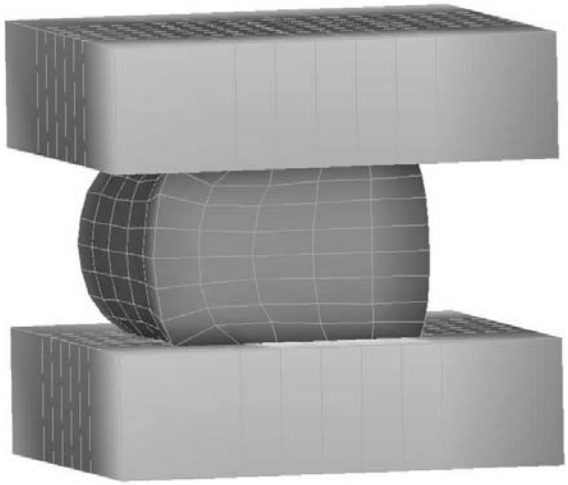

Figure 8.4. The deformed shape of the 10×5×5 element model. The mass is 473 kg and the compression 30 mm.

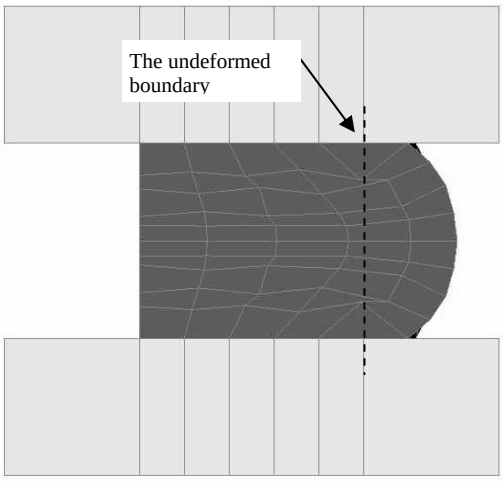

Figure 8.5. View of the figure 8.4 from the symmetry plane. The view plane has no deformation perpendicular to plane

8.3 Results from the shock test simulations

Some selected shock tests are simulated in LS-DYNA. The selected situations are the cases with the highest respective the lowest input acceleration for all three masses. The cases where the drop table has bounced are skipped. The curves over the acceleration and deformation relative the drop table or the locked surface on the model and the input acceleration are presented in figures 8.5-8.10. The simulations are made for both the Yeoh and Arruda & Boyce material models.

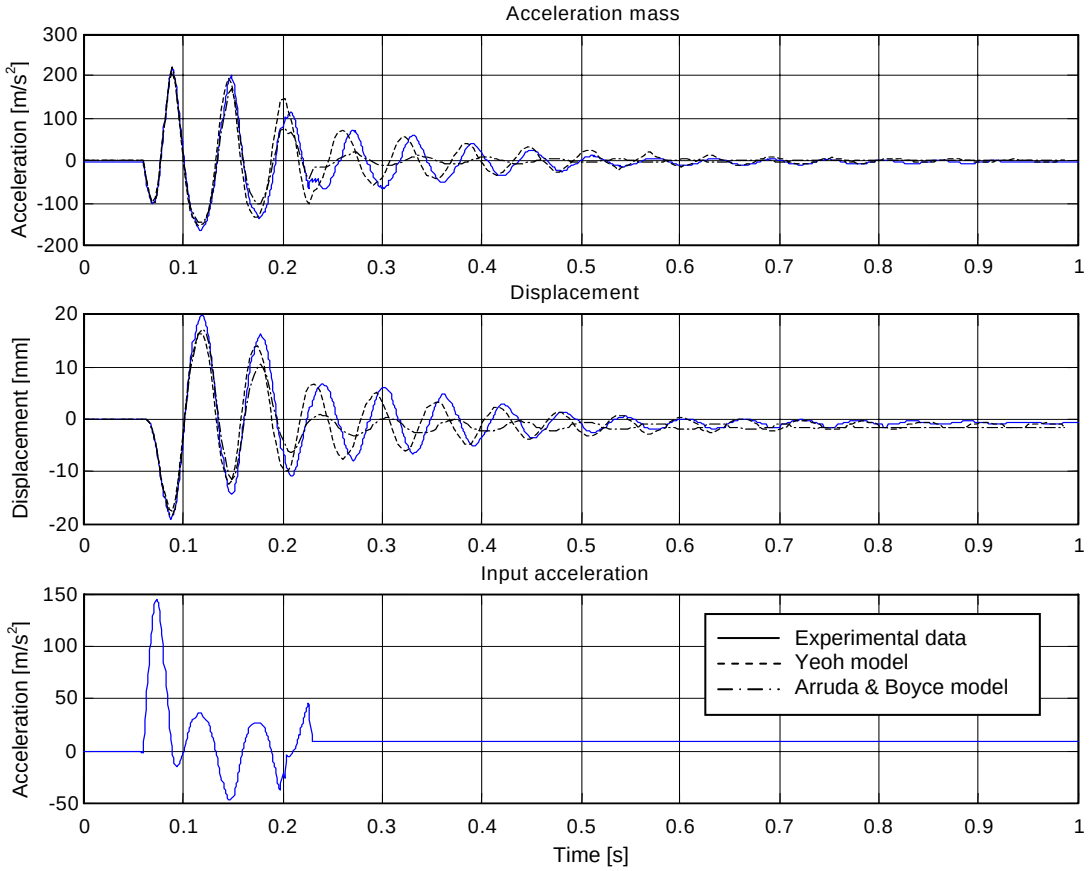

Figure 8.5. Results from the shock simulations with the Yeoh model respective the Arruda & Boyce model. The weight of the mass is 215 kg and the drop height is 150 mm

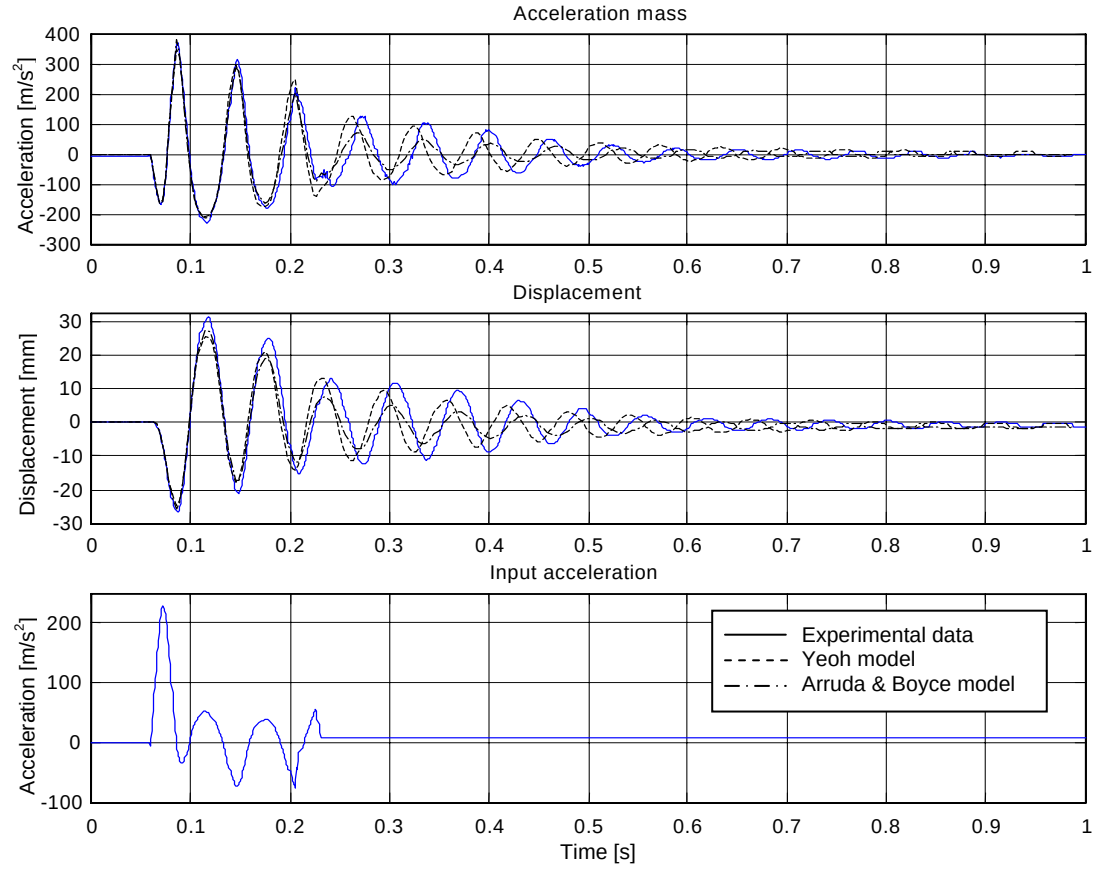

Figure 8.6. Results from the shock simulations with the Yeoh model respective the Arruda & Boyce model. The weight of the mass is 215 kg and the drop height is 300 mm

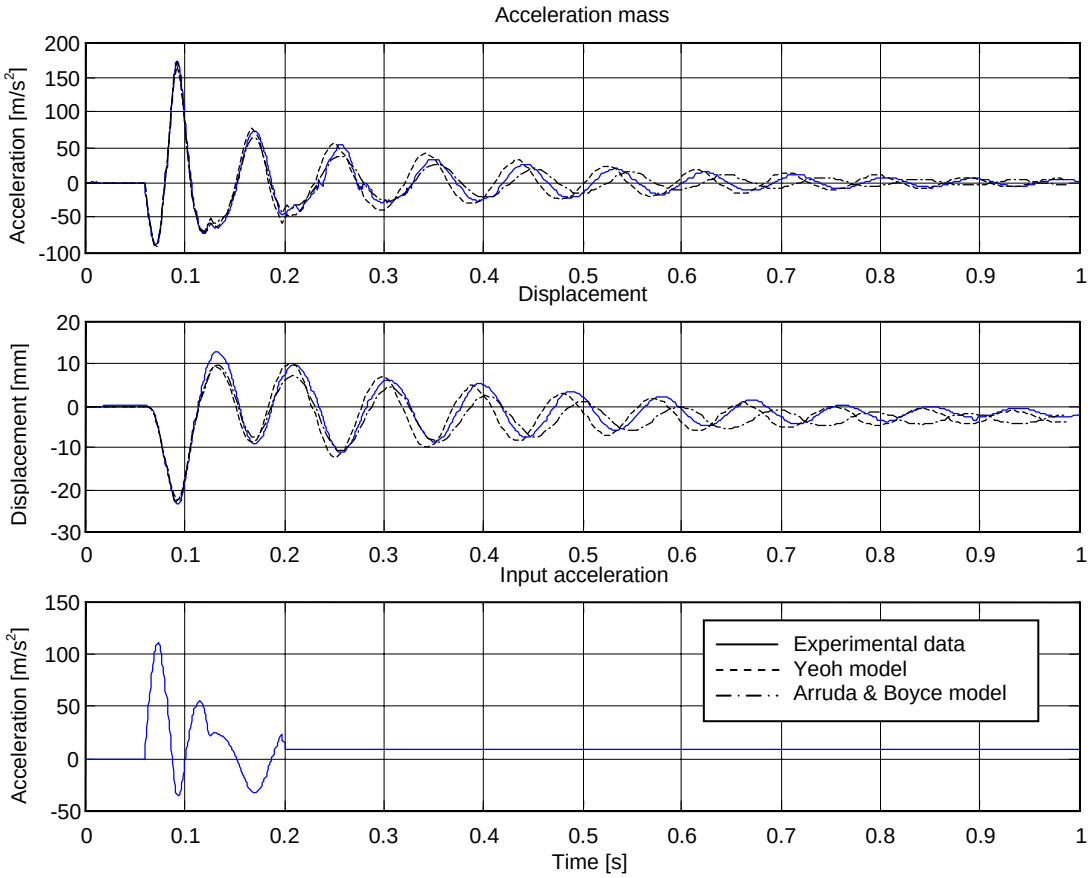

Figure 8.7. Results from the shock simulations with the Yeoh model respective the Arruda & Boyce model. The weight of the mass is 473 kg and the drop height is 100 mm

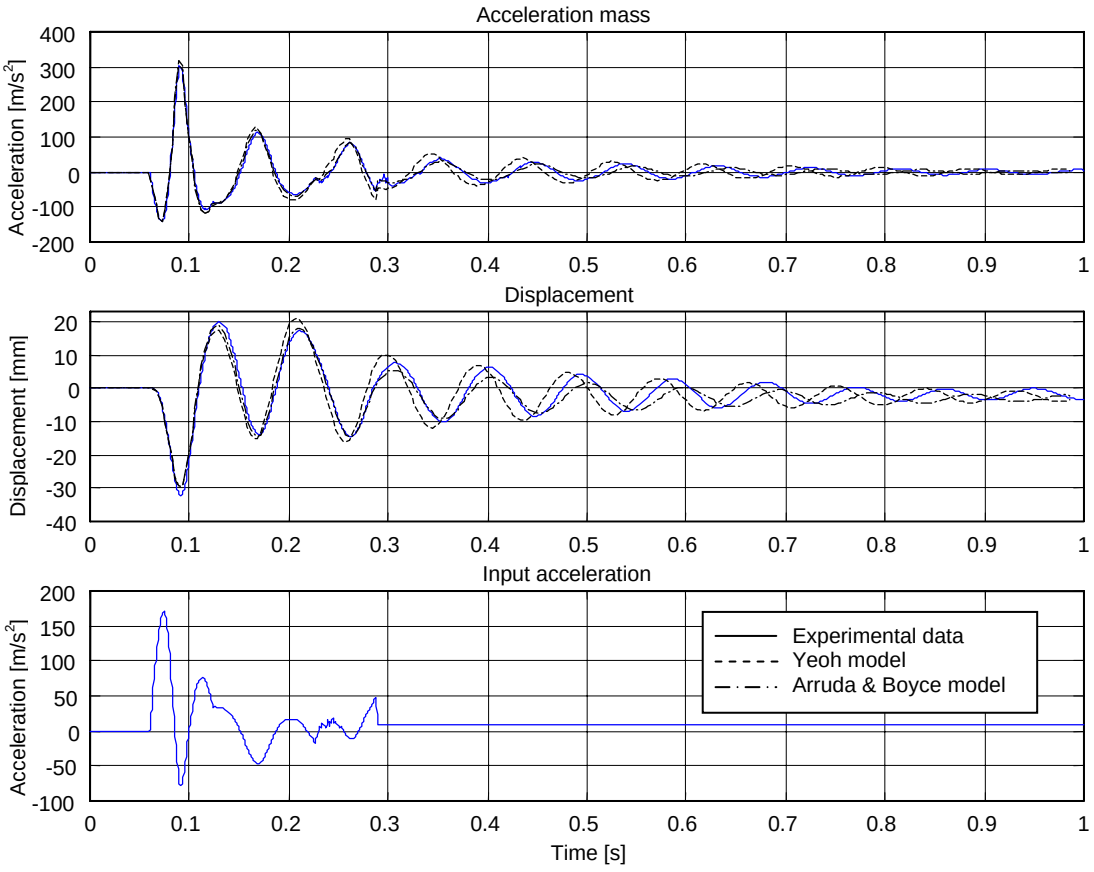

Figure 8.8. Results from the shock simulations with the Yeoh model respective the Arruda & Boyce model. The weight of the mass is 473 kg and the drop height is 200 mm

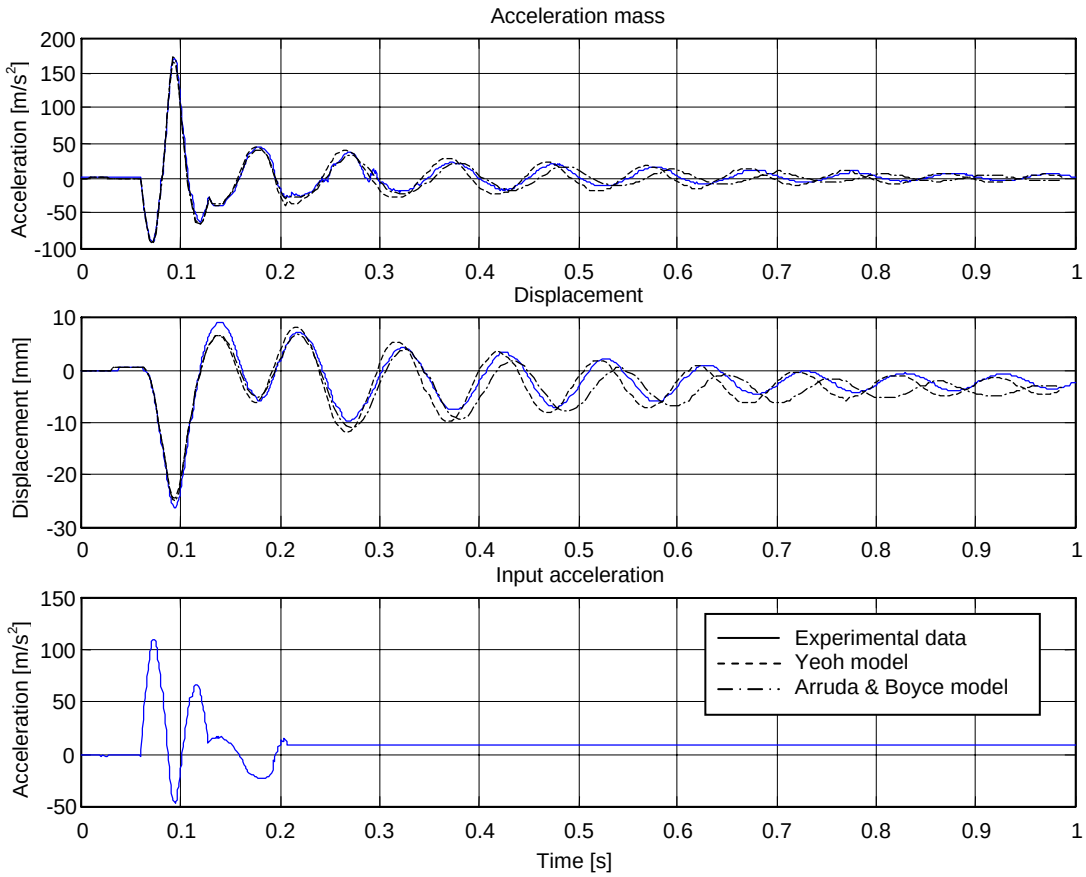

Figure 8.9. Results from the shock simulations with the Yeoh model respective the Arruda & Boyce model. The weight of the mass is 590 kg and the drop height is 100 mm

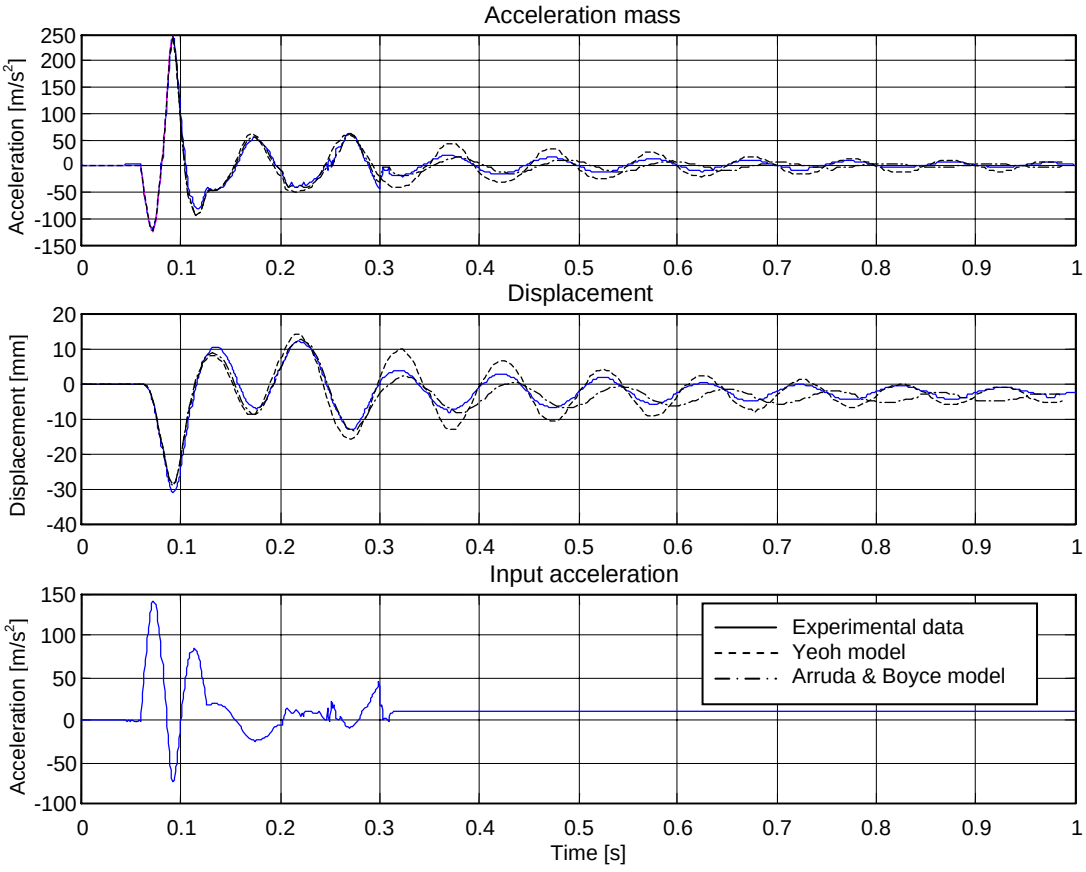

Figure 8.10. Results from the shock simulations with the Yeoh model respective the Arruda & Boyce model. The weight of the mass is 590 kg and the drop height is 150 mm

A comparison between the simulations and the experimental test can be made easier if any numerical values can be obtained. It is however not easy to find a way of doing it at the shock phase since the oscillations are not harmonic. The free vibrations can easily be measured if a simple system consisting of a linear spring, a damper and a mass is assumed. the equation of motion for this system can be expressed as [5]

$$ma(t) + cv(t) + kx(t) = 0 \tag{8.1}$$

the solution to the equation is

$$x(t) = \left[x(0)\cos\omega_D t + \left(\frac{v(0) + x(0)\xi}{\omega_D} \right) \sin\omega_D t \right] e^{-\xi\omega t} \tag{8.2}$$

where

$$\omega = \sqrt{\frac{k}{m}} \qquad \xi = \frac{c}{2m\omega} \qquad \omega_D = \omega\sqrt{1-\xi^2} \tag{8.3}$$

If equation (8.2) is fitted to the displacement curves at the free vibration phase is it possible to find out the frequency and the damping for the different material models and for the experimental data. The results of it are presented in the table below.

	Exp. data	Yeoh	A & B
215 kg 150mm			
frequency [Hz]	16.6	16.3	15.1
damping ξ	0.053	0.044	0.05
215 kg 300 mm			
frequency [Hz]	15.9	16.2	15.1
damping ξ	0.048	0.044	0.05
473 kg 100 mm			
frequency [Hz]	10.9	11.0	10.2
damping ξ	0.041	0.042	0.049
473 kg 200 mm			
frequency [Hz]	10.8	11.0	10.3
damping ξ	0.044	0.042	0.048
590 kg 100 mm			
frequency [Hz]	9.9	9.9	9.2
damping ξ	0.04	0.042	0.049
590 kg 150 mm			
frequency [Hz]	9.9	10	9.3
damping ξ	0.04	0.042	0.049

The calibration of equation (8.2) to the experimental data was not perfect. The frequency in the experiment had a tendency to increase when the amplitude decreases due to the amplitude dependency and non-linear elastic behaviour. The equation (8.2) does not cover those effects.

8.4 Evaluation of the results

8.4.1 Comparison between Arruda & Boyce and Yeoh

The simulations with the Yeoh model correspond quite well with the experiment. The largest error can be found in the displacement at the first peaks during the shock phase. The tension peak has a deviation of about 28 % for the worst case 590 kg with the drop height of 100 mm. An explanation of this is given in next section. The Arruda & Boyce model shows also good results in the shock phase. The two models follow each other in most cases.

The damping in the free vibration phase seems also to fit quite well (cf. previous table). It can be noticed that both models seem to be out of phase in the free vibration phase. One reason can of course be that the stiffness deviate, but the frequency is quite alike. So the main reason is probably that LS-DYNA cannot handle the high input frequencies. It can clearly be seen in figure 8.10 that the models especially the Yeoh model do not follow high frequency acceleration response. This together with fact that most of the higher frequencies generated by the brake on the drop table is neglected from the input acceleration make the phase drift.

Figure 8.5 and 8.6 show a phenomenon that is hard to find an explanation for. The Arruda & Boyce model gives a too small response in the free vibration phase. Obviously is there a damping mechanism that affects the model. It is possible that the damping is controlled by the frequency. The higher frequency achieved by the 215 kg mass, displays in the shock phase more damping compared with the Yeoh model. The two lower frequencies worked considerably better. It is also possible that superposed higher frequencies, at for example just over 0.2 s in figure 8.5, damp the Arruda & Boyce model quite a lot. The phenomenon seems however not come from the parameter fit since the parameters generate a damping curve with just a slightly increasing damping. The magnitude is at most about twize the one for the damping at 20 Hz. This makes it precarious to use the Arruda & Boyce model until there is an explanation.

8.4.2 Amplitude dependency

The results from the simulations especially for the Yeoh model behave quite well, the largest deviations are in most case in the shock phase. The error of the displacement can be up to 28 %, while the accelerations seem to fit better. One part of the decrease in extension and compression can be traced from the fact that the amplitude dependency is not included in the material models. A. I. Medalia [13] shows that the dynamic stiffness and especially the phase angel, i.e. the damping, are very dependent on the amplitude. The change in dynamic stiffness does not affect this case very much since the amplitude is so high that the stiffness is almost constant, see figure 8.11. The change in amplitude affects on the other hand the damping quite a lot. Figure 8.12 shows the phase angle depended on the strain amplitude on different rubber types. It can be seen that the

damping for natural rubber (NR) increases with falling amplitudes. The translation to the tension and compression scale is done with equation (5.4) and (6.11). The comparison is built on the assumption of equal strain energy. Both graphs shows filled natural rubber not necessarily same compound, unfortunately is the hardness unknown.

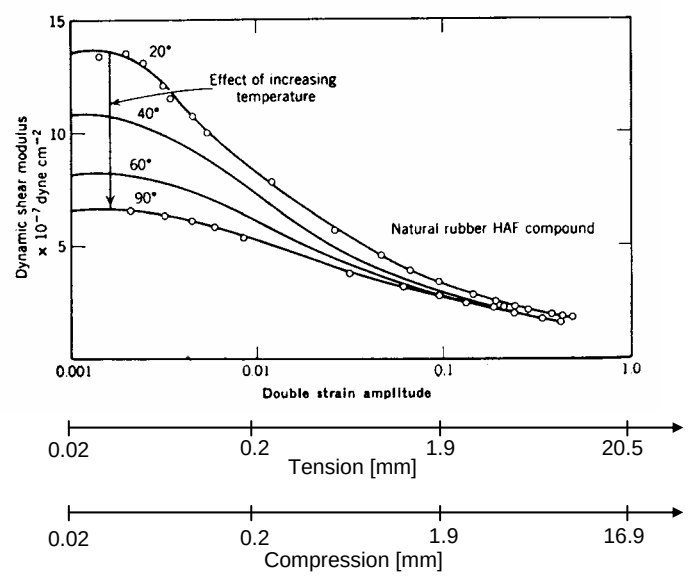

Figure 8.11. Dynamic shear modulus for filled natural rubber. (Source: Medalia [12]).

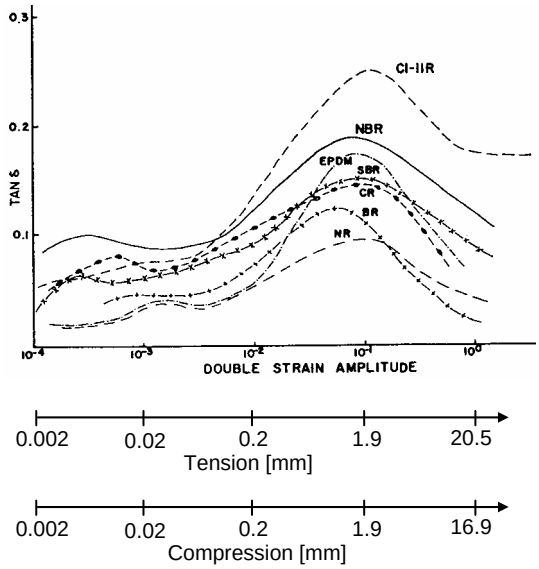

Figure 8.12. Phase angle different rubber types. The natural rubber is marked NR. (Source: Medalia [12]).

The fact that the damping is too high in the shock phase can also be established by the results of a FE simulation where the viscoelastic behaviour is disabled and the hyperelastic parameters are adjusted to be valid for the initial stiffness. The Yeoh model is used on the case with a mass of 215 kg and a drop height of 300 mm. The used hyperelastic material constants are C_{10} = 0.6899 C_{20} = -0.06899 and C_{30} = 0.00689, i.e. the approximate relation for the constants is used. This would correspond to an approximate initial shear modulus of 1.38 MPa compared to the original of 1.06 MPa. Figure 8.13. shows the result.

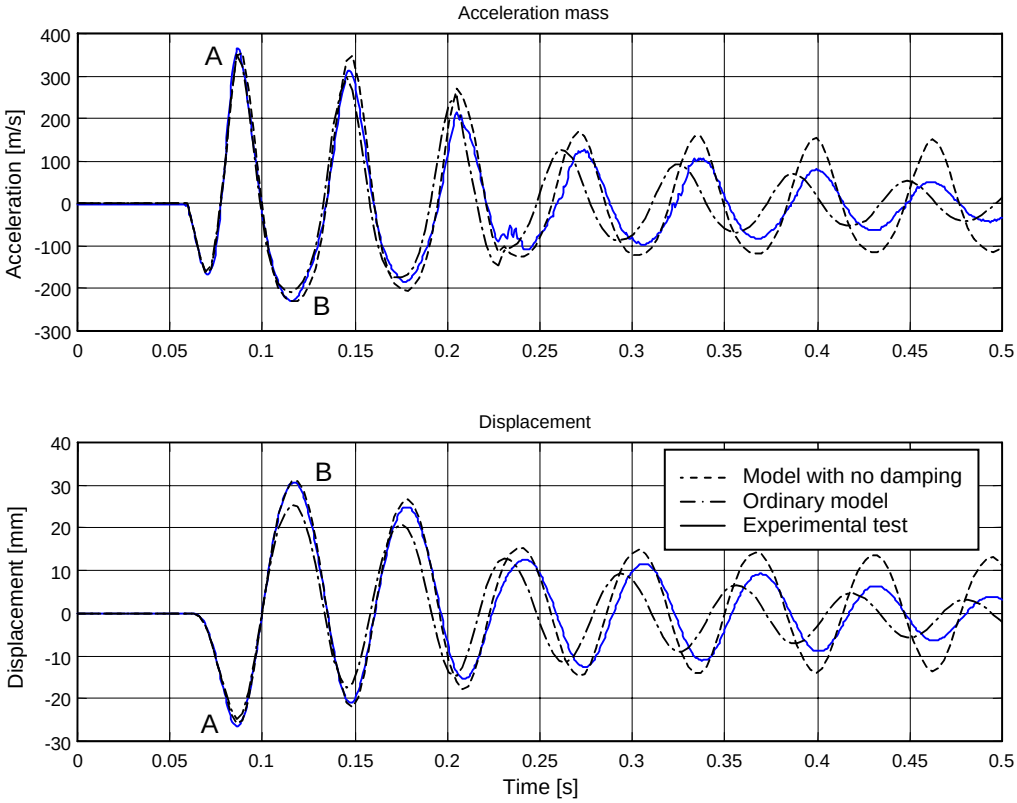

Figure 8.13. The FE model without any damping compared to the ordinary FE model and the experimental test. Mass 215 kg and drop height 300 mm

The model mimics the experimental result considerable better at the first two peaks *A* and *B* with a material model without any damping. But when the amplitude decrease more damping must be included, cf. also figure 8.12. The displacement at point *B* is affect by the damping and if the shock phase is of particular interest is it possible that a material model without any damping is more suitable. If the important quantity is just the transmitted acceleration the deviation at point *B* is so small that the damped model seems to be a better choice.

These conclusions are not surprising, since the visco- hyperelastic material models cannot model amplitude dependency.

8.4.3 Frequency dependency

The frequency dependency on the material models are harder to evaluate, since neither the stiffness nor the phase angle vary much at these relative low frequencies, see figure 8.14.

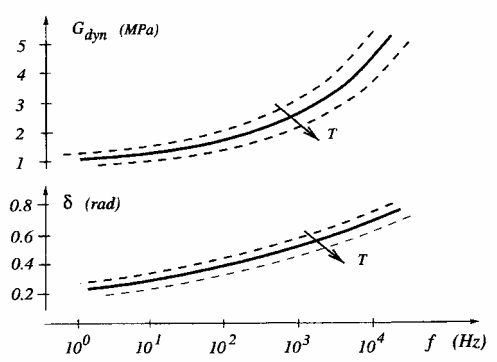

Figure 8.14. The frequency dependency of the dynamic modulus and the phase angle. (Source: Austrell [3]).

It is also difficult to separate the more dominant amplitude dependency from the frequency dependency. The achieved frequencies from the Yeoh model at the free vibrations phase match the measured ones quite well (see table in section 8.3). The largest deviation is about 2 %. The Arruda & Boyce shows generally a bit too low frequencies, it can be explained by the fact that the Arruda & Boyce model is weaker at small strains than the Yeoh model. It is of course impossible to trace the cause of this behaviour. The reason can be wrong weight of the mass, the hyperelastic behaviour has also a deviation from the real elastic behaviour and finally the parameter fit of the visco-elastic parameters is very approximate. The calibration is made at a corresponding uniaxial amplitude of about 6mm. The achieved damping is not quite as good as the achieved frequency the largest error is about 18 % for both models. The damping is however influenced by the shock phase so it is very difficult to find out if the frequency dependency of the damping is correct.

9 Conclusion

The results from the simulations correspond quite well to the experimental results. Especially the Yeoh model gives remarkable good results despite the many approximations in the calibration of the model. There are, of course, also other sources of error, like the measurements in the material tests and the shock test. The approximations and errors have, of course, affected the results, but it seems like the corrections of both the static and dynamic stiffness have worked quite well. A comparison of the results from the simulations and the tests indicate, also, that measuring errors were not significant. If they were significant the accuracy of results would differ more between the different conditions. The fact that the material tests were done in shear deformation and the shock tests in tension and compression eliminates the possibility that the material models are valid for just one deformation mode.

The two examined models, Yeoh and Arruda & Boyce, show in most cases a similar behaviour. The Arruda & Boyce model did, however, in the cases with the lowest mass not respond very well. The reason could unfortunately not be found. This effect makes the model insecure to use and it is not advisable to use it before any explanation can be found.

Unfortunately, the rubber material is more dependent on the strain amplitude than the strain frequency at these relatively low frequencies. The frequency dependency can almost be neglected in this frequency range. It would be much more useful to have an amplitude dependent material model than a frequency dependent one. The calibration of the material models to a amplitude of about 6 mm works quite well. The deviations at the shock phase where the amplitude are considerable higher are quite large due to too high damping, while the free oscillation phase is better. It is possible that a fit to higher amplitude is better, this was not tested since it would require the whole dynamic modulus curve.

Today, with the visco-hyperelastic models it is necessary to choose if the results shall be accurate in the shock phase or in the free oscillation phase. To achieve an accurate result in the shock phase is it recommended to use a purely hyperelastic model where no damping exist. The Yeoh model with the following constants

$C_{10} = 0.6899$
$C_{20} = -0.06899$
$C_{30} = 0.00689$

worked quite well.

If the free oscillations are of importance it is better to use the visco- hyperelastic model where the hyperelasticity is described by the Yeoh model. The following constants are used in the simulations

C_{10} = 0.529
C_{20} = -0.0958
C_{30} = 0.0293

and

G_1= 0.487 MPa	G_2= 0.241 MPa	G_3 = 0.123 MPa	G_4= 0.00190 MPa
t_{r1} = 0.00119s	t_{r2} = 0.690 s	t_{r3} = 0.0196 s	t_{r4} = 0.248 s

It would be interesting to find out the response of the models in a case with considerable higher input accelerations. It was, however, impossible to achieve higher accelerations in the shock test with a frequency of less than 20 Hz. The compression of the dampers would be too high in that case. The absence of experimental tests made any simulations meaningless, since the results could not be evaluated.

A material model dependent on the strain amplitude is, of course, in the future desirable. But it is also important to fit the existing models to proper test results. When a new rubber element is developed is it advisable to obtain test data from real test specimen. The test that shall be performed is a simple shear test where the elastic behaviour is measured and a dynamic shear test where the dynamic modulus and the phase shift are measured. The frequency and the amplitude shall cover the whole region. It is also advisable to do some tests at higher frequencies in order to obtain asymptotic values. Finally a compression and tension test can be useful to verify the hyperelastic model and the tests can also be used in the calibration of the material model. The simple shear test specimen can for example be shaped like the example in figure 5.2. Further details are for example described in Austrell's thesis [3].

10 References

[1] ABAQUS/Standard Version 5.8, Hibbitt, Karlsson & Sorensen Inc.

[2] Arruda, E. och Boyce, M., *A Three-Dimensional Constitutive Model for the Large Stretch Behaviour of Rubber Elastic Materials*, The Journal of the Mechanics and Physic of Solids, Vol. 41, No. 2, 389-412, 1993.

[3] Austrell, P-E., *Modeling of elasticity and damping for filled elastomers.* Report TVSM-1009, Division of Structural Mechanics, Lund University, 1997.

[4] Christensen, R.M., *A Nonlinear Theory of Viscoelasticity for Application to Elastomers*, Journal of Applied Mechanics, Vol. 47, 762-768, 1980.

[5] Clough, R.W. and Penzien J., *Dynamic of Structures second edition*, McGraw-Hill Inc, 1993.

[6] Godvindjee, S. and Simo J.C., *Mullins´ effect and the strain amplitude dependence of the storage modulus*, International Journal of Solids Structures, Vol. 29, No.14/15, 1737-1751, 1992.

[7] Hibbitt, Karlsson and Sorensen, *ABAQUS/Standard User's Manual Version 5.8*, 1998.

[8] *LS-DYNA Theoretical manual Version 950*, Livermore Software Technology Corporation, 1998.

[9] *Inspection Test & Trials Report: ITR-0035*, Kockums AB, 1990

[10] LS-DYNA Version 950d, Livermore Software Technology Corporation.

[11] Lundgren, E., Lectures notes: Continuum Mechanics, Division of Mechanics, Lund University, 1999.

[12] Matlab version 5.3, the MathWorks Inc.

[13] Medalia, A.I., *Effects of Carbon Black on Dynamic Properties of Rubber Vulcanizates*, Rubber Chemistry and Technology, Vol. 51, 437-523, 1978.

[14] *National encyklopedin*, Bokförlaget Bra Böcker AB, Höganäs, 1989-1996.

[15] Ogden, R.W., *Non-linear Elastic Deformations*, Dover Publications Inc., New York, 1997.

[16] Odqvist, K.G. *et al., Formelsamling i Hållfasthetslära*, Department of Solid Mechanics, Royal Institute of Technology, Stockholm, 1990.

[17] Ristinmaa, M. and Ottosen, N.S., *Large Strain Plasticity and Thermodynamics*, Report CODEN:LUTFD2/(TFHF-3072)/1-145/1996, Division of Solid Mechanics, Lund University, 1996.

[18] Yeoh, O.H., *Charaqcterization of elastic properties of carbon-black-filled rubber vulcanizates*, Rubber Chemistry and Technology, Vol. 63, 792-805, 1990.

Appendix A

The dynamic modulus and the phase shift are here presented in tables. The values are calculated with no adjustments for error like bending modes included in the fundamental simple shear deformation. Description of the calculations can be found in section 5.2.3.

The dynamic modulus G_{dyn} [MPa]:

Shear strain amplitude	Frequency [Hz]				
	1	5	10	15	20
0.015	1.23	1.28	1.28	1.16	1.12
0.031		1.23	1.26	1.11	1.11
0.046	1.17	1.20	1.24	1.10	1.12
0.062		1.18	1.24	1.08	
0.077	1.15	1.16	1.12		
0.092		1.15			
0.11	1.12	1.14			
0.12					
0.14	1.11				

The phase shift δ:

Shear strain amplitude	Frequency [Hz]				
	1	5	10	15	20
0.015	0.0546	0.0664	0.0737	0.025	0.0828
0.031		0.0706	0.0749	0.057	0.0919
0.046	0.0609	0.0747	0.0711	0.0703	0.0954
0.062		0.0723	0.0295	0.0763	
0.077	0.0581	0.0715	0.0061		
0.092		0.0725			
0.11	0.0578	0.0758			
0.12					
0.14	0.0555				

Appendix B

A compression test was performed at Kockums. The test object, i.e. the damper, was first compressed two times in order to condition the damper. The real test was then made with a deformation rate of 0.09 mm/s. The next test with a rate of 8 mm/s (the limit of the test machine) was made just to see if there was any difference between the deformation rates. The stress is calculated as the engineer stress. the force divided by the original area (85 mm × 75 mm). The stretch is calculated as

$$\lambda = 1 - \frac{\delta}{65} \tag{B.1}$$

where δ is the compression.

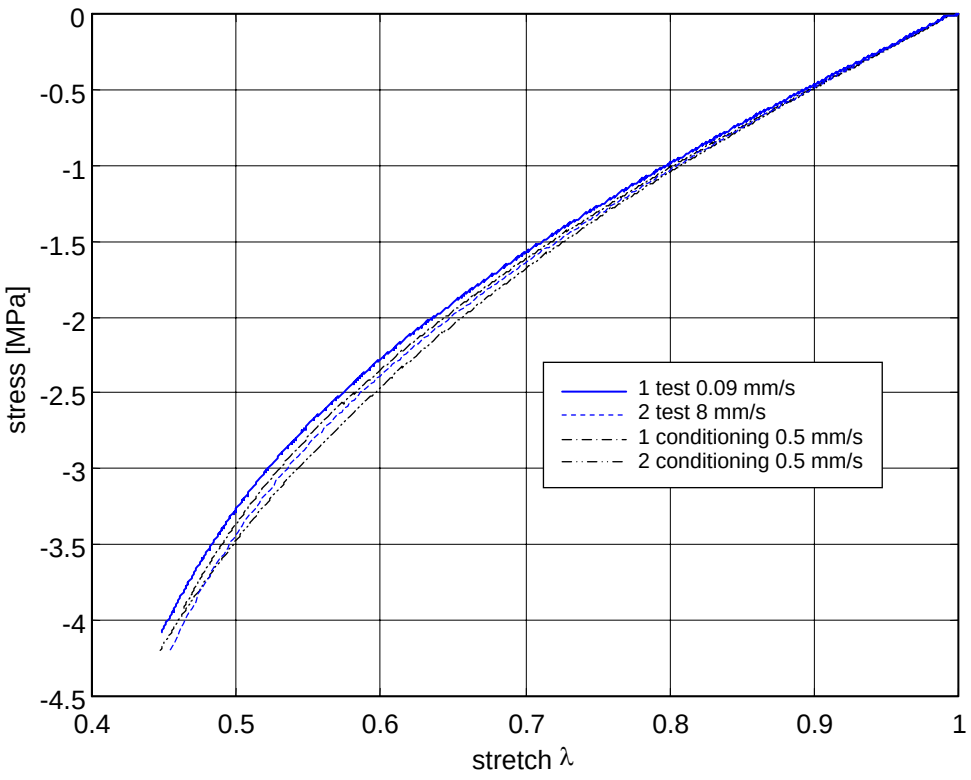

Figure B.1. Compression tests made at Kockums.

Appendix C

In this section are all measurements from the shock tests presented. The test arrangement with the accelerometer and displacement transducer setup are described in section 7.1. It is also referred to figure 7.6 and equation (7.1) for a description of the notations a_g, a_{tot} and x.

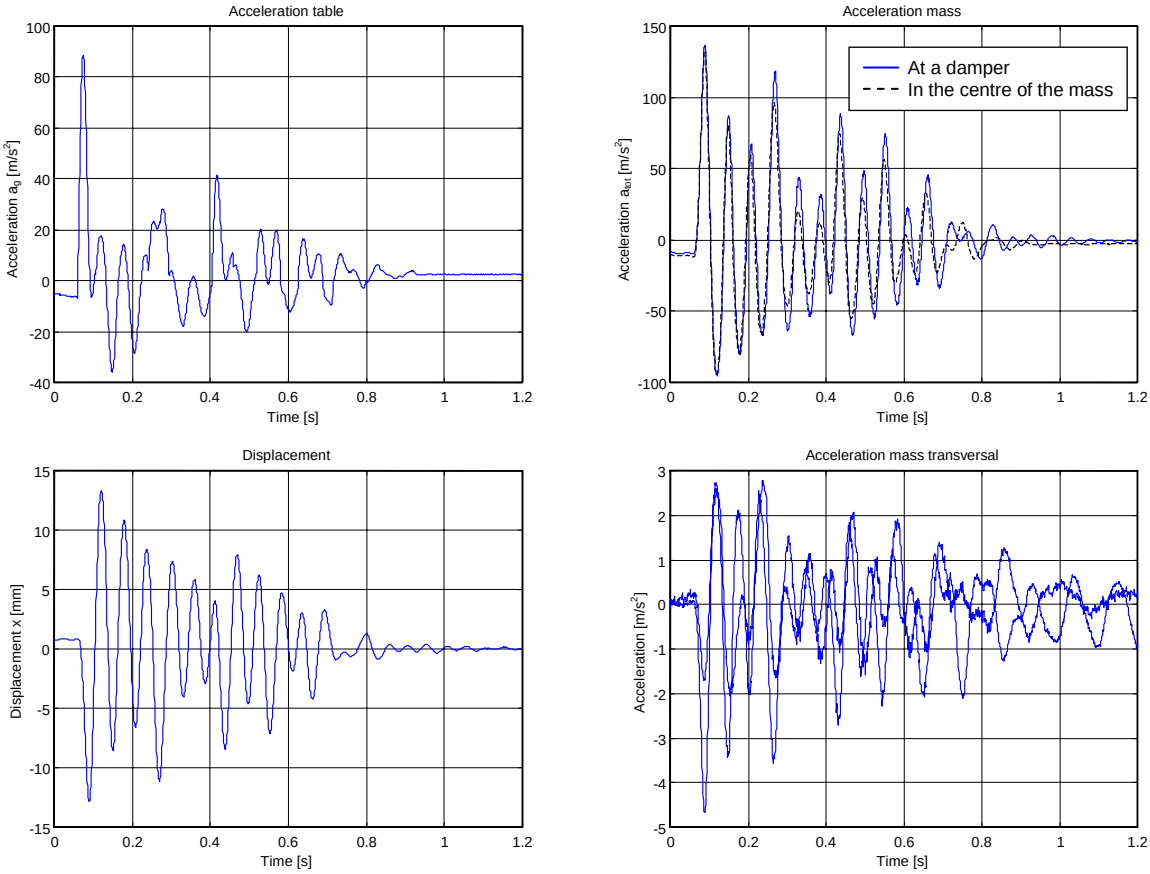

Figure C.1. Mass 215 kg and drop height 75 mm

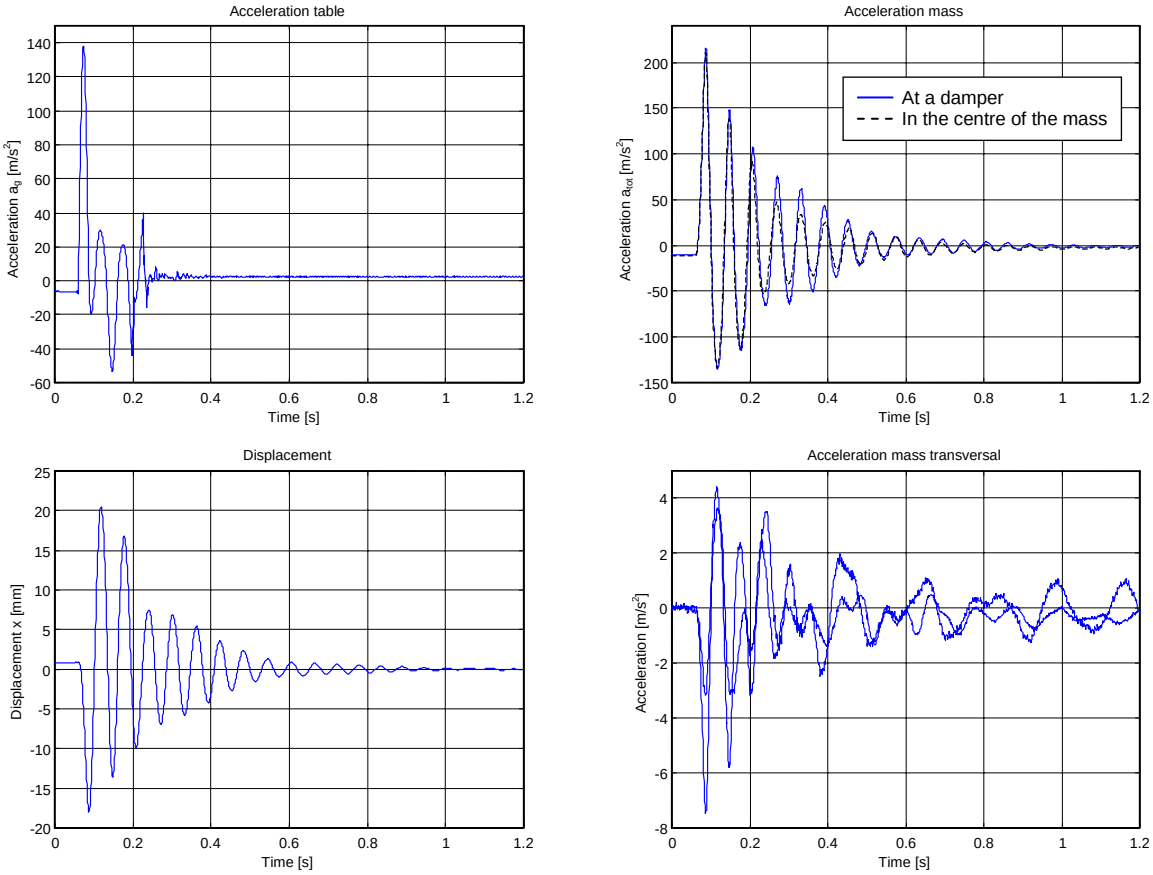

Figure C.2. Mass 215 kg and drop height 150 mm

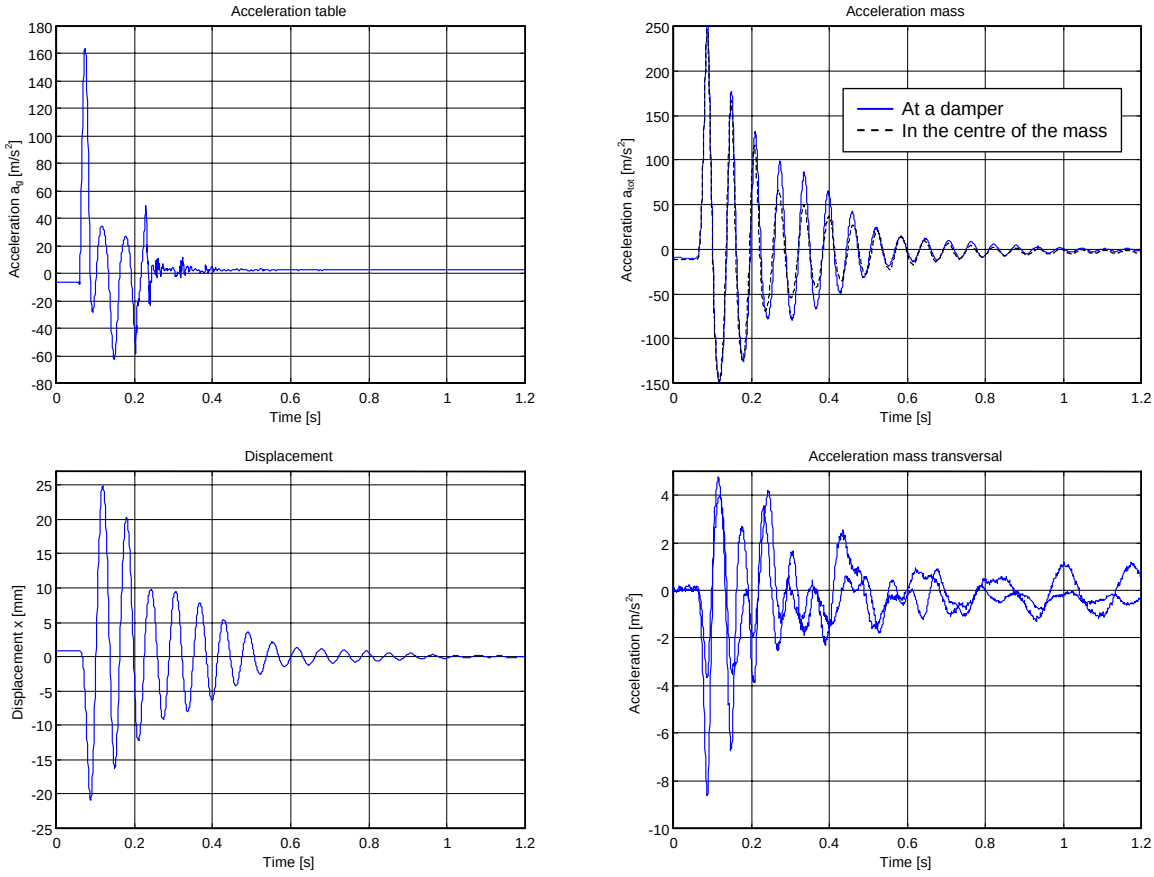

Figure C.3. Mass 215 kg and drop height 190 mm.

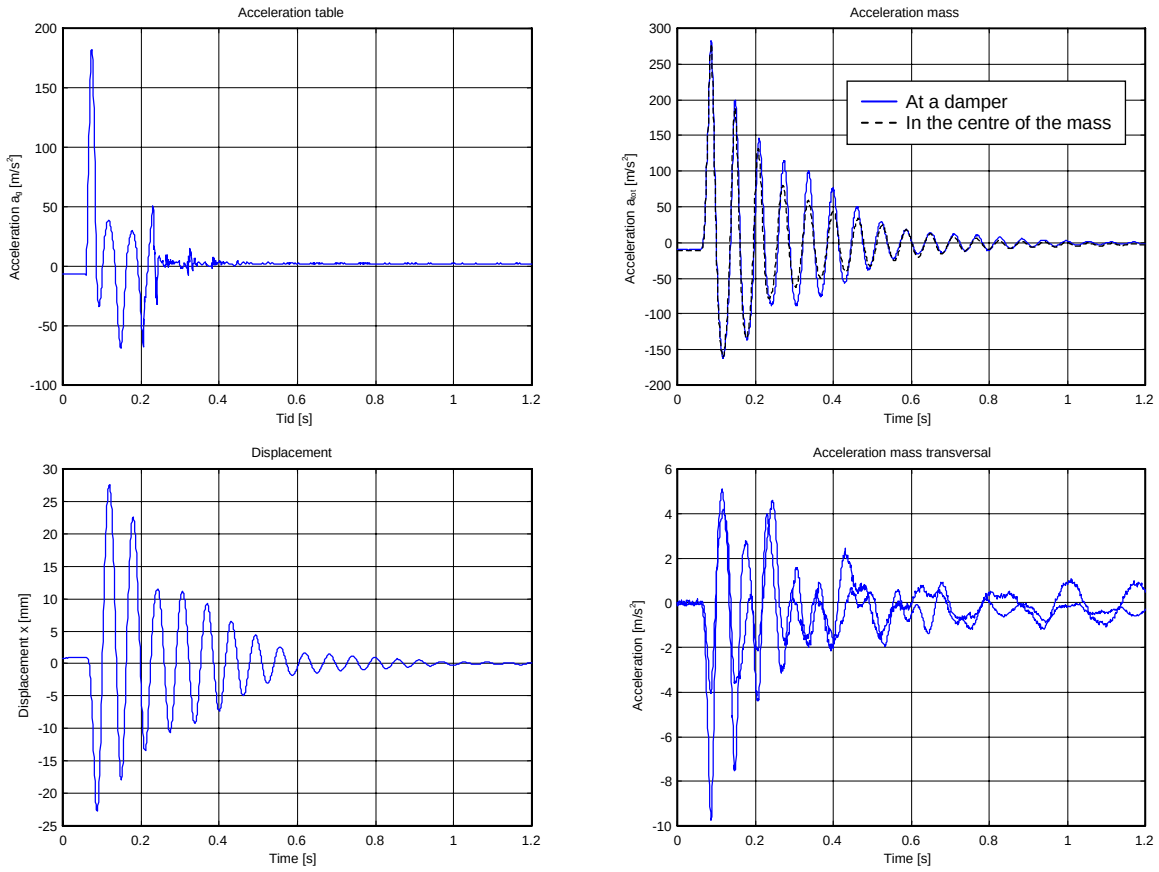

Figure C.4. Mass 215 kg and drop height 225 mm.

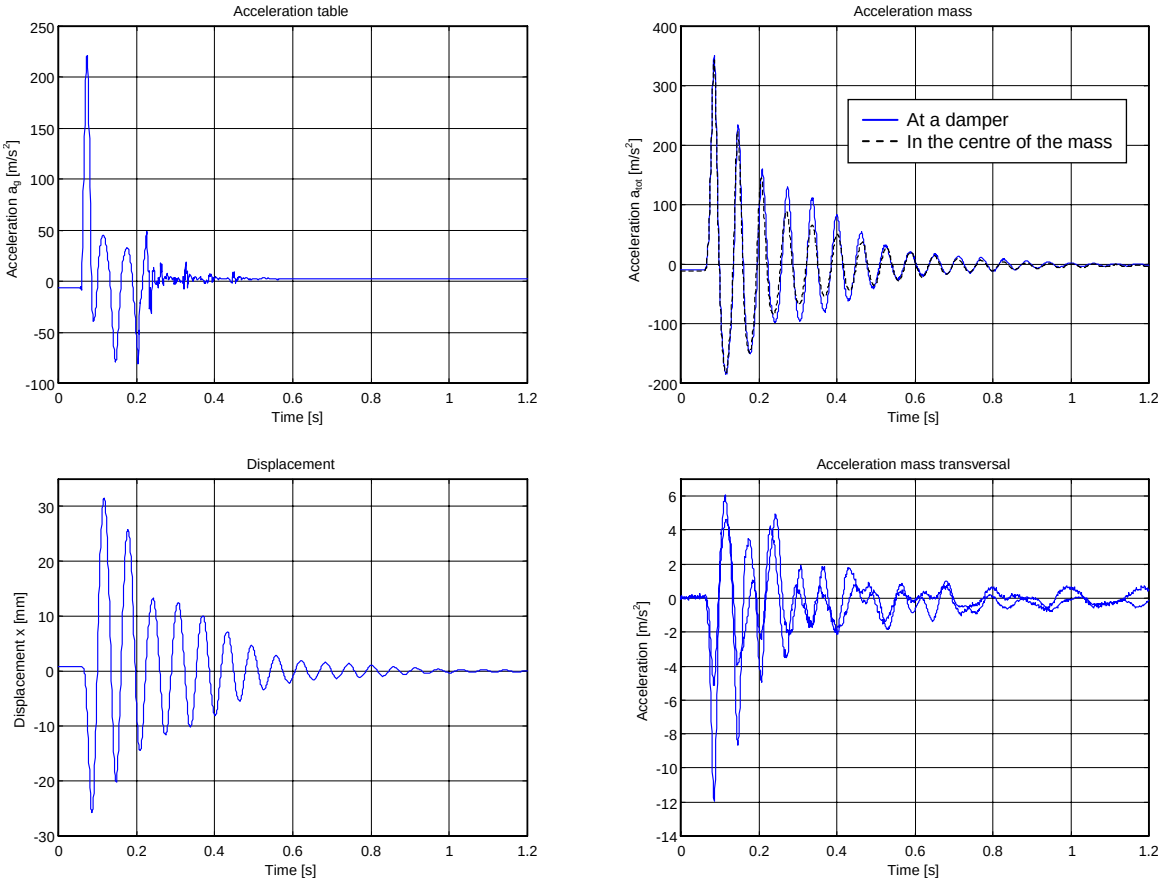

Figure C.5. Mass 215 kg and drop height 300 mm.

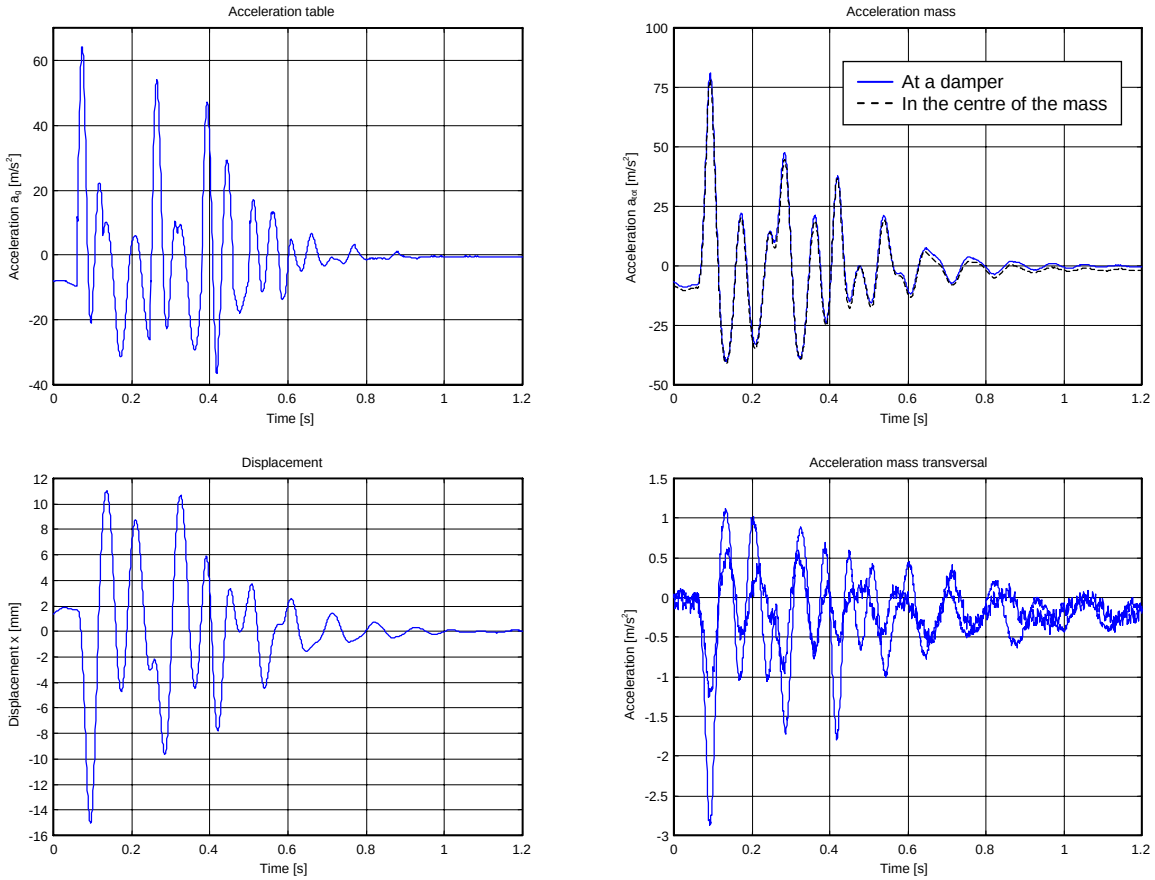

Figure C.6. Mass 473 kg and drop height 50 mm (test 1).

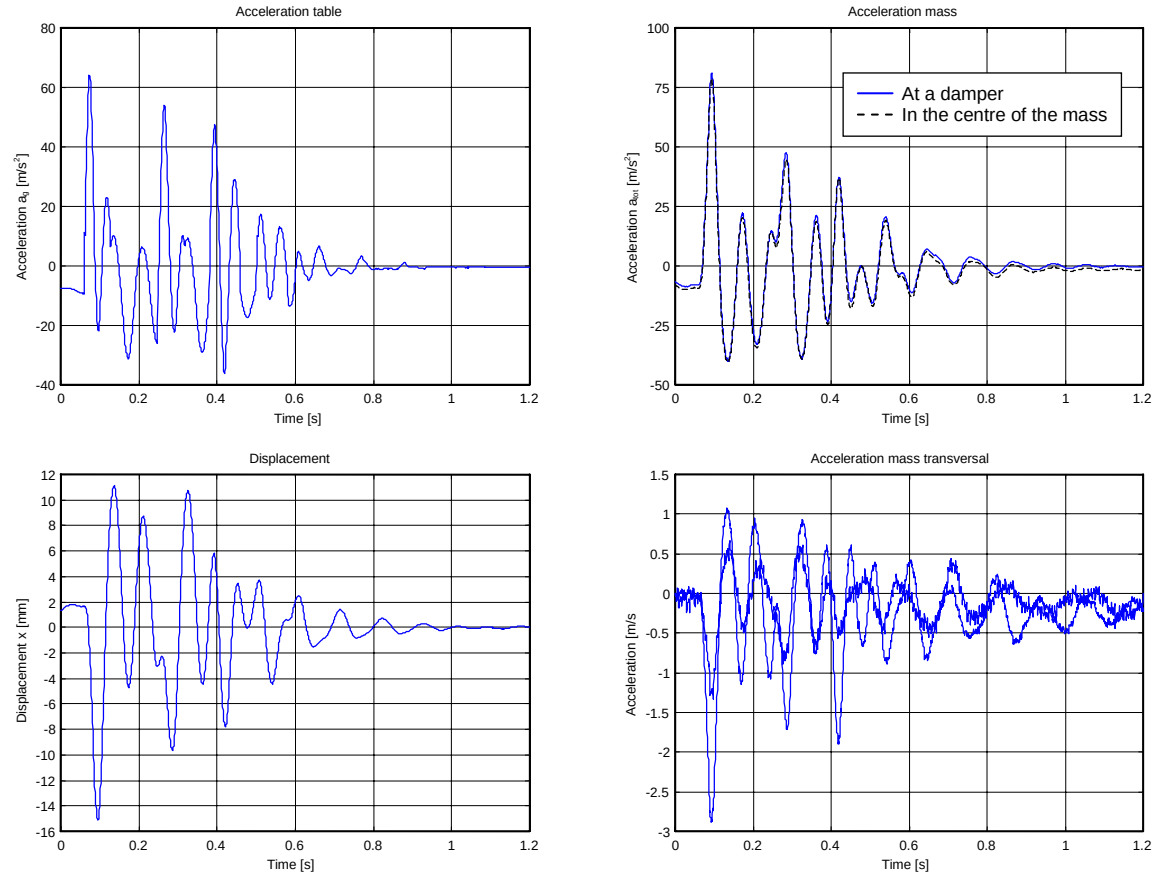

Figure C.7. Mass 473 kg and drop height 50 mm (test 2).

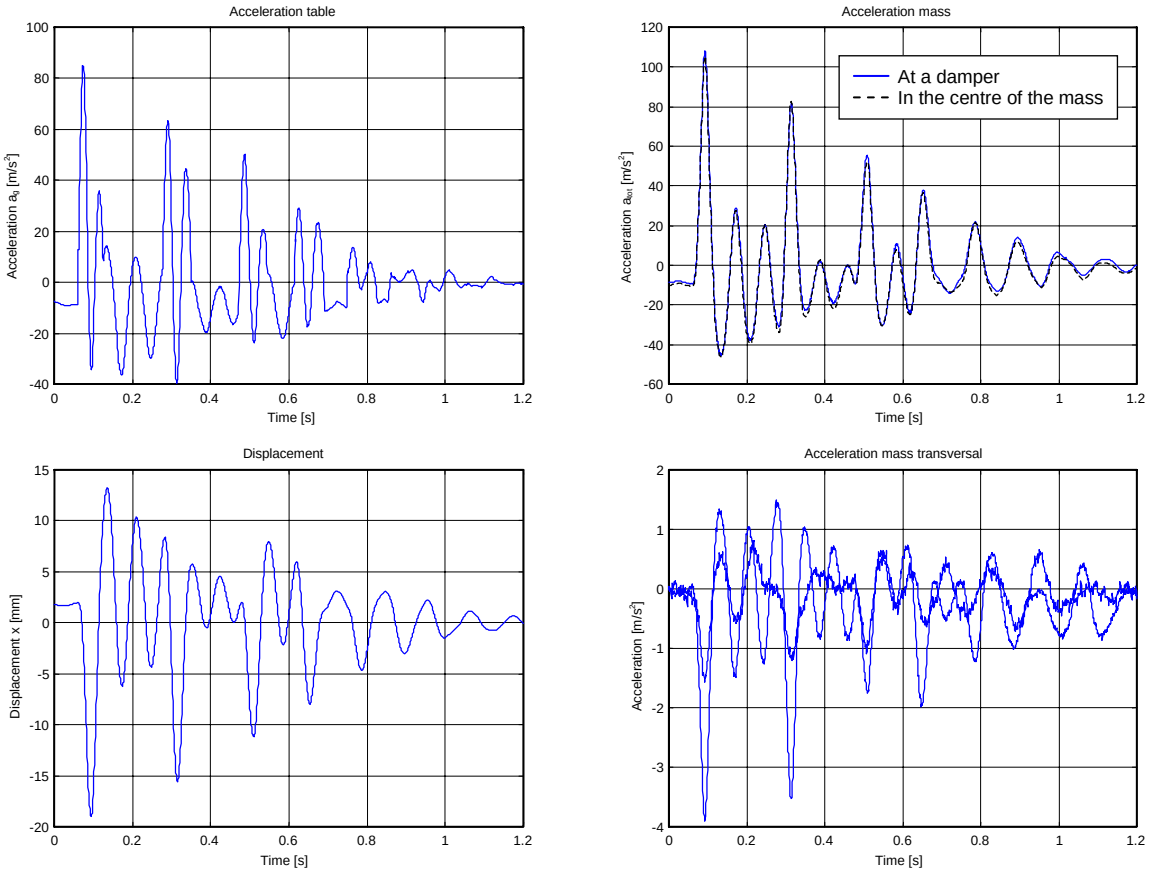

Figure C.8. Mass 473 kg and drop height 75 mm.

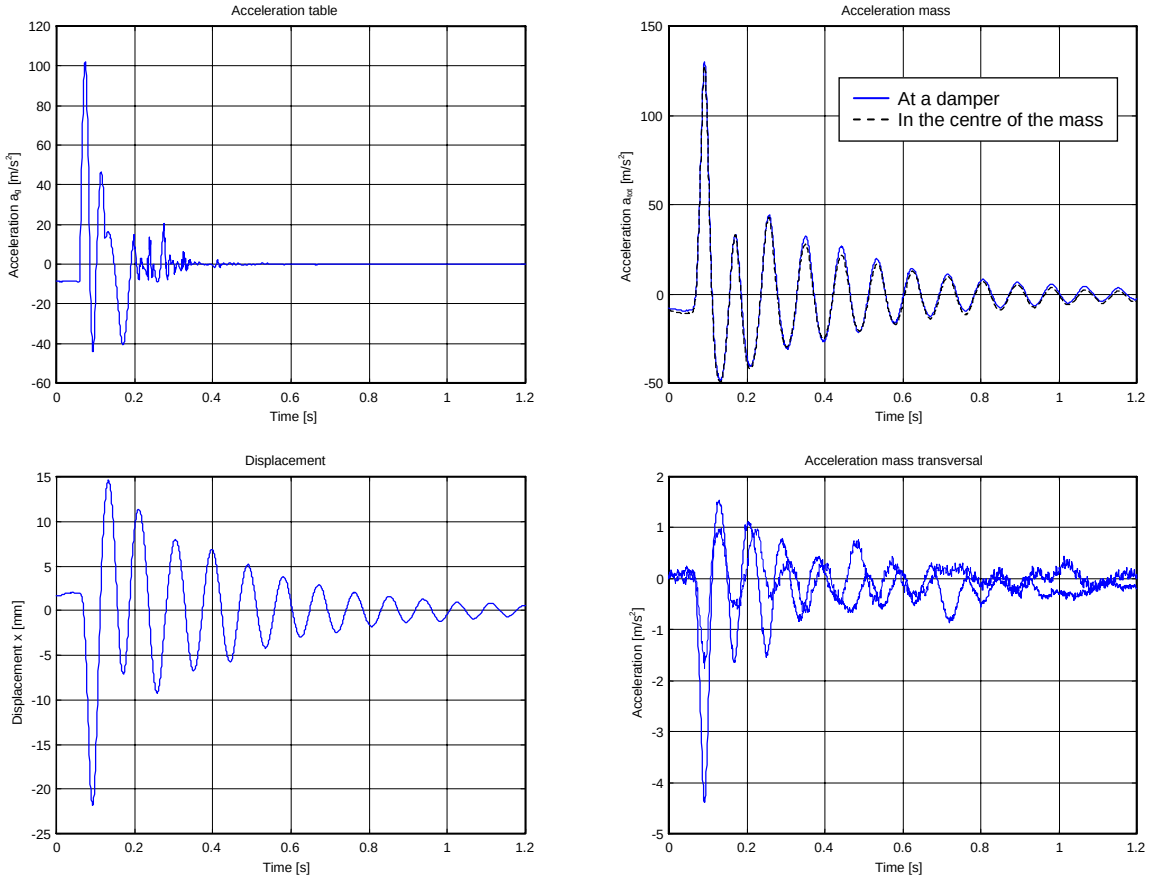

Figure C.9. Mass 473 kg and drop height 100 mm.

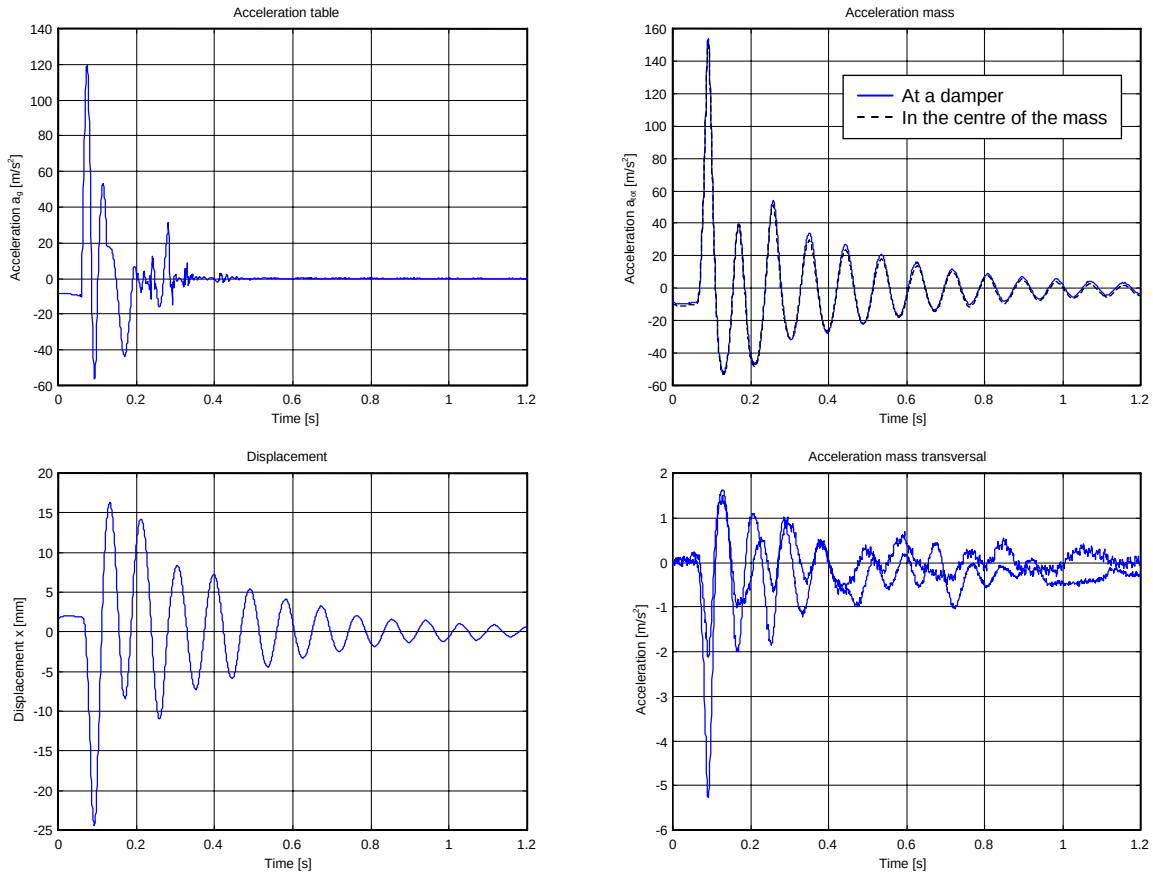

Figure C.10. Mass 473 kg and drop height 125 mm.

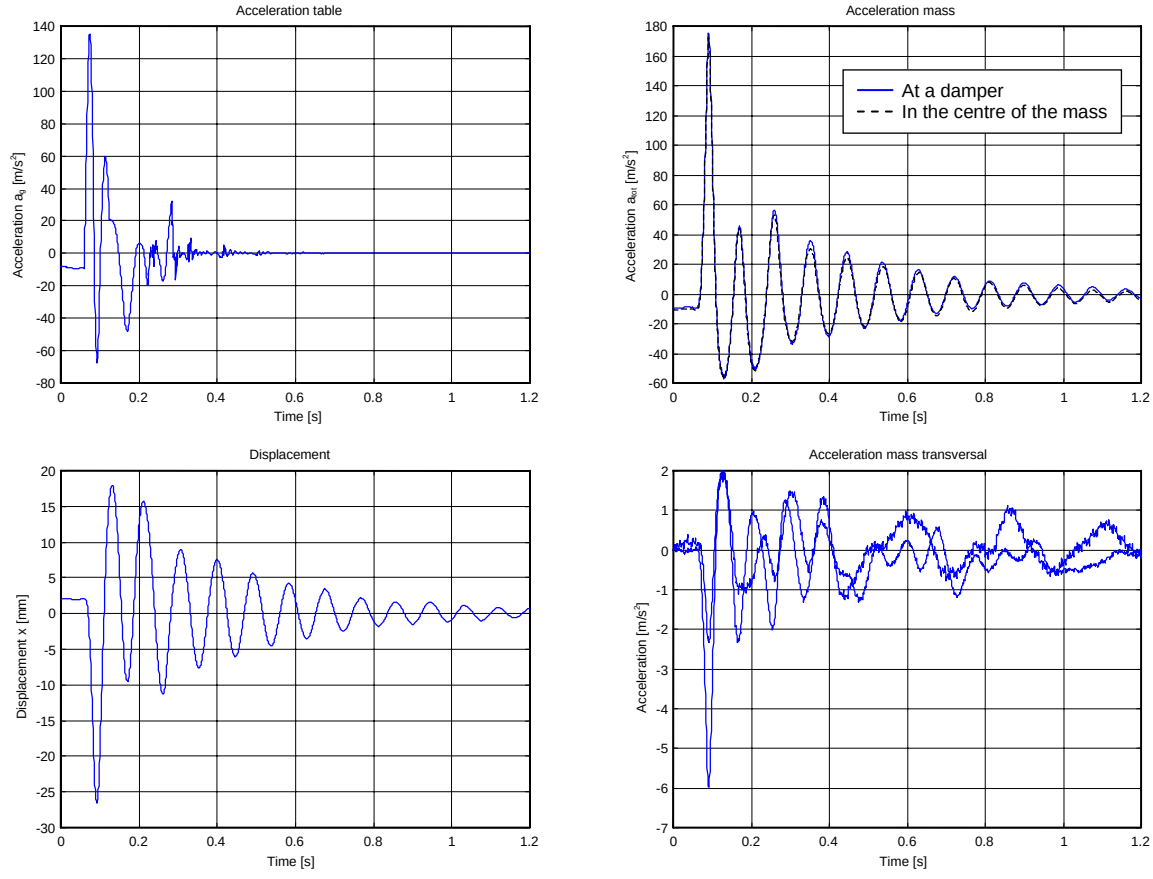

Figure C.11. Mass 473 kg and drop height 150 mm.

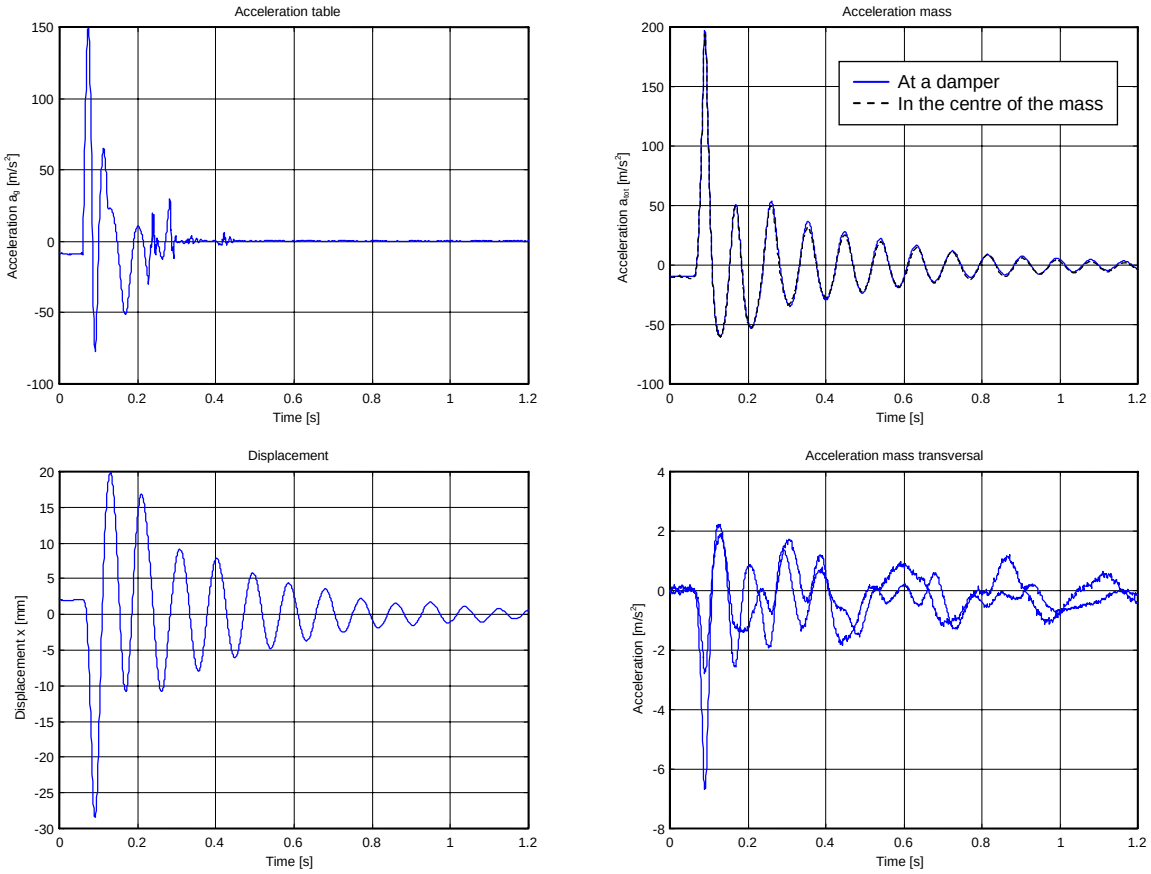

Figure C.12. Mass 473 kg and drop height 175 mm.

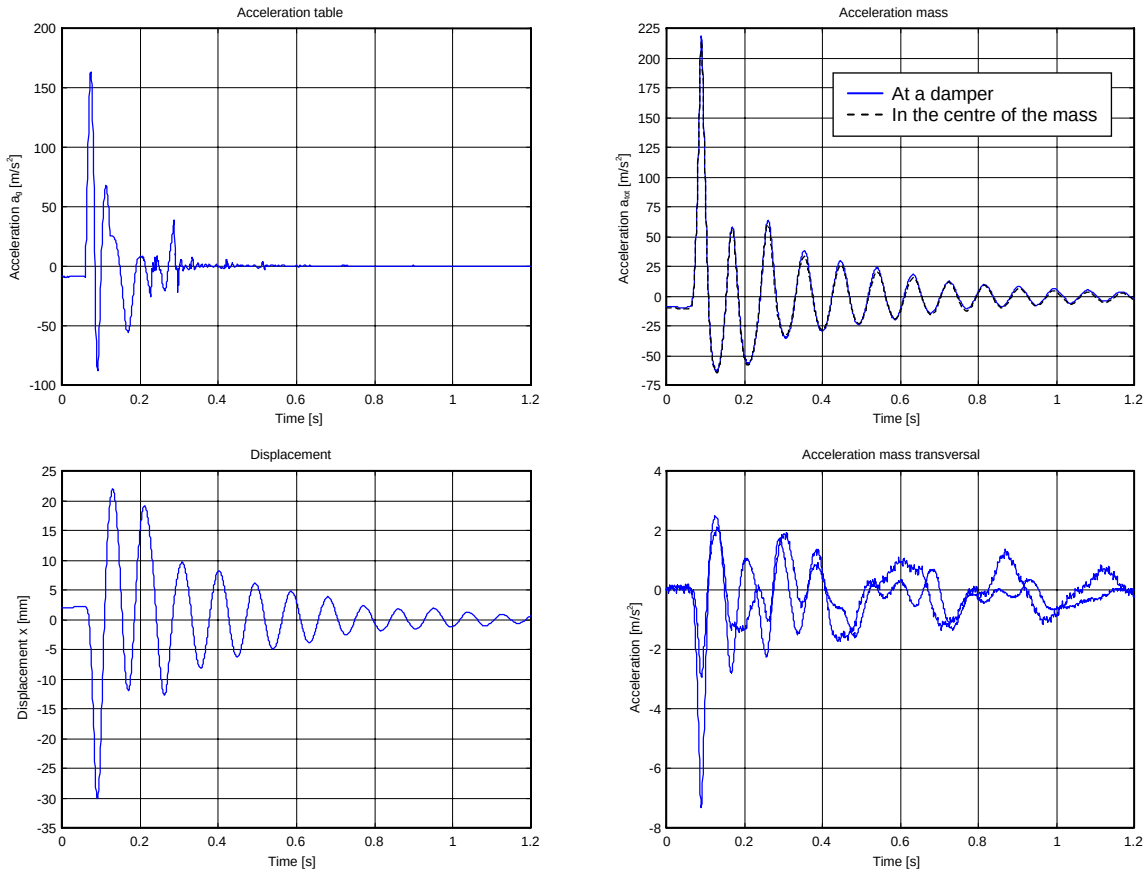

Figure C.13. Mass 473 kg and drop height 200 mm.

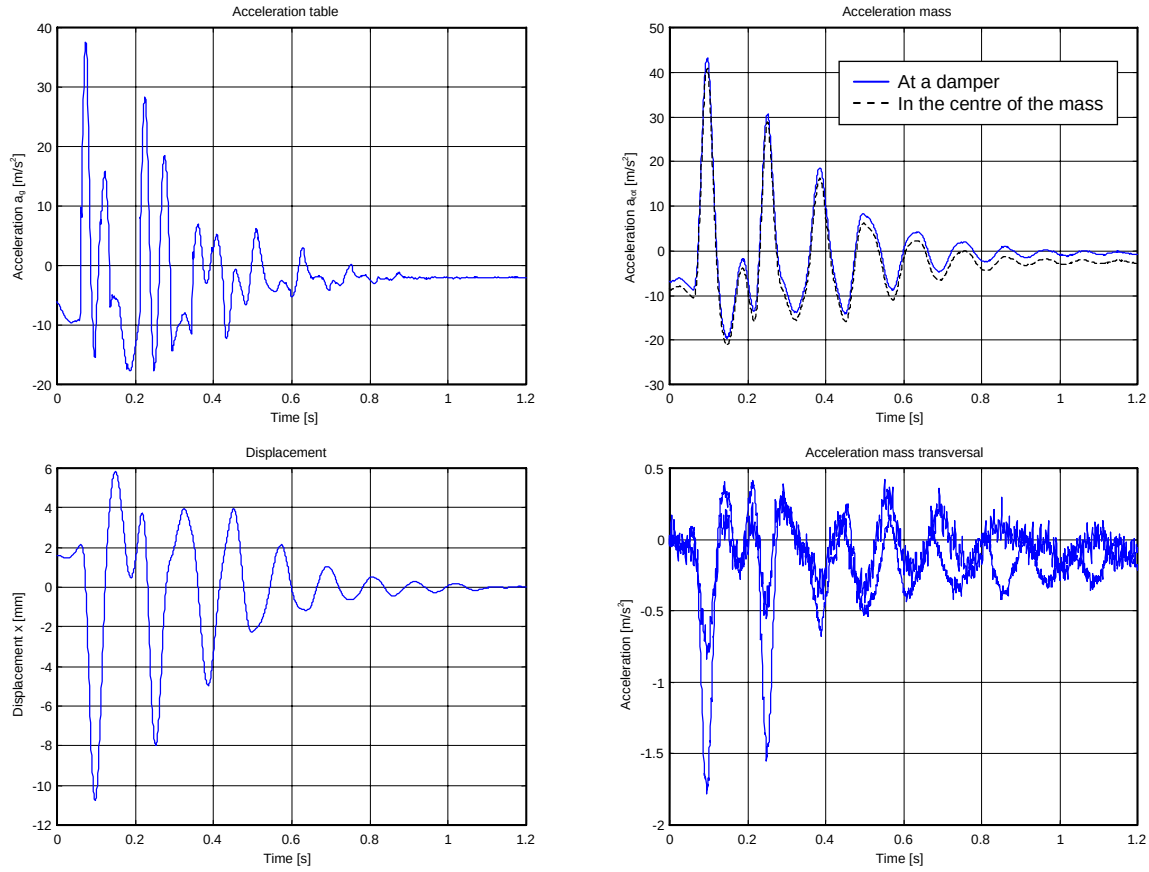

Figure C.14. Mass 590 kg and drop height 25 mm.

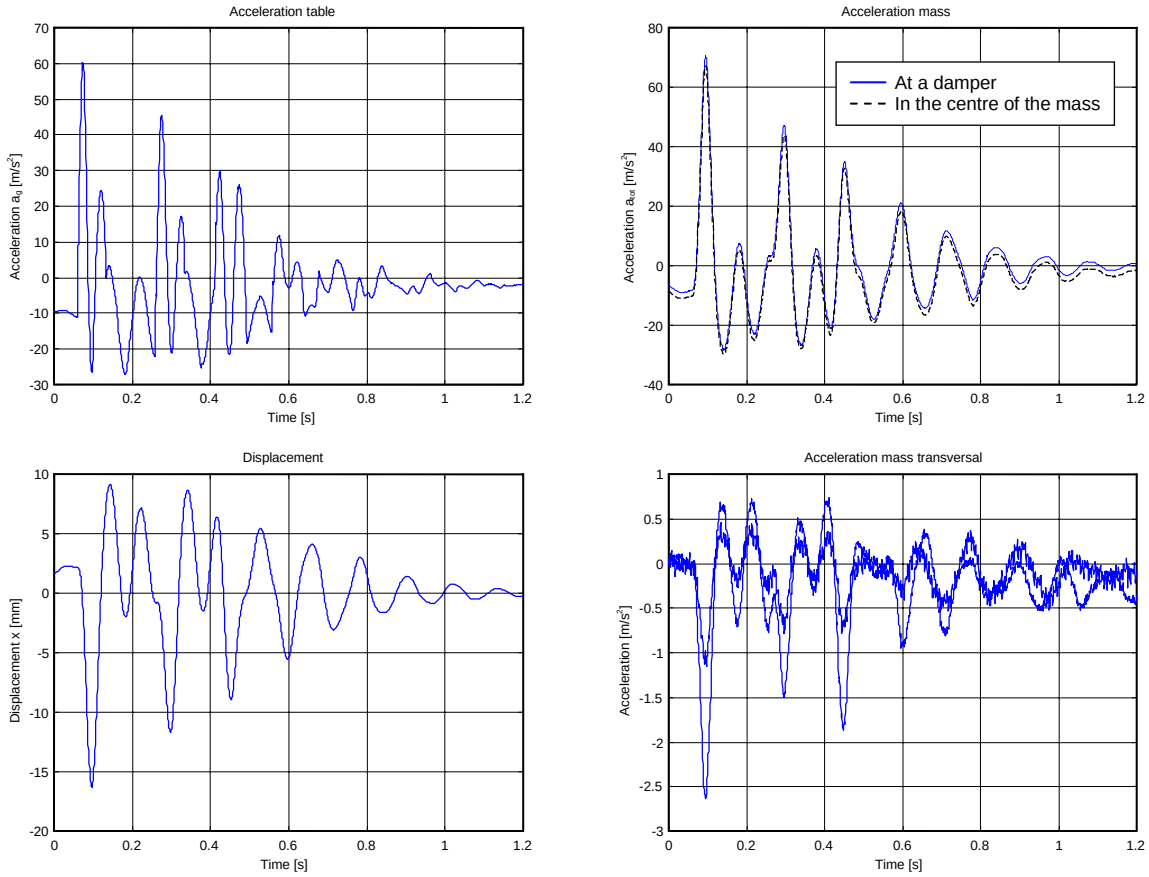

Figure C.15. Mass 590 kg and drop height 50 mm.

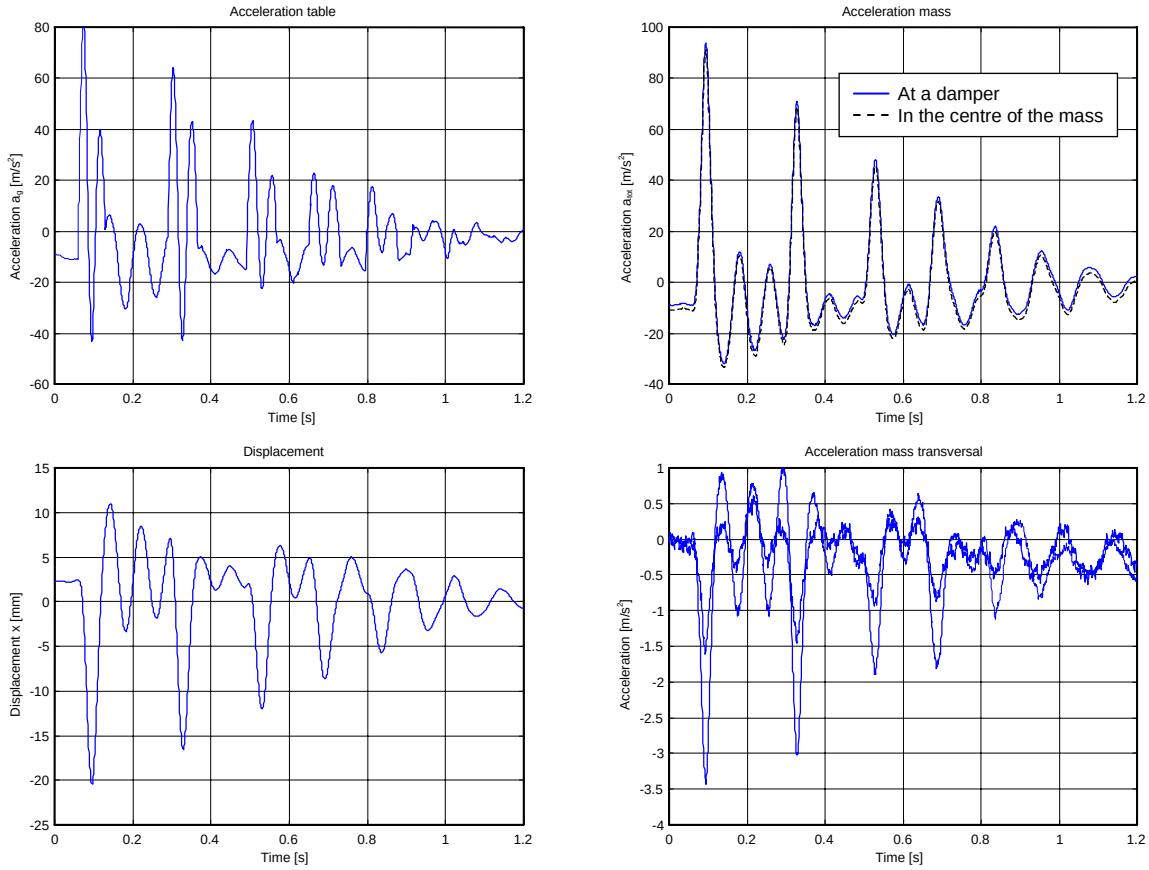

Figure C.16. Mass 590 kg and drop height 75 mm.

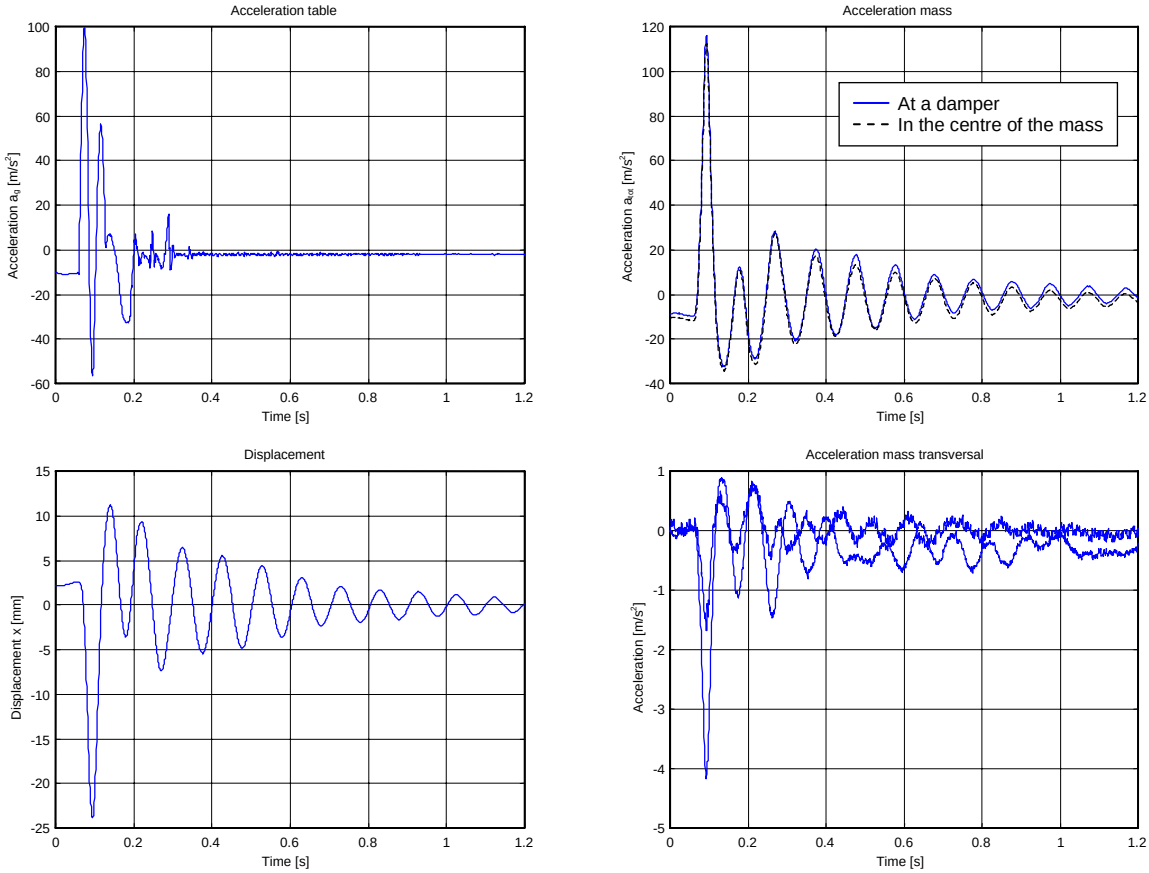

Figure C.17. Mass 590 kg and drop height 100 mm.

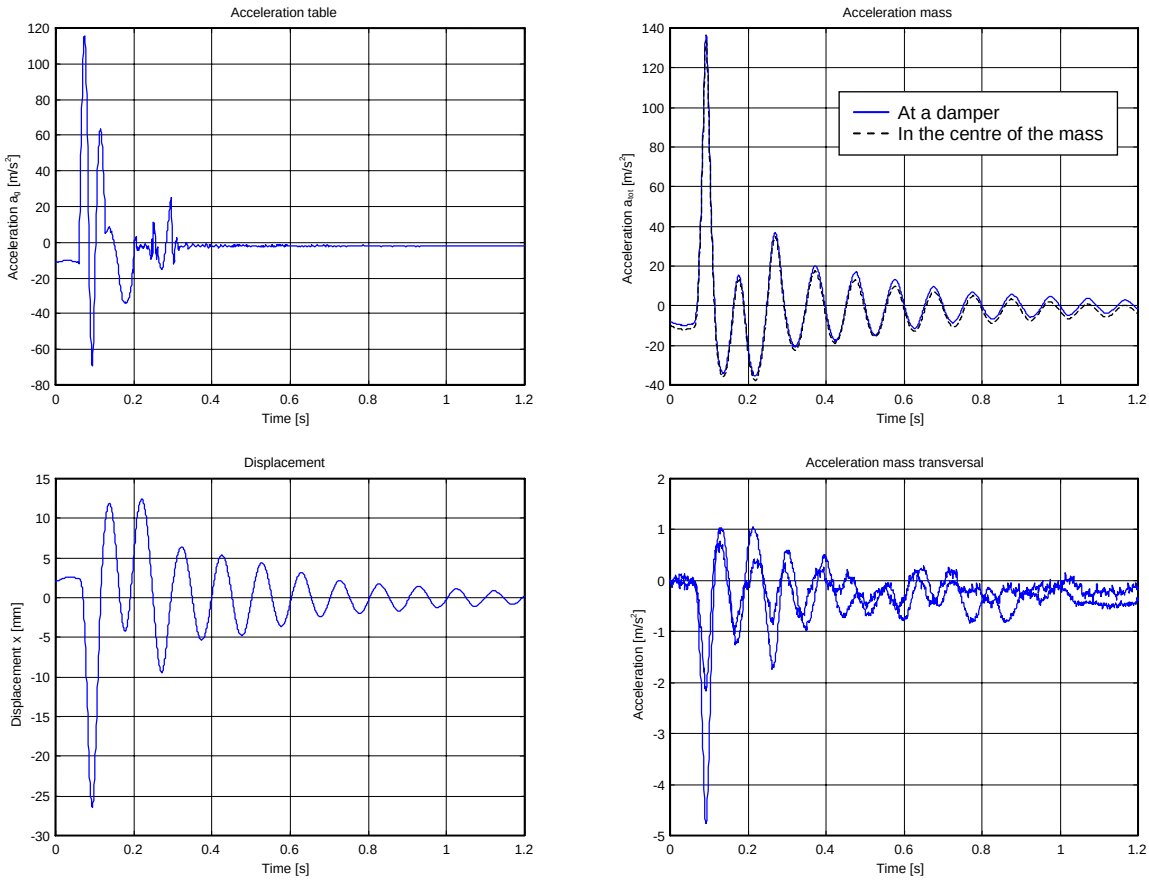

Figure C.18. Mass 590 kg and drop height 125 mm.

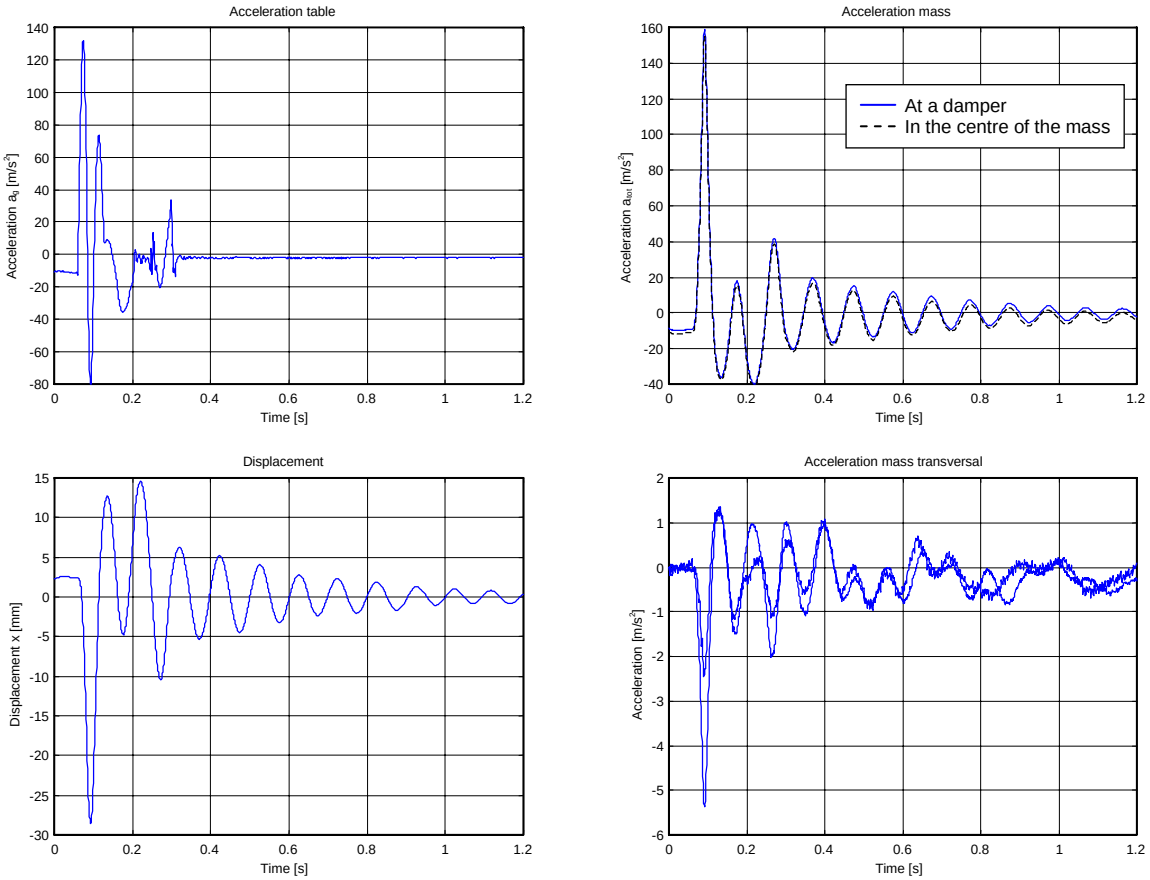

Figure C.19. Mass 590 kg and drop height 150 mm.